BINDING EFFICIENCY OF COAL-DERIVED BINDERS TOWARDS ANODE BUTTS

Final Technical Progress Report

Start Date: June 1, 2003
End Date: June 30, 2004

Principle Investigator: Dr. John M. Andresen
Report Issue: June 2004

Internal Agreement No. 2485-TPSU-DOE-0350,
For Award No.: DE-FC26-98FT40350

The Energy Institute
Penn State University
C-211 Coal Utilization Lab
University Park PA 16802

DISCLAIMER

ABSTRACT

This work can be divided into three parts: the study of the performance of alternative binder pitches, the physical and chemical properties of the butt materials, and the interaction of different pitches on different parts of the butt materials. There are four binder pitches used in this work: standard coal tar pitch (SCTP), petroleum pitch (PP), coal-extracted pitch (WVU), and gasification pitch (GP). The results of this study show that the petroleum pitch offers a potential to be used as additives to the standard coal-tar pitches for use as binders in the aluminum anode production, while the addition of coal-extracted pitch and gasification pitch give comparable anode properties when the ratio of standard coal tar pitch to the alternative pitch is greater than 50:50. Further work should be conducted to study the causes of improvement of adding alternative pitches to better understanding the roles of the binders from various types of pitches.

Three industrial anode butts, with and without recycled butt material, were studied. Non-destructive X-Ray imaging was used to quantify the spatial distribution of density and porosity in the sample. Apparent and absolute densities were measured and the specific pore volumes were calculated as a function of the distance from the airburn side. The results from the X-Ray CT and the densities and pore volume measurement showed a decrease in apparent density, and an increase in absolute density and specific pore volume from the center of the core to the surfaces. The anode butt that did not contain recycled butt material in the original formulation showed a higher reactivity with air at the airburn side while it had lower reactivity with CO_2 at the electrolytic side. It can be confirmed from this work that the main factors that derived the change in air and CO_2 reactivities of the anodes along the electrolytic surface to the airburn surface were the concentration of the inorganic contents, e.g. sodium, calcium, etc., and the porosity of the carbon material.

The experimental-scale anodes made from the top and bottom of the butt materials gave quite lower green apparent densities than the anodes made from the

middle part of the butt materials. These results were linked with high porosity of the top and bottom of the butt materials that inhibited the pitch to penetrate well into the pores. However the effect of porosity was weakened in the baked apparent density. Anodes that made from the pitch mixture that contained 20% PP and 20%GP gave comparable baked density to the anodes made from SCTP only. Whereas the anodes that were made from the pitch mixture that contained 20% WVU gave somewhat lower baked densities than the SCTP only and these results were caused by a high pitch loss of this pitch after baking.

TABLE OF CONTENTS

LIST OF TABLES

LIST OF FIGURES

1. Introduction

Carbon anodes are manufactured from calcined petroleum coke, butt fillers and coal tar pitch. Since the demand of the coal tar pitch in the aluminum industry accounts for about 75% of the pitch market [1] and the production of coal tars is rapidly decreasing in the United States as well as throughout the world [2], the development of alternative binders were considered in this work. Coal tar binder pitches are traditionally obtained from coal tars that are the by-product of bituminous coal coking process used to make coke for blast furnaces in iron production. During the manufacturing of carbon anodes coal tar pitch is mixed with calcined petroleum coke, where petroleum coke is the by-product from the delayed coker in a refinery. Remaining parts of spent anodes from the aluminum production, namely butts, are also crushed and used as filler [3].

The alternative binder pitches considered in this work are petroleum pitch (PP), coal-extracted pitch (WVU), and gasification pitch (GP). Petroleum pitch is a residue produced from heat-treatment and distillation of petroleum fractions. A production of coal-extracted pitch involves a prehydrogenation of coal followed by extraction using a dipolar solvent. Gasification pitches are distilled by-product tars produced from the coal gasification process. The mix of binder, filler and some additives are heated to about 50°C above the softening point of the pitch, typically 160°C. This temperature is sufficient to enable the pitch to wet the carbon particles [4]. The mix is then either extruded, vibrated or pressed to form a green anode. The wetting of coke by pitch is very important to the anode property. The pitch has to flow over the coke surface and has to enter into the surface porosity to generate a cohesive paste. Quinoline insolubles or QI play an important role in filling the spaces between petroleum and recycled anode coke particles on which the pitch is supported and prevent the pitch from fully penetrating the pores of the coke particle [4]. It is generally accepted that pitches with up to 15 %wt QI yield better anodes [5]. The only pitch studied in this work that contains QI is the SCTP, whereas the others contain about 0.1 wt% or less of QI. Mixing of the SCTP and the alternative pitch creates a various content of QI to the mixture.

The Hall-Héroult process, where alumina is reduced by carbon to produce aluminum, is currently the largest user of premium carbon products worldwide consuming over 11 million tons in form of carbon anodes annually [1]. To improve the economics of the process, anode butts, the unused parts of the anode remaining from operation in the reducing pot, are crushed and used as filler in the production of new anodes. About 20% of the anode is recycled butt material that accounts for over 300,000 tons annually [2]. The lower part has been in contact with the hot electrolyte experiencing temperatures in the range of 930 to 980°C. The lower part of the anode may also have been consumed by CO_2 burn, where typically the binder coke is attacked selectively. CO_2 burn may also affect the side of the anode. Further, the top part of the anode may reach temperatures of 350 to 600°C depending on the protective cover of electrolyte material, and air burn may also take place. Hence, the butt chemistry may differ significantly from that of petroleum coke, where the lower part of the butt may be altered due to the interaction with the cryolite as well as the modification of the surface chemistry due to the burn-off from CO_2. The top part of the butt could be highly oxidized during the air burning, while the middle part of the butt may not be affected by any of the above.

The objectives of this work were to determine:

1. the performance of each alternative binder pitch from various sources of pitches
2. the physical and chemical properties of the butt materials from different conditions in the reducing pots
3. the interaction of different pitches on different parts of the butt materials

To fulfill the first objective, each alternative pitch was mixed with a standard coal tar pitch (SCTP) at various mixtures and laboratory-scale test anodes were formed and studied. The ratio of pitch:coke:butt remained constant for the whole study. Mixing of the SCTP and the alternative pitch creates a various content of QI to the mixture. This may provide a suitable level of QI that gives a good laboratory-scale anode property.

A range of tests were performed to study the physical and chemical properties of the butt materials. This work examined the spatial distribution of physical properties such as densities and porosities of anode butts as a function of their position in the reducing pot. X-Ray Computed Tomography (X-Ray CT) was used to non-destructively study the overall structure of an anode butt. Other physical properties such as apparent density, and absolute density were directly measured. The thermal gravimetric analyzer (TGA) was used to examine the air and CO_2 reacitivities at different conditions. Alcoa Co., Ltd. provided the Inductively Coupled Plasma (ICP) analyses of different inorganic contents, e.g. sodium, fluoride, aluminum, etc. to different parts of the anode butts. Finally, attempts were made to determine the relationships among these physical and chemical properties.

The last part of this study was to examine how different pitches interact with different parts of the butt material, i.e. bath side, middle, and electrolytic side. Since these different parts of the anode butts have experienced different conditions such as different temperatures, chemical exposure, etc. These effects may cause different properties throughout the anode butt. Since a certain amount of butt materials were crushed and recycled to make a new anode, the output of this study may be used to improve the property of the anode and, hence, improve the economy of the pre-baked anode production.

2. Experimental

The experimental can be divided into three different parts: the binder pitch study, the anode butt study, and the pitch/butt study.

2.1 Binder Pitches Study

2.1.1 Materials

Four types of pitch were used in this study: two standard coal tar binder pitches (SCTP-1), a petroleum pitch (PP-1), a coal-extracted pitch (WVU-5), and a gasification pitch (GP-1). The properties of each pitch are summarized in Table 1. Petroleum coke

and recycled anode butts were crushed and aggregated into three different sizes: (i) Fines: >200 mesh size; (ii) Intermediate: 60-200 mesh size; and (iii) Coarse: <60 mesh size

Table 1 Properties of pitches.

Property	SCTP-1	SCTP-2[1]	GP-1	GP-2	PP-1[1]	WVU-4[2]	WVU-5[2]
Softening Point (°C)	112.5	111.9	115	130	111.9	127.1	112.2
Quinoline Insolubles (wt%)	13.6	15.9	<0.1	<0.1	0.1	<0.1	<0.1
Toluene Insolubles (wt%)	27.8	30.9	N.A.	N.A.	3.2	N.A.	N.A.
Coking Value (wt%)	N.A.	57.9	N.A.	N.A.	47	43.9	50.3
Ash Content (wt%)	N.A.	0.29	N.A.	N.A.	0.08	0.1	0.2
Specific Gravity @ 25°C	N.A.	1.34	N.A.	N.A.	1.246	1.2	1.25
Sulfur Content (wt%)	N.A.	0.56	N.A.	N.A.	1.21	N.A.	N.A.
Metal							
Calcium (ppm)	N.A.	49	N.A.	N.A.	5	N.A.	N.A.
Chlorine (ppm)	N.A.	18	N.A.	N.A.	15	N.A.	N.A.
Iron (ppm)	N.A.	269	N.A.	N.A.	19	N.A.	N.A.
Lead (ppm)	N.A.	38	N.A.	N.A.	N.D.	N.A.	N.A.
Nickel (ppm)	N.A.	4	N.A.	N.A.	4	N.A.	N.A.
Phosphorous (ppm)	N.A.	N.D.	N.A.	N.A.	N.D.	N.A.	N.A.
Potassium (ppm)	N.A.	39	N.A.	N.A.	2	N.A.	N.A.
Silicon (ppm)	N.A.	439	N.A.	N.A.	377	N.A.	N.A.
Sodium (ppm)	N.A.	N.D.	N.A.	N.A.	54	N.A.	N.A.
Vanadium (ppm)	N.A.	3	N.A.	N.A.	8	N.A.	N.A.
Zinc (ppm)	N.A.	80	N.A.	N.A.	0	N.A.	N.A.

N.A. = Not Available
N.D. = Not Detectable
[1] Data provided by Koppers Co., Ltd
[2] Data provided by the West Virginia University

2.1.2 Compositions of Experimental-Scale Anodes

All experimental-scale anodes in this work were made using the following compositions:

Pitch:Butt:Coke = 22:29:49

Fine:Intermediate:Coarse = 40:35:25

2.1.3 Mixing and Forming

The aggregate fillers and binders, which weighed about 15 grams in total, were mixed at about 50°C above the softening point of the pitch mixture. The CARVER cylindrical mold with an inside diameter of 28.58 mm was preheated to about 10°C above

the softening point of the pitch mixture. The hot mix was placed into the mold and rapidly pressed at 9,000 psi for 2.5 minutes. The final green anode was cylindrical in shape with typically 28.60 mm. in diameter and 13.00-14.00 mm in height.

2.1.4 Baking

The green anodes were baked with a low heating rate to about 1075°C over a period of 5-6 days prior to cooling. The temperature profile was 25°C/hr from 25°C to 125°C; 3.5°C/hr from 125 to 600°C; 100°C/hr from 600 to 1075°C; hold at the temperatures between 950 and 1075°C for 6 hours; and cool down in the furnace to room temperature.

2.1.5 Properties Measurement

The green and baked anodes were weighed to the nearest 0.001 gram and their dimensions were measured by a caliper to the nearest 0.01 millimeter. The apparent densities of both green and baked anodes were calculated by a ratio of mass and volume. The amount of pitch loss after baking was calculated by assuming that all the weight loss was resulting from the pyrolysis of pitch. Finally, the volume change of the baked anodes relative to the green ones was calculated.

2.2 Anode Butts Study

The experiments conducted using industrial anode butts, BUTT-1, BUTT-2, and BUTT-4 collected from different plants. The bath temperature was about 960°C and the pots were operated at 4.6 volts and 100,000 to 350,000 amps. The height of a new anode was 58 centimeters prior to setting in the pot and this height reduced to 18 centimeters when the butt was removed after approximately 24 days of service. Butt-2 contained recycled anode butts in the formulation of the original anode and had experienced standard operating conditions in the pot as well as a preparation for recycling. Butt-4 was

a butt from an anode that originally did not contain any recycled anode-butt material. Table 2 summarizes the conditions of these two anode butts.

Table 2 Characteristics of selected anode butts.

Anode butt code	Characteristics
Butt-1	-About 24 days of operation in the pot. -Formulation of original anode included recycled butts.
Butt-2	-About 24 days of operation in the pot. -Formulation of original anode included recycled butts.
Butt-4	-About 24 days of operation in the pot. -Formulation of original anode did not included recycled butts.

The samples used in this study were cored from the center of the butts (core #5) and had approximately 51 millimeters O.D. These samples were first scanned with the X-Ray CT scanner using a large focal spot source at 200 kV. X-Ray Tomography (CT) is a non-destructive method for obtaining three-dimensional attenuations of an object. The attenuation maps depend on bulk density and apparent atomic number of the material. With proper calibration the distribution of parameters such as density, porosity, and composition can be acquired. Samples shorter than 150 millimeters were scanned parallel to the axial axis of the sample with a resolution of about 400 microns. Samples longer than 150 millimeters were scanned perpendicular to the axial axis with a resolution of about 300 microns.

The middle core of each anode butt (see Figure 1), namely Core #5, was sliced perpendicular to the axial axis into sections approximately 5 millimeters thick. Different names were given to call each slice of the core, i.e. T1, T2, T3, …, M1, M2, M3,…, B4, B3, B2, B1, as shown in Figure 2. T1 represents the most top and B1 represents the most bottom of the core. The diameter and thickness of each slice were measured to the nearest 0.01-millimeter by a Caliper. The weight of each slice was measured to the nearest 0.0001 gram. The apparent density (ρ_{app}) was calculated by the ratio of mass and volume. Each slice was later cracked into smaller pieces approximately 1-3 grams. About 5-6 grams of sample were weighed to the nearest 0.0001-gram and the absolute volume was performed by a Helium substitution using the Quantachrome

Multipcynometer. The absolute density (ρ_{abs}) was calculated by the ratio of mass and volume. The specific pore volume (v_P) was calculated by

$$v_P = \frac{1}{\rho_{App}} - \frac{1}{\rho_{abs}} \qquad \text{Equation (1)}$$

Parts of each slice of the anode butt Core #5 were sent to Alcoa Co., Ltd to perform the ICP analyses to measure the concentrations of inorganic materials, e.g. sodium, fluoride, aluminum, etc. of each section of the butt core. Only Butt-2 was used in the thermal analyses. The leftover materials from the ICP analyses of each slice were crushed to pass a 200-mesh size screen. About 9-11 mg of the +200 mesh size of each slice was used in a thermal gravimetric study. Separate tests were done to ensure that the particle size and the amount of the sample for a TGA run were appropriate to eliminate the effect of mass transfer throughout the sample bed. Three TG analyses were performed: (1) non-isothermal air reactivity from the room temperature to 800°C at 10°C/min; (2) isothermal air reactivity at approximately 500°C; and (3) isothermal CO_2 reactivity at approximately 960°C. The experimental procedures of this part of the study were schematically summarized in Figure 3

A simple and systematic reactivity test was developed by Jenkins et al. [6]. In this work, about 9-11 mg of sample was placed in a TGA apparatus and heated the sample up at 50°C/min to the target temperature with dry nitrogen at a rate of 100 cm^3/min. After the temperature was stabilized at the target temperature, dry air or CO_2 was introduced isothermally at a rate of 100 cm^3/min. The weight loss of the sample was continuously recorded. Typically, the burn-off (versus time) curve exhibited a rectilinear part over a period of about 40% of the char that was gasified [6] (see Figure 24), and followed by a decrease in slope. A maximum reactivity was observed in this rectilinear region and was calculated by

$$R_{\max} = -\frac{1}{m_C}\frac{dm_C}{dt} \qquad \text{Equation (2)}$$

where R_{max} is a maximum reactivity at a desired temperature (mg h^{-1} mg^{-1}), m_C is the initial mass of char on an ash-free basis (mg). dm_C/dt is the maximum weight loss rate (mg h^{-1}) or the slope of the burn-off versus time. The reactivity (Equation (2)) also can be written in term of the conversion, $X_C = \frac{m_{c0} - m_c}{m_{c0}}$, as follows:

$$R = \frac{1}{1 - X_C}\frac{dX_C}{dt} = kC_C \qquad \text{Equation (3)}$$

The burn-off versus time plot can be normalized using a dimensionless time scale, i.e. $t/\tau_{0.5}$, where $\tau_{0.5}$ is the time at a fractional burn-off of 0.5 [7]. The typical shape for most chars derived from coals of a wide range of ranks exhibit similar shapes of the burn-off versus $t/\tau_{0.5}$. However, this normalized burn-off curve is not sufficient to offer the 'characteristic' shape for all type of cokes because of the complexity of the char gasification reactions. The initial slow increase in the slope of the TGA plot is due to the opening of closed pores and enlarging of existing pores to increase the accessibility of reactant gas during the induction period. The slope increases as burn-off increases until a maximum is reached. Then the slope starts to decline, slowly decreasing to complete burn-off. The decrease in slope results from decreases of amount of gasifiable material and from lower reactive area due to the coalescence of pores as burn-off proceeds.

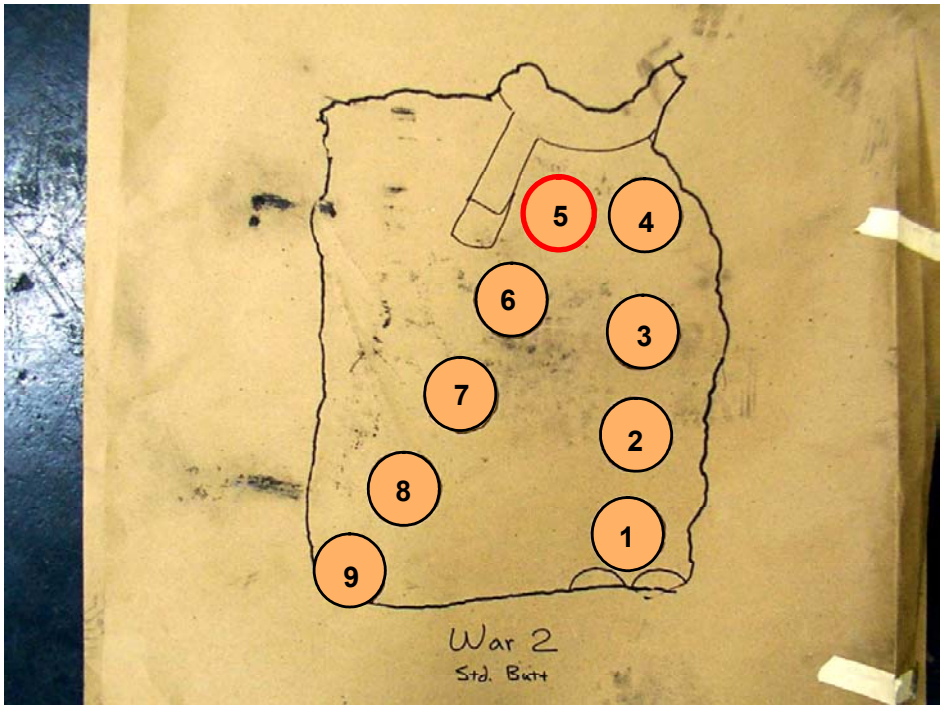

Figure 1 Position of the Core #5 in the anode butt.

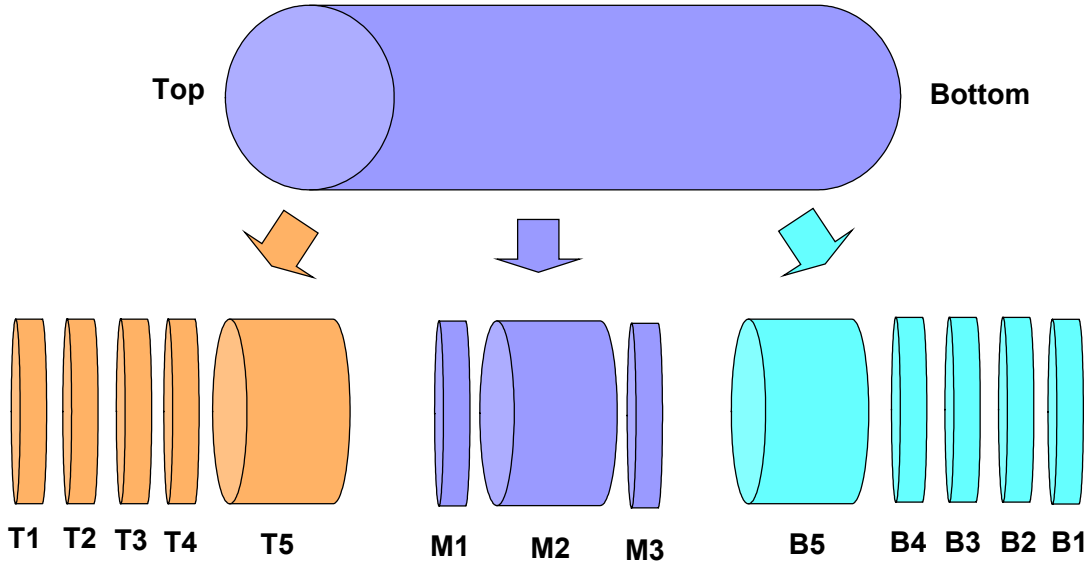

Figure 2 Names of different slices of the cut anode butt.

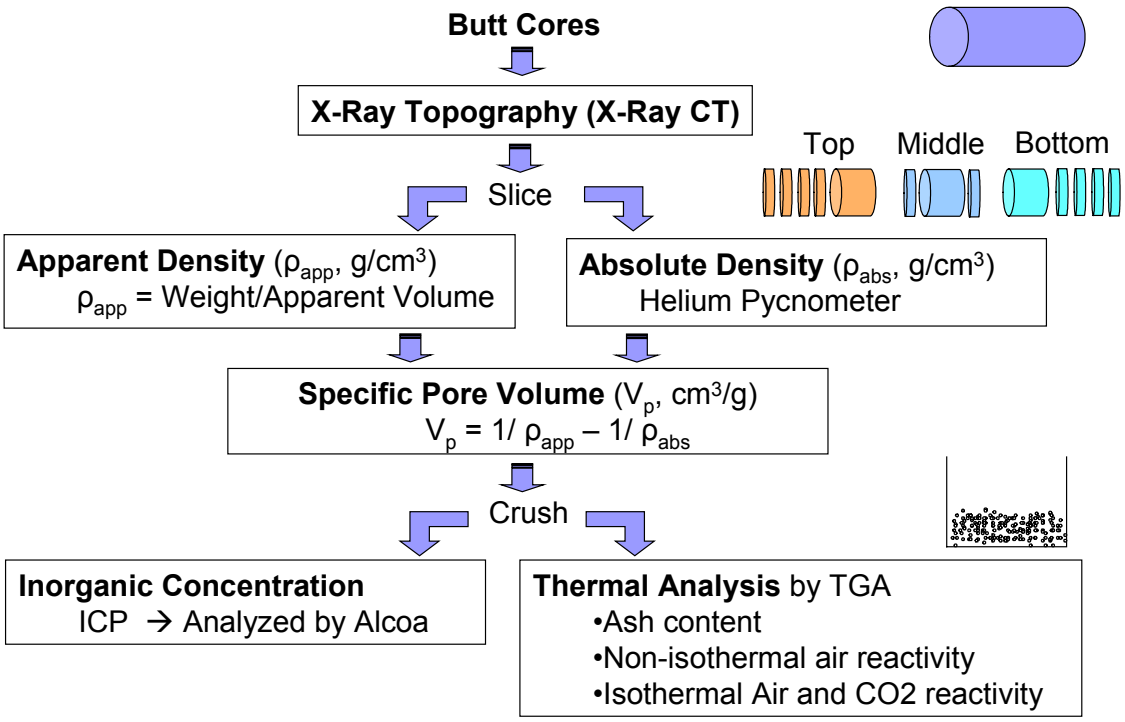

Figure 3 Experimental procedure.

2.3 Pitches/Butts Study

In this part of the study, the procedures of making a laboratory-scale anode and the property measurement of the anode were the same as described in Section 2.1. The pitch:coke:butt ratio remained the same, i.e. 22:49:29. However, there were some minor changes in the material used in the compositions of the anode as follows:

2.3.1 Pitch

Since the limited amount of the SCTP-1, which was used in the study of pitches in Section 2.1, the SCTP-2 was used instead and its property is shown in Table 1. Four different compositions of pitch mixture were used to make the laboratory-scale anodes: (1) 100% SCTP-2; (2) 20% PP-1 and 80% SCTP-2; (3) 20% WVU-5 and 80% SCTP-2; and (4) 20% GP-1 and 80% SCTP-2. All percentages are in weight basis. 20% of the

alternative pitches were used because it was shown in the pitches study (see Section 3.1) that up to 50% of the alternative pitch may be added to balance the SCTP to give comparable properties of the laboratory-scale anode made by only SCTP.

2.3.2 Coke

The same ratio and coke materials were used as those laboratory-scale anodes made in Section 2.1.1 and 2.1.2.

2.3.3 Butt materials

Because of the limited amount of butt material obtained from the Butt-2 Core #5 from the anode butts study in Section 2.2, Butt-2 Core #3 was employed in this study. Core #3 was sliced into different sections as shown in Figure 2. Only the most top (T1), middle (M1), and the most bottom (B1) were crushed to fine, intermediate and coarse sizes. Each part of the butt materials, i.e. T1, M1, and B1, was mixed with coke and pitch mixture. Hence four experimental anodes were made from each of T1, M1, or B1, i.e. (1) 100% SCTP-2; (2) 20% PP-1 and 80% SCTP-2; (3) 20% GP-1 and 80% SCTP-2; and (4) 20% WVU-5 and 80% SCTP-2.

3. Results and Discussion

3.1 Binder Pitches Study

In this study, three different alternative pitch sources were investigated, namely gasification pitch (GP-1 and –2), petroleum pitch (PP-1), and coal-extracted pitch (WVU 4 and –5). Each type of pitch was mixed with the standard coal tar pitch (SCTP) at various percentages while maintaining the total pitch content of 22 wt%. Because of a limited amount of SCTP, two samples of SCTP, namely, SCTP-1 and –2, were used. Both SCTPs have a comparable softening point; however, the SCTP-2 has a slightly higher QI and TI than the SCTP-1 as shown in Table 1. Figure 4 to Figure 8 show the apparent and baked densities of the green and baked anodes, %pitch loss and %volume

change of the experimental-scale anodes of the SCTP-1 + GP-1, SCTP-1 + GP-2, SCTP-2 + PP-1, SCTP-2 + WVU-4, and SCTP-2 + WVU-5 mixtures, respectively.

The experimental-scale anodes made from SCTP-1 and -2 gave slightly different green and baked densities, however, the SCTP-1 gave quite lower pitch loss and volume change after baking than the SCTP-2. The higher in pitch loss and volume change after baking of the SCTP-2 might cause by a higher QI in this pitch than the SCTP-1. The higher QI fraction could give rise to the alpha resin fraction in pitch. The alpha resins consist of two subdivisions: the fine spherical materials (typically below 2 μm in diameter) and the mesophase generated by the alpha-resins. The former has favorable properties and gives a better anode because it has a higher carbon to hydrogen ratio (between 3.5 and 4) which causes the pitch not to undergo excessive swelling and the fine particles could fill up the pores. On the other hand, the mesophase is large in the particle size (up to 80 μm) and has a carbon to hydrogen ration between 3.5 to 4. These characteristics inhibit the pitch to fill in the finer pores and also cause a higher swelling. Consequently, a pitch that contains more proportion of the mesophase gives more swelling and a lower apparent density in a baked anode [5]. However, the chemistry of pitches is not in the scope of this study. A further investigation will be needed to understand the causes of these results.

Table 3 A comparison of the properties of green and baked experimental-scale anodes made from SCTP-1 and SCTP-2.

Properties	Experimental Anodes Made from	
	SCTP-1 (QI =13.6%)	SCTP-2 (QI = 15.9%)
Green Apparent Density (g/cm^3)	1.695±0.03	1.719±0.0002
Baked Apparent Density (g/cm^3)	1.589±0.03	1.542±0.003
% Pitch Loss	28.14±4.38	33.8±0.1
% Volume Change	0.03±2.89	3.2±0.2

The results of this section can be divided into two parts: the discussion of the softening point effect and the effect of adding alternative pitches. Since GP and WVU

studied here have two different softening points, i.e. the softening point of GP-1 and WVU-5 is about 110-115°C and it is about 126-130°C for GP-2 and WVU-4 (See Table 1). It is worth discussing the effect of higher softening point pitches here. A comparison between GP-1 and GP-2 and between WVU-4 and WVU-5 shows that the higher softening point pitches give poorer properties to the anodes, i.e. slightly lower green apparent density, significant lower baked apparent density, significant higher pitch loss and higher volume change after baking. Factors that affect the anode properties from different softening point pitches are the mixing temperature and the chemistry of pitch itself. The mixing temperature directly affects the wettability between pitch and coke. However, a comparison between the green apparent densities between Figure 4(a) and Figure 5(a) for GP and between Figure 7(a) and Figure 8(a) for WVU pitches shows that the mixing temperature is only a minor effect to the anode quality. Pitches with higher softening point only gave slightly lower green apparent density anodes than those made from the lower softening point pitches. Both higher softening point GP and WVU pitches gave a significant reduction in baked apparent density as compared to the pitches with lower softening point. These results are due to the higher in pitch loss after baking of these higher softening point pitches. This effect may cause by the chemistry of pitches. The effect of QI is not the reason here since both low and high softening point GP and WVU pitches did not contain a significant amount of QI. Other chemistry of pitches drove these results. Again, it is worth in the future studying the pitch chemistry to develop knowledge of this field.

The effect of adding alternative pitches to the apparent densities of the green and baked laboratory-scale anodes is shown in Figures 4(a), 5(a), 6(a), 7(a), and 8(a) for GP-1, GP-2, PP-1, WVU-4, and WVU-5, respectively. The apparent densities of the green anodes made from a mixture of SCTP and the alternative pitch are quite similar to those when the SCTP was used only. However, this trend does not keep up for the apparent baked densities. The more ratio of the alternative pitch to the SCTP, the more decrease in the apparent densities for all alternative pitches except PP-1. The addition of PP-1 gives an improvement in apparent densities for both green and baked anodes (Figure 6(a)). The main factor for the reduction in baked density is due to the increase in loss of binder

during baking as shown in Figures 4(b), 5(b), 6(b), 7(b) and 8(b). The pitch loss is defined as a reduction in anode weights before and after baking over the initial pitch content (22%) since the weight loss of the coke material can be neglected. The addition of GP and WVU to the SCTP tends to give higher pitch loss than the PP. Also, for all SCTP + alternative pitch studied here, the addition of the alternative pitch more likely gives a lower volume change of the baked anodes as compared to the baked anodes with SCTP only as shown in Figures 4(c), 5(c), 6(c), 7(c), and 8(c).

The reason of the high loss of pitch content in the anodes with higher alternative pitch concentration may result from the lack of QI as well as the difference in molecular composition. The QI plays a very important role in how pitches perform excellent binder functions, i.e. wetting and penetrating petroleum coke particles during mixing and forming, and bridging between pitch-coke particles during baking [4]. Although the importance of QI is well established, the optimum amount of QI in binder pitch is still not clear [4]. Because pure alternative pitches give comparable or higher green apparent density, it can be hypothesized that these pitches wet and penetrate petroleum coke well but they lack of a capability to prevent pitch from escaping the inter- and intra-pores. However, these alternative pitches need to be optimized in terms of pitch loss prior to commercial interest.

Of all pitch mixtures studied here, the addition of an alternative pitch shows quite similar trends, i.e. SCTP gives a lower pitch loss and higher volume change compared to the pure alternative pitches. Among all three alternative pitches, the addition of WVU and GP shows poorer properties of the anodes among all three mixtures, i.e. high pitch loss and low baked densities, while the addition of PP-1 shows little impact on the properties of the anodes for most SCTP-PP-1 compositions. The addition of GP and WVU also gives comparable anode properties when the SCTP:WVU/GP ratio is greater than 50:50. The comparison of the properties of the anode made from 20-25% and 50% alternative pitches and those made from 100% SCTP-1 and –2 is shown in Figure 9 and Figure 10 for the apparent density, Figure 11 for the pitch loss and Figure 12 for the volume change after baking.

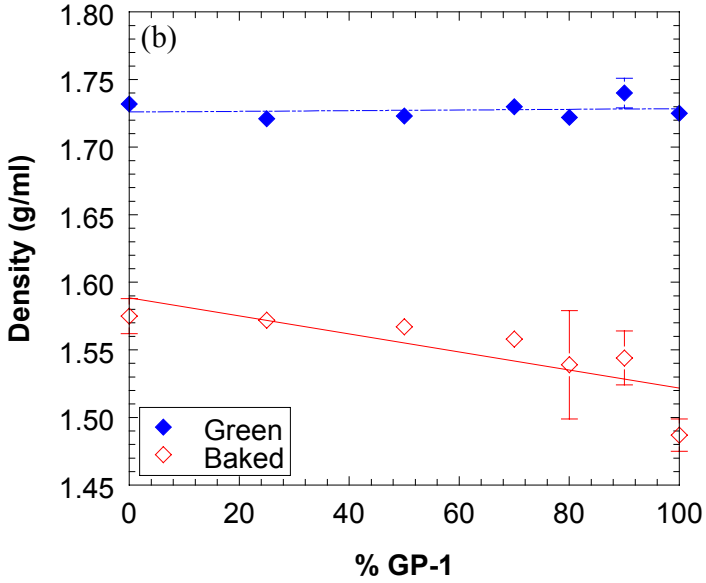

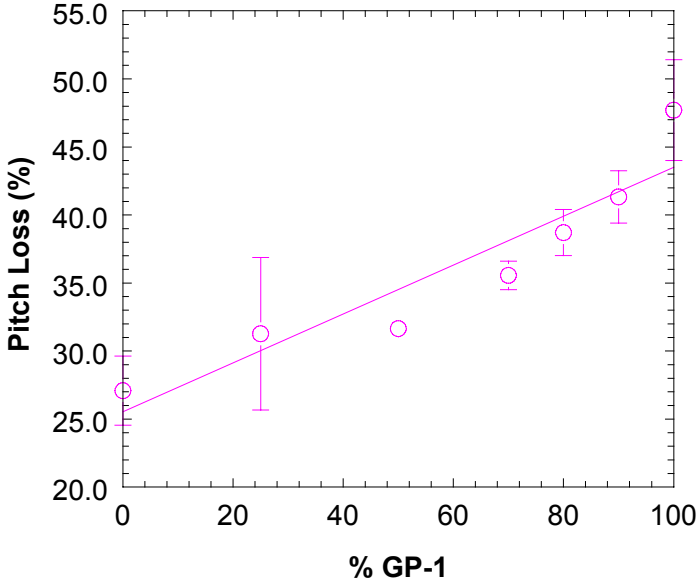

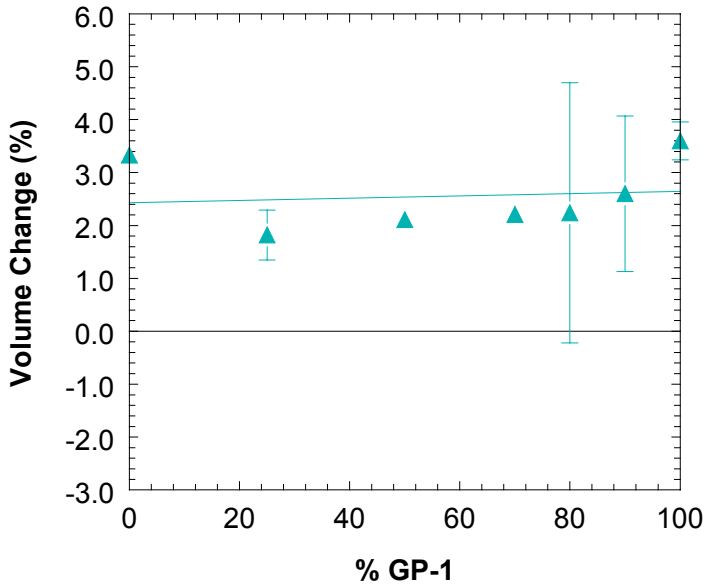

Figure 4 Properties of green and baked anodes prepared by using different pitches compositions varying from 0% GP-1 (or 100% SCTP-1) to 100% GP-1 (or 0% SCTP-1): (a) Apparent densities of green and baked anodes; (b) Percentages of pitch loss after baked; (c) Percentages of volume change after baked. The error bars show the standard deviations of each experimental set. The dashed lines show the linear relationship of the mixtures

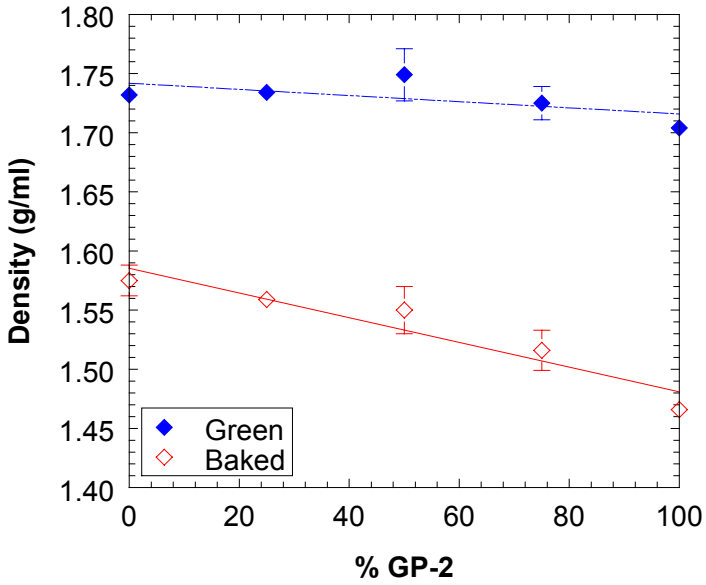

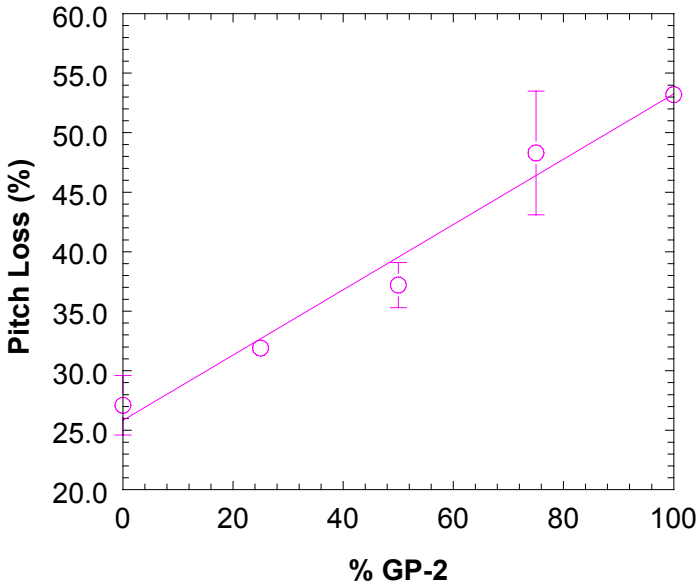

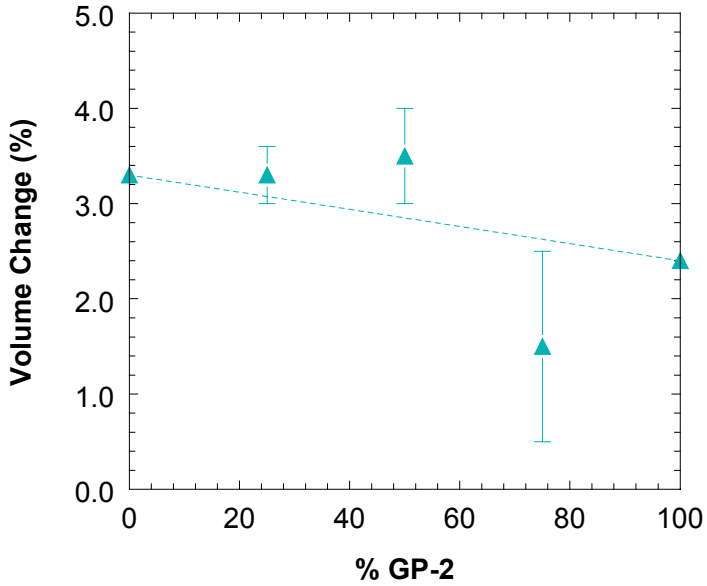

Figure 5 Properties of green and baked anodes prepared by using different pitches compositions varying from 0% GP-2 (or 100% SCTP-1) to 100% GP-2 (or 0% SCTP-1): (a) Apparent densities of green and baked anodes; (b) Percentages of pitch loss after baked; (c) Percentages of volume change after baked. The error bars show the standard deviations of each experimental set. The dashed lines show the linear relationship of the mixtures

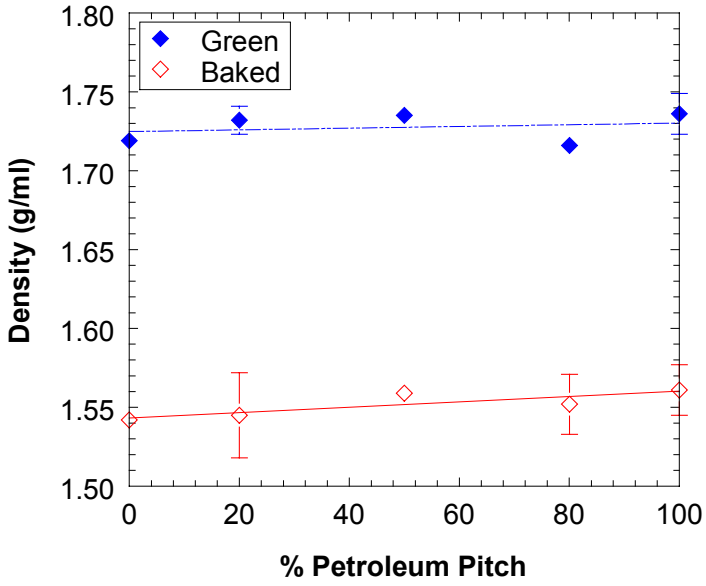

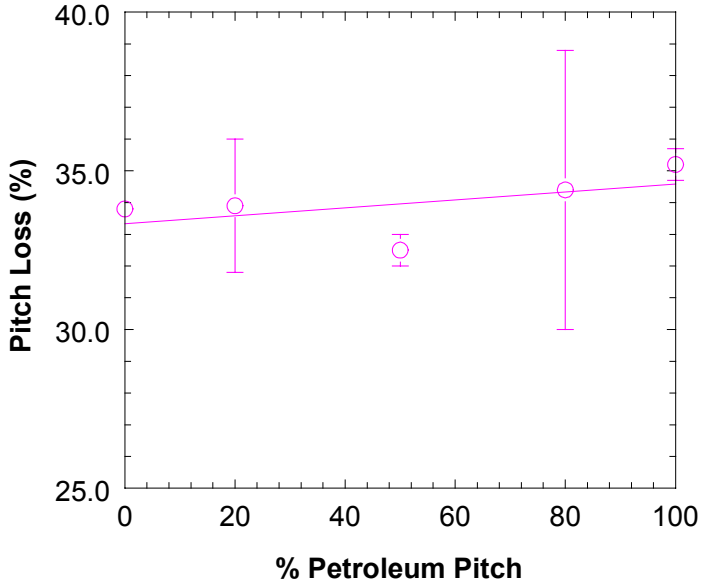

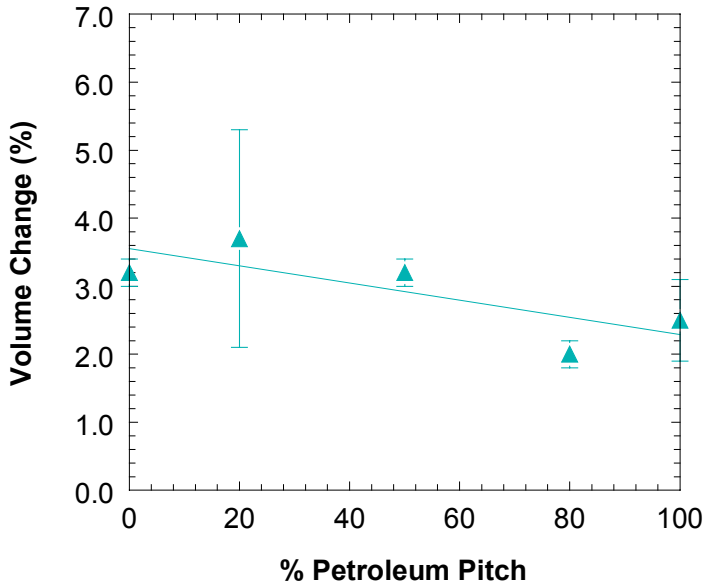

Figure 6 Properties of green and baked anodes prepared by using different pitches compositions varying from 0% PP-1 (or 100% SCTP-2) to 100% PP-1 (or 0% SCTP-2): (a) Apparent densities of green and baked anodes; (b) Percentages of pitch loss after baked; (c) Percentages of volume change after baked. The error bars show the standard deviations of each experimental set. The dashed lines show the linear relationship of the mixtures.

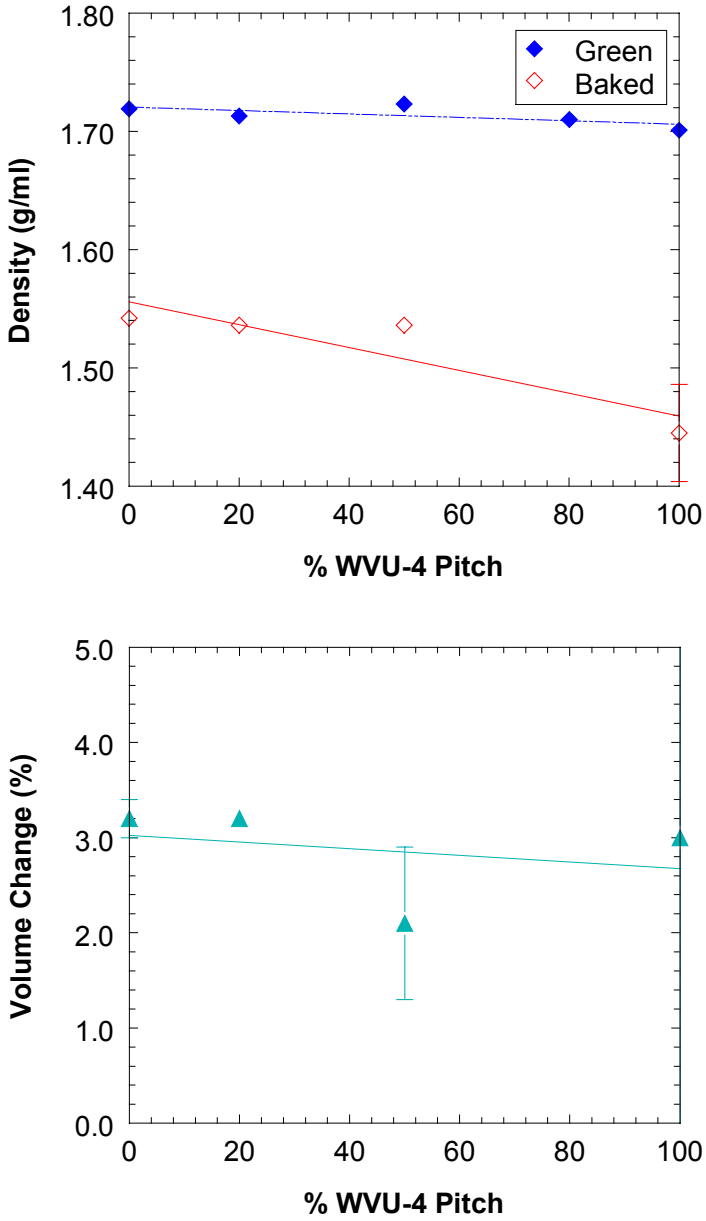

Figure 7 Properties of green and baked anodes prepared by using different pitches compositions varying from 0% WVU-4 (or 100% SCTP-2) to 100% WVU-4 (or 0% SCTP-2): (a) Apparent densities of green and baked anodes; (b) Percentages of pitch loss after baked; (c) Percentages of volume change after baked. The error bars show the standard deviations of each experimental set. The dashed lines show the linear relationship of the mixtures.

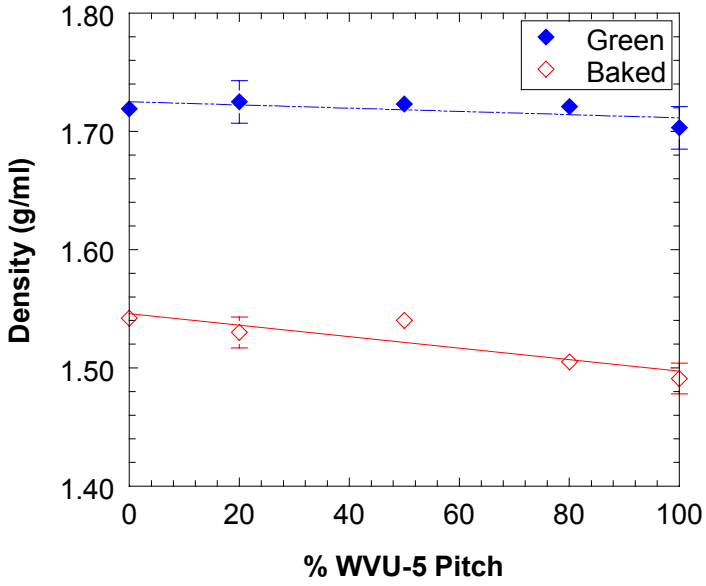

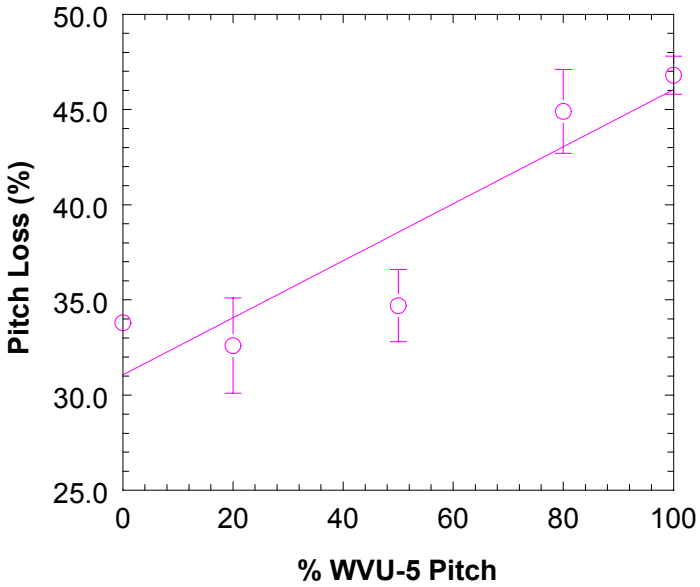

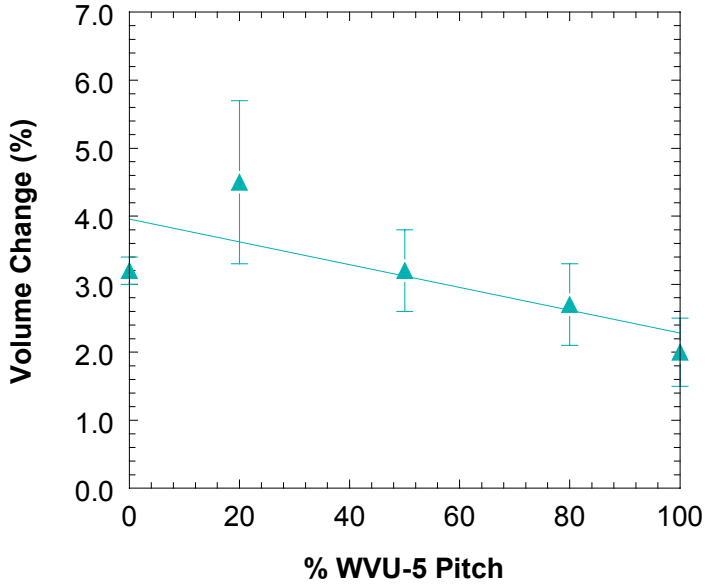

Figure 8 Properties of green and baked anodes prepared by using different pitches compositions varying from 0% WVU-5 (or 100% SCTP-1) to 100% WVU-5 (or 0% SCTP-1): (a) Apparent densities of green and baked anodes; (b) Percentages of pitch loss after baked; (c) Percentages of volume change after baked. The error bars show the standard deviations of each experimental set. The dashed lines show the linear relationship of the mixtures.

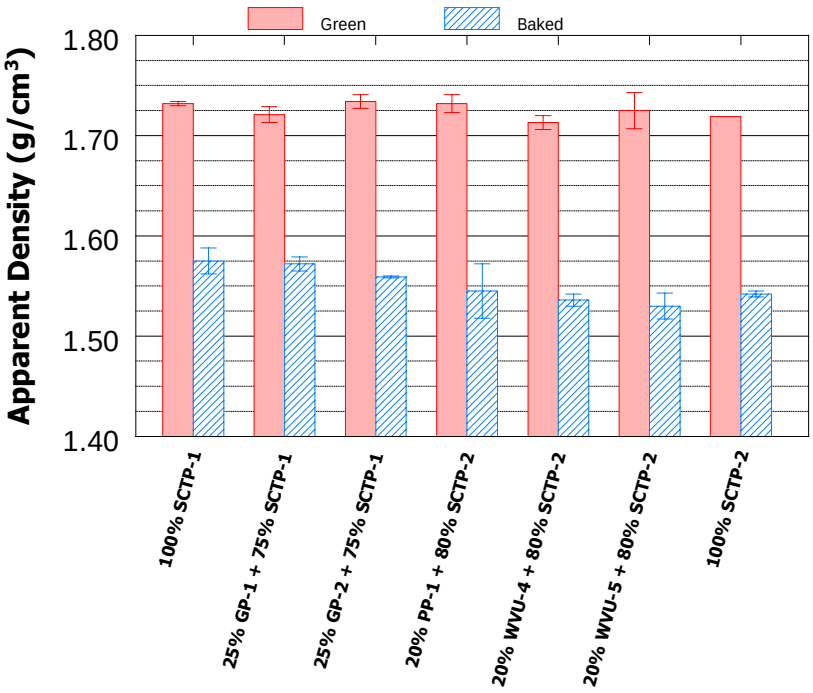

Figure 9 Green and baked apparent densities of the experimental-scale anodes made from 20-25 %wt alternative pitch (GP-1, -2, PP-1, WVU-4, and –5) as compared to the anodes made from 100% SCTP-1 and –2.

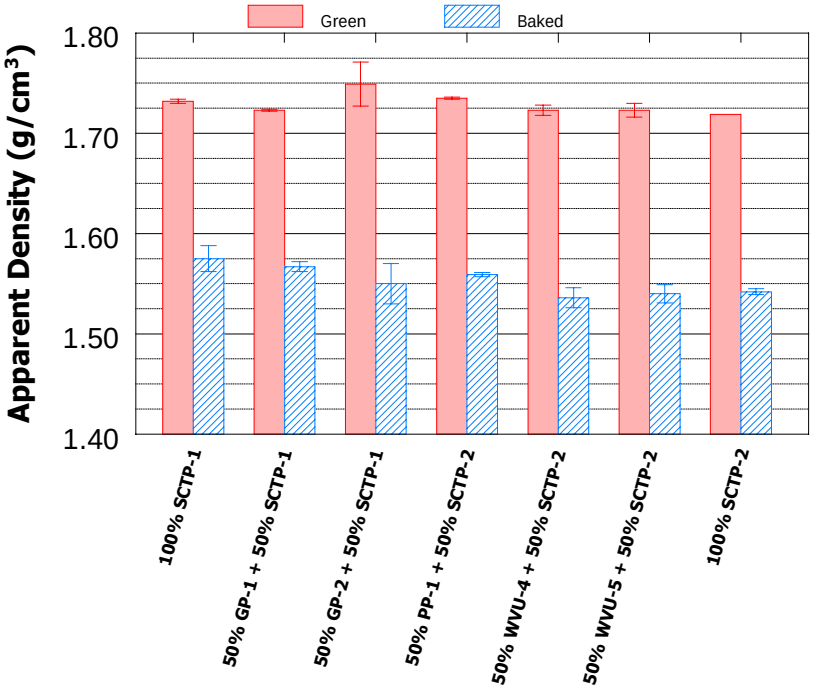

Figure 10 Green and baked apparent densities of the experimental-scale anodes made from 50 %wt alternative pitch (GP-1, -2, PP-1, WVU-4, and –5) as compared to the anodes made from 100% SCTP-1 and –2.

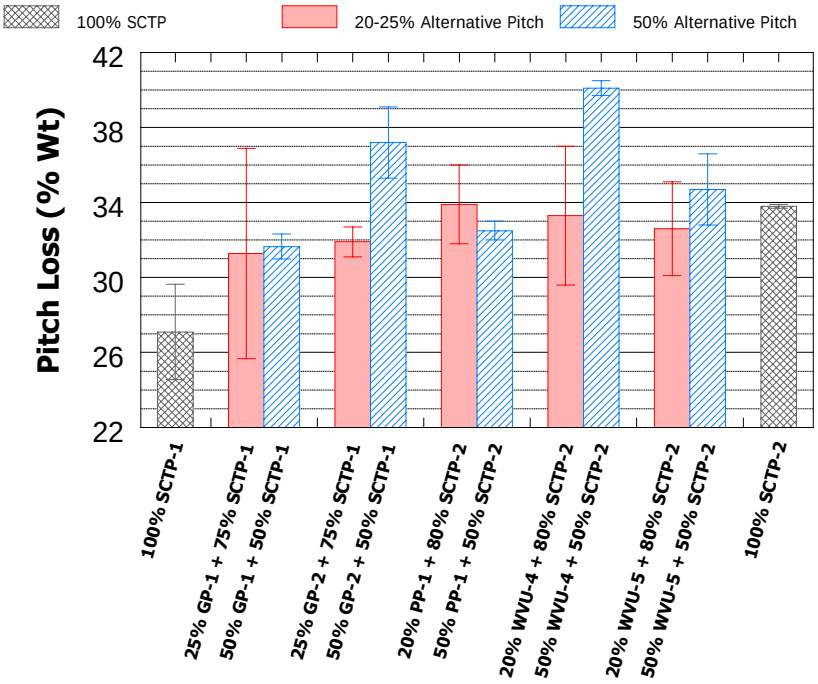

Figure 11 Percentages of pitch loss of the experimental-scale anodes made from 20-25 %wt and 50 %wt alternative pitch (GP-1, -2, PP-1, WVU-4, and –5) as compared to the anodes made from 100% SCTP-1 and –2.

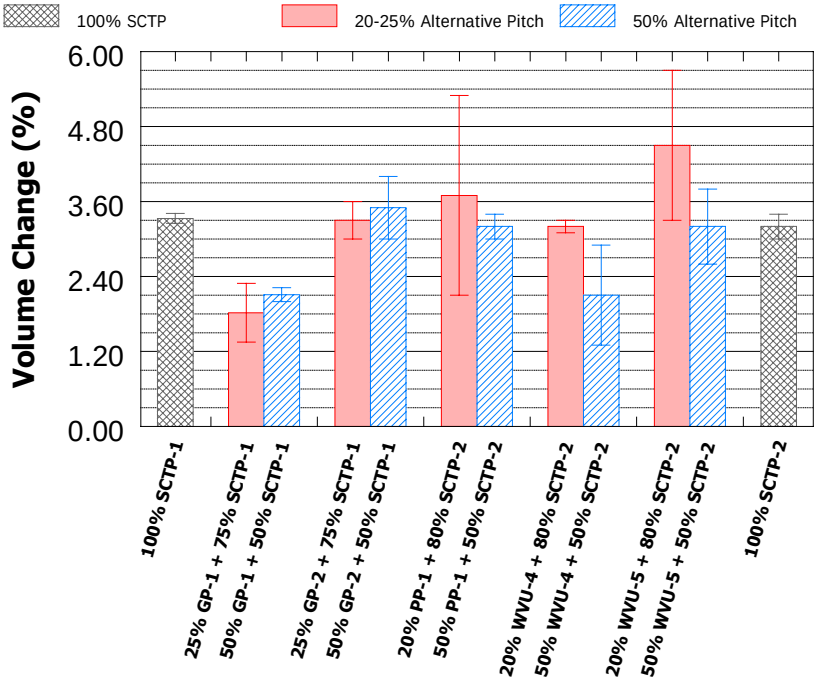

Figure 12 Volume changes of the experimental-scale anodes made from 20-25 %wt and 50 %wt alternative pitch (GP-1, -2, PP-1, WVU-4, and –5) as compared to the anodes made from 100% SCTP-1 and –2.

3.2 Anode Butts Study

3.2.1 X-Ray CT and Physical Properties Results

The X-Ray CT of all the anode butt samples received from the Alcoa Co., Ltd. was shown in our previous report [8]. In this final report, we focus on the physical and chemical properties of the anode butts as a function of distance from the airburn side. Only the Core #5 of Butt-1, -2, and -4 were studied. The tested properties are apparent density, absolute density, specific pore volume, chemical analyses, ash content, and air and CO_2 reactivities. The chemical analyses were performed by the Alcoa Co., Ltd using the ICP technique. The other tests were performed by the Energy Institute, PSU.

Three radial CT slices—the airburn end, middle, and electrolytic end—of Butt-1, and Butt-4 samples, and an axial slice of Butt-2 sample are shown in Figure 13(a), Figure 14(a), and Figure 15(a), respectively. The variation in density and rough heterogeneities are seen throughout the sample. A brighter color at the electrolytic end shows a higher density of the carbon material compared to a darker color at the rest of the core. This indicates a densification of the structure of the carbon that has been in contact with the electrolytic bath. A slightly lighter color at the airburn end of the anode butt shows a higher density of the carbon material that has experienced the air burn-off. The black spots indicate that various sizes of pores are distributed throughout the butt samples.

The results from the CT scanning agree quite well with the absolute density as shown as a function of distance from the airburn side for all three butts (Figure 13 (b) for Butt-1, Figure 14(b) for Butt-2, and Figure 15(b) for Butt-4). All anode butts tend to follow the same patterns in terms of physical properties. The absolute densities are higher at both ends and are quite uniform at the middle, while the apparent densities are quite lower at both ends and perform uniformly at the center. As a result, the calculated specific pore volumes, as calculated by Equation (1), are higher at both ends and quite uniform at the middle of the anode butt. From these results, the CT observation is an effective tool to non-destructively analyze the physical properties of an object. However, the axial axis scanning shown here does not properly relate the pore distribution to the

apparent density and the specific pore volume. This relationship is clearly explained in Figure 13(a) and Figure 15(a) where Butt-1 and –4, respectively, were scanned perpendicular to the axial axis. Three CT slices are shown: airburn side, middle, and electrolytic side. The airburn side (left) shows high porosity (dark spots) which the electrolytic end (right) shows high density and low porosity. The CT observation are confirmed by the apparent and absolute densities measurements and the calculation of the specific pore volumes as shown in Figures (b), (c), and (d), respectively, of Figure 13 for Butt-1 and Figure 15 for Butt-4.

All Butt-1, -2 and -4 gave similar results in terms of physical properties throughout the cores, where both anode butts exhibited a major change in densities and pore volume at a distance about 20 millimeters from both airburn and electrolytic ends. The apparent density is quite uniform at the center and decreases toward both airburn and electrolytic ends. The absolute density also exhibits quite uniformly at the center, and increases toward both ends, however. This contradiction between the apparent and absolute densities is seen by an increase in specific pore volume from uniform values at the center to higher values at both ends. The results obtained in this study were similar to those obtained by Cutshall and Bullough [9] who observed a decrease in apparent density and an increase in porosity from the center of the core to the electrolytic surface. The high density sites associated with the large porosity at both ends indicates the connection of these properties to the reactions occurred at the airburn and the electrolytic ends.

Butt-4 shows slightly lower apparent and absolute densities than Butt-1 and -2 since Butt-4 did not contain recycled butt material. Butt-4 also shows a significantly higher specific pore volume at the airburn side and a lower specific pore volume at the electrolytic side, indicating a high reactivity with air from the anode butt. These results indicate that Butt-4 has a higher reactivity with CO_2 than the anode butt which originally contained recycled butt material. The observation discussed here confirmed previous results that sodium content greatly promotes CO_2 reactivity and may be assigned to variations in anode consumption rates [10, 11].

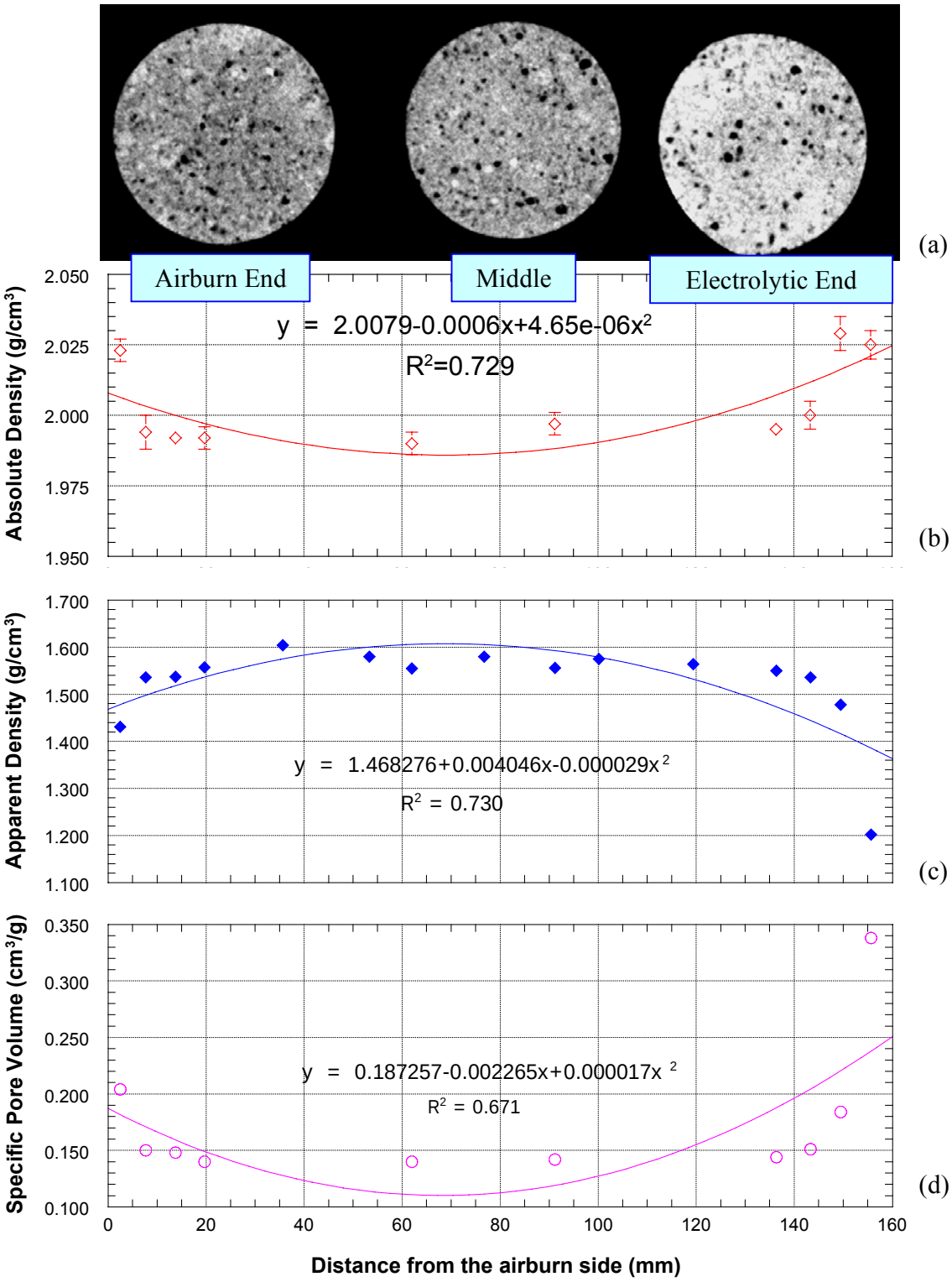

Figure 13 (a) Radial scanning of the X-Ray CT with the same intensity color maps, (b) absolute density (◇), (c) apparent density (◆), and (d) specific pore volume (○) of the Butt-1 Core #5 at different distance from the airburn side. The solid lines show the polynomial relationship of these properties with the distance from the airburn side.

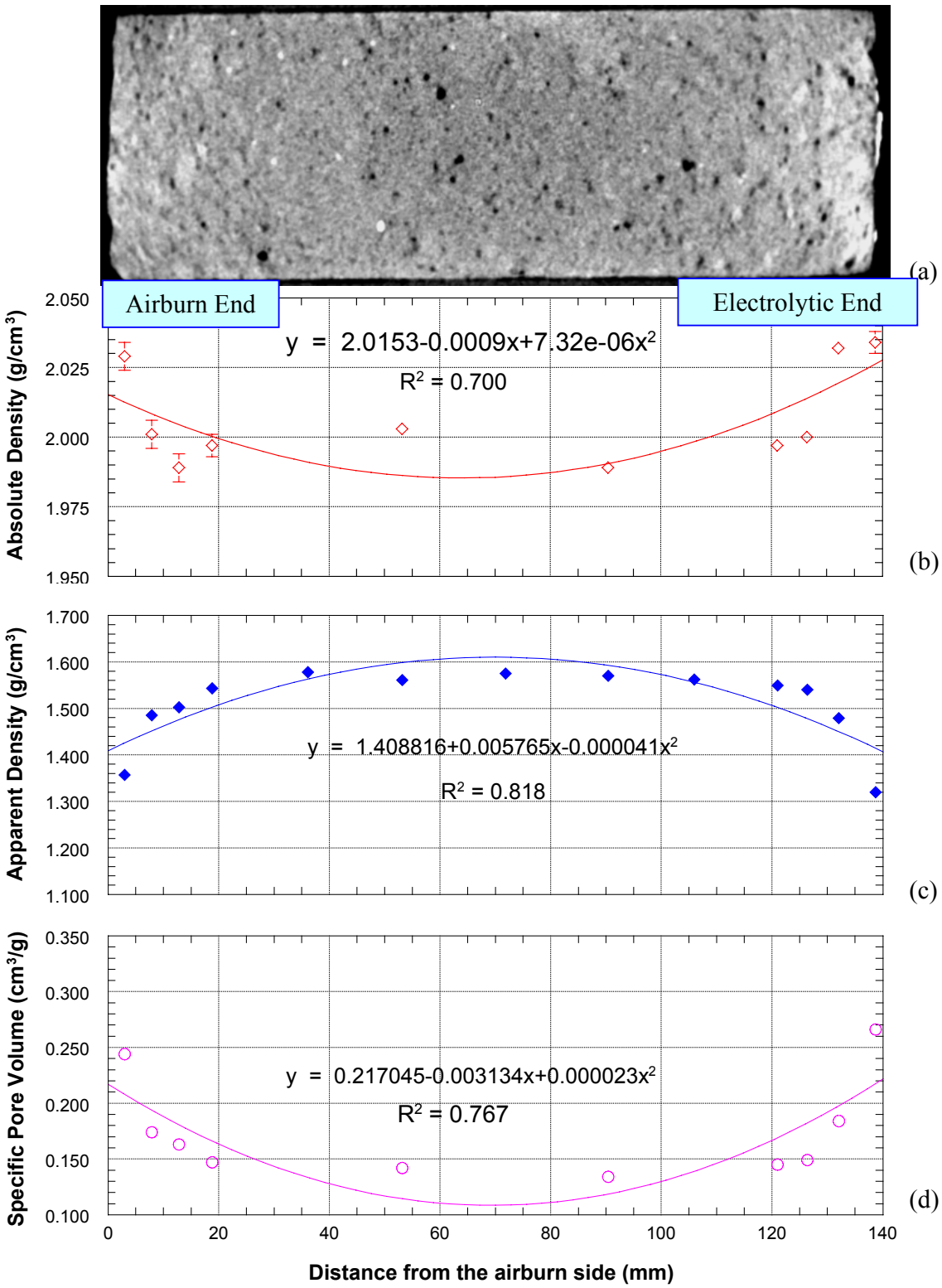

Figure 14 (a) Axial scanning of the X-Ray CT with the same intensity color maps, (b) absolute density (◇), (c) apparent density (◆), and (d) specific pore volume (○) of the Butt-2 Core #5 at different distance from the airburn side. The solid lines show the polynomial relationship of these properties with the distance from the airburn side.

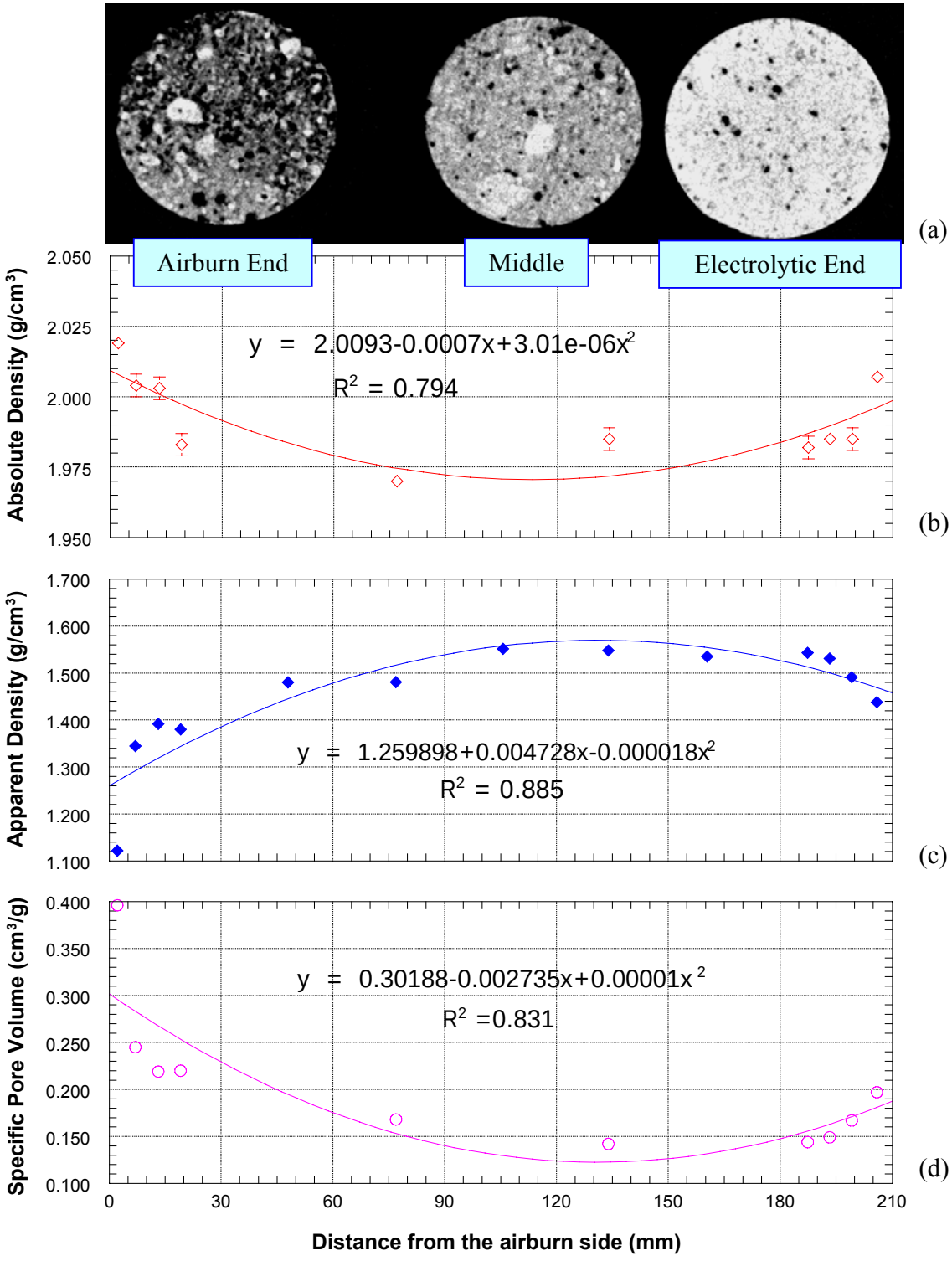

Figure 15 (a) Radial scanning of the X-Ray CT with the same intensity color maps, (b) absolute density (◇), (c) apparent density (◆), and (d) specific pore volume (○) of the Butt-4 Core #5 at different distance from the airburn side. The solid lines show the polynomial relationship of these properties with the distance from the airburn side.

3.2.2 Chemical Analyses

The chemical analyses of Butt-1 and -2 were performed using ICP technique and Butt-4 by the ICP/MS technique by Alcoa Co., Ltd. Figure 16, Figure 17(a), and Figure 18 show the ICP results of Butt-1, -2, and -4, respectively. All anode butts exhibit similar results. As shown by a comparison Figure 19, the most top butt material (T1) contains more inorganic contents than the butt material from the middle and the most bottom (B1). Only aluminum, sodium and fluoride were analyzed in Butt-1, and -2. Fluoride content appears to be the highest concentration and follows by sodium and aluminum, respectively, for both anode butts. Various types of inorganic matters except fluoride were analyzed in Butt-4 as shown in Figure 18. Among T1, M3 and B1 samples, T1 contains the highest concentration for most inorganic contents presented here. Iron content in this sample is very high especially in the T1 sample, i.e. 2700 ppm. B1 and M3 also contain rather high iron content, i.e. 420 and 340 ppm, respectively. Other major inorganic contents are sulfur, sodium, aluminum and calcium. It has been shown that the presence of inorganic contents can enhance the reactivity of chars under oxidation [12]. Walker et al. [12] summarized that the reactivity of chars (or cokes) made from lignites in CO_2 and air followed same order as followed: Na > K > Ca. Iron appeared to be less reactive than the raw chars. Since T1 contains rather higher sodium and calcium than M3 and B1, it can be presumed that T1 would exhibit a fairly higher reactivity in both CO_2 and air than the rest of the butt samples. Although the GC/MS was not performed in Butts -1 and -2, the amount of inorganic contents in these two butts should not be very different than what have been shown in Butt-4.

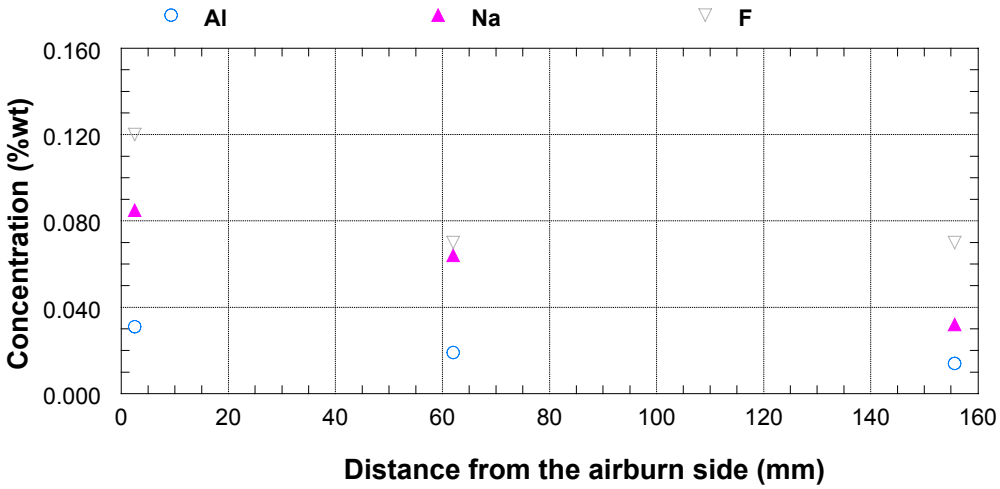

Figure 16 Concentration of aluminum, sodium and fluoride at different positions from the airburn side of Butt-1 Core #5.

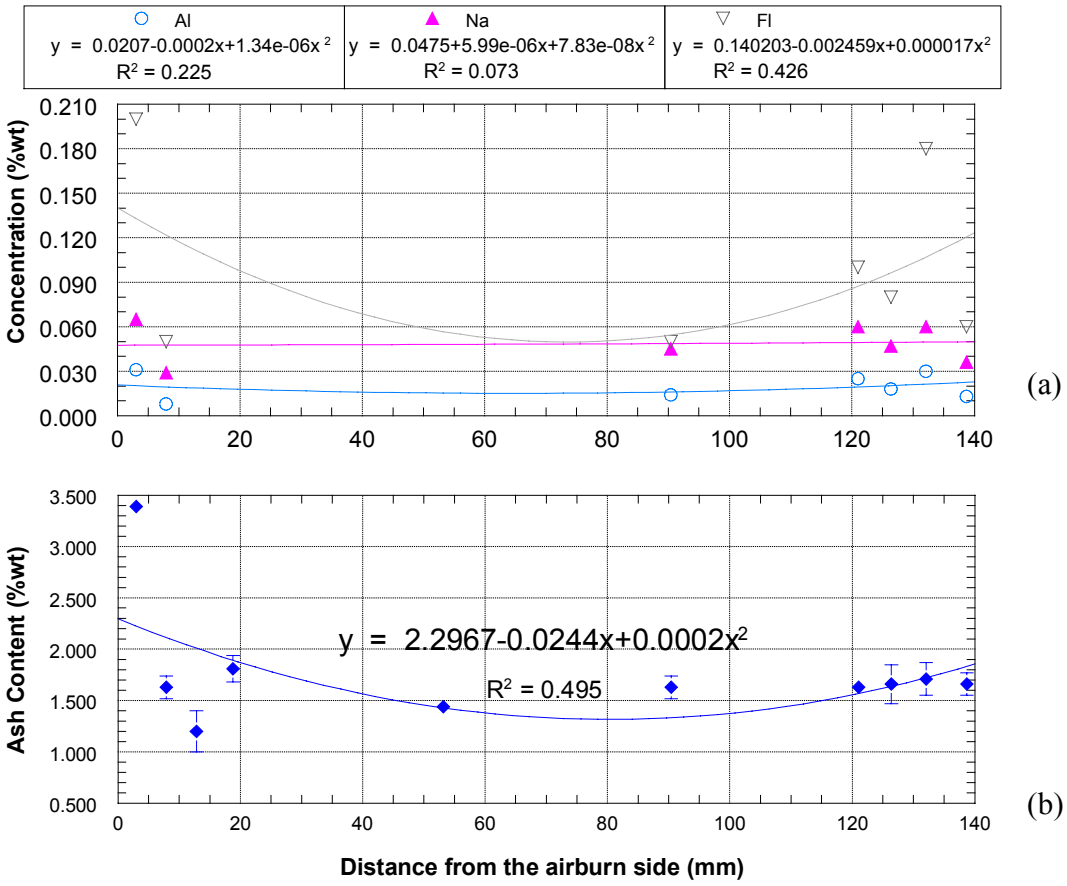

Figure 17 Properties of the Butt-2 Core #5 as a funcition of the airburn side: (a) Concentration of aluminum, sodium and fluoride. (b) Ash content. The solid lines show the polynomial relationship of these properties with the distance from the airburn side.

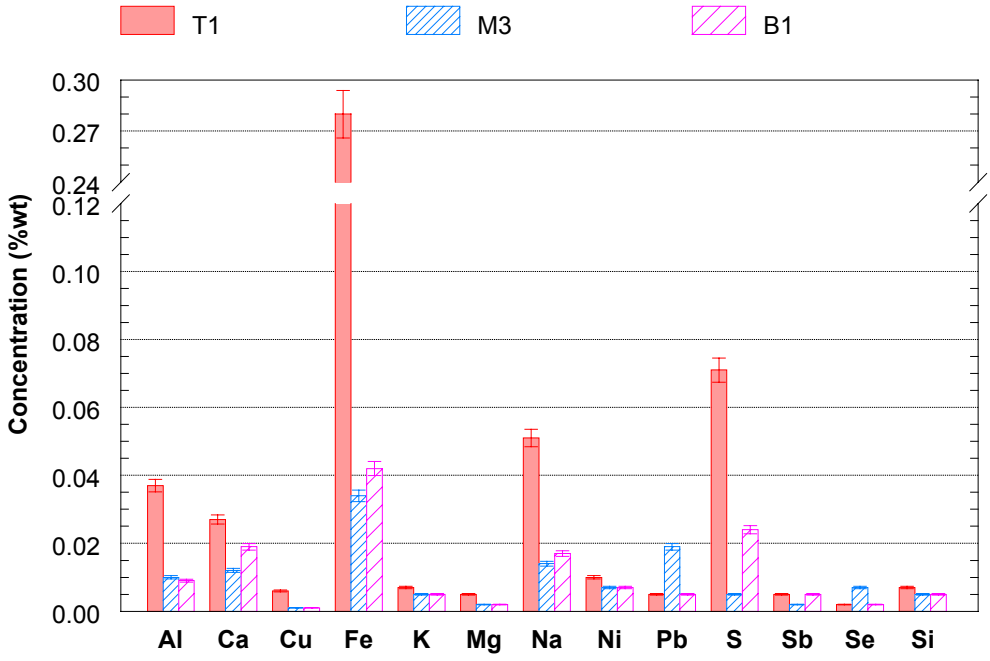

Figure 18 ICP/MS analyses of Butt-4

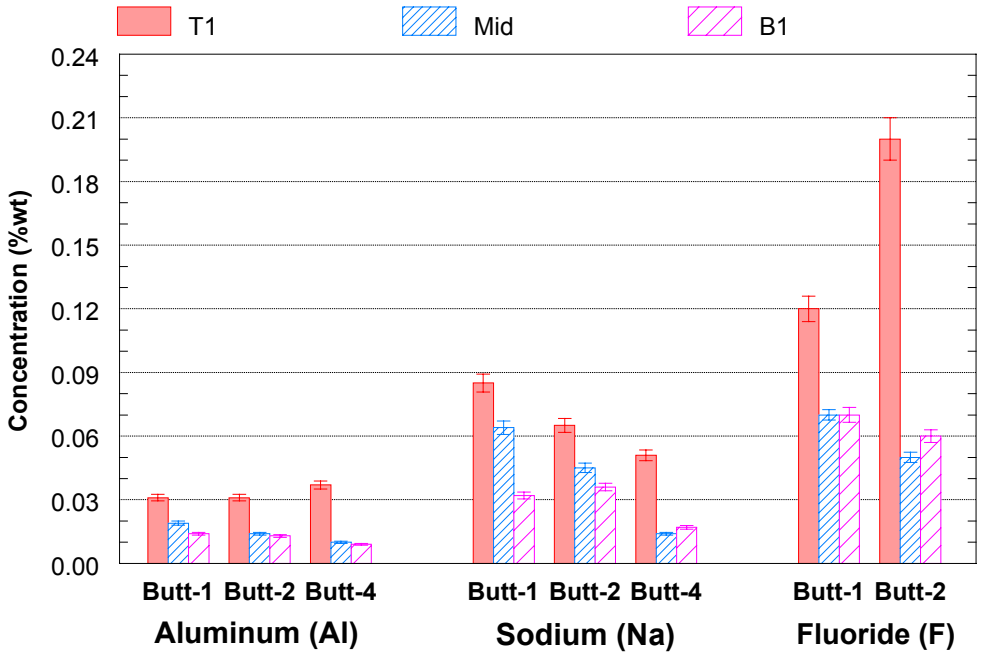

Figure 19 Comparison of aluminum, sodium and fluoride concentrations of the top, middle, and bottom part of Butt-1, -2, and -4.

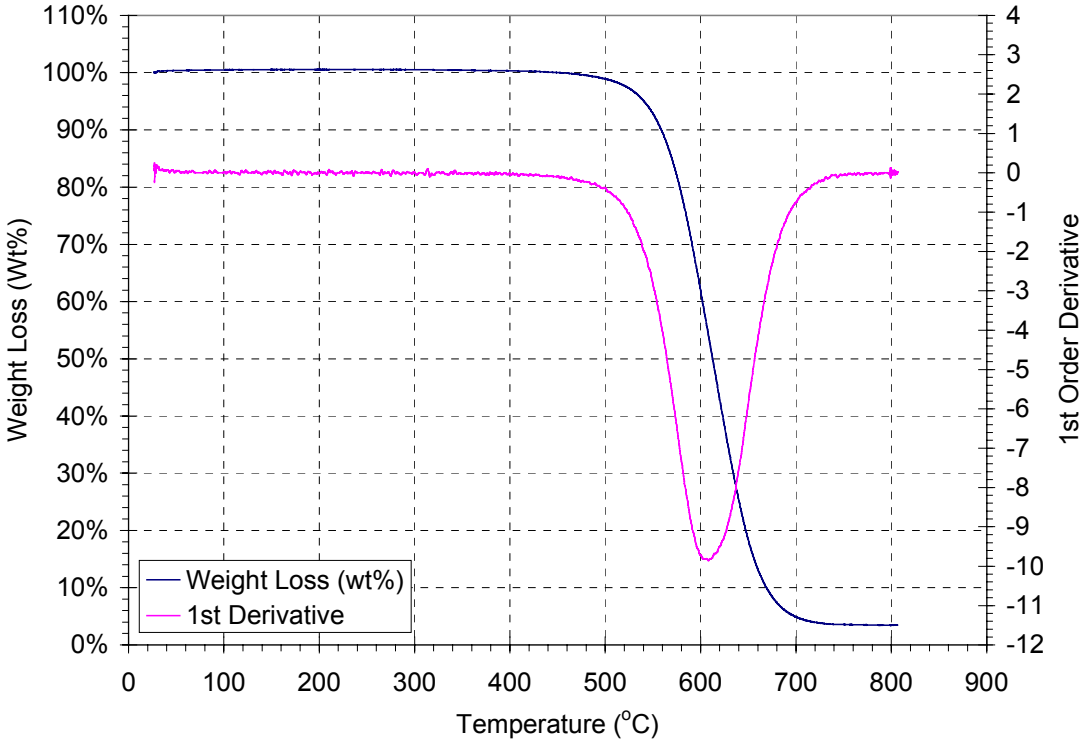

Figure 20 Typical TGA plots.

3.2.3 Thermal Analyses: Non-Isothermal Air Reactivity

Typical TGA plots are shown in Figure 20. The weight loss plot shows a slight weight gain at the temperature close to 100°C due to the oxygen adsorption to the carbon surface. At the temperature about 350°C the carbon material starts oxidizing with oxygen and the material weight starts to decrease. The rate of weight loss decreases as the temperature increases until it reaches a maximum rate of weight loss which is shown by the minimum value of the derivative weight loss plot. The rate of weight loss then decreases and diminishes at about 800°C.

The weigh loss and the derivative weight loss plots of samples from Butt-2 Core #5 from the airburn end to the electrolytic end are shown in Figure 21 and Figure 22, respectively. Both weight loss and derivative weight loss indicate a high air reactivity of the most top sample (T1), and a fairly lower reactivity of the samples from the middle

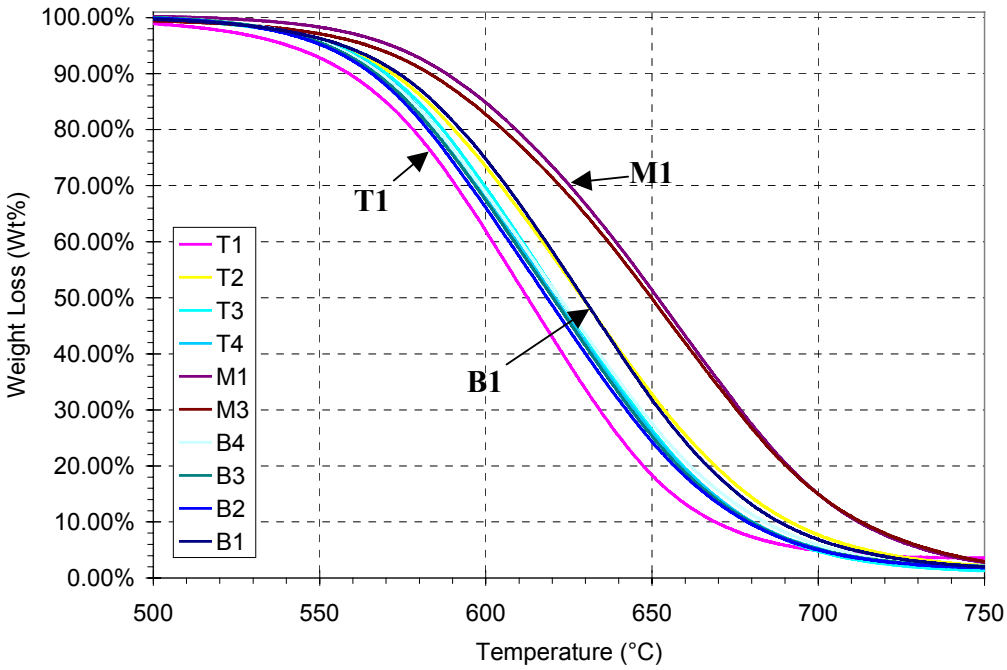

Figure 21 TGA weight loss v.s. temperatures of BUTT-2 Core #5 from top to bottom of the anode butt.

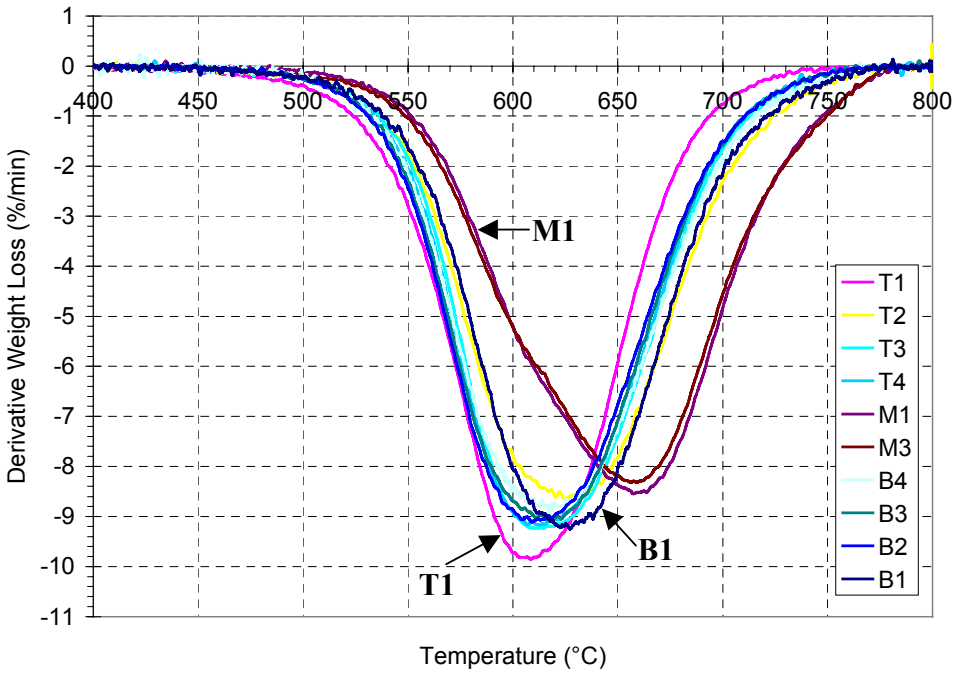

Figure 22 First derivative of weight loss v.s. temperatures of BUTT-2 Core #5 from top to bottom of the anode butt.

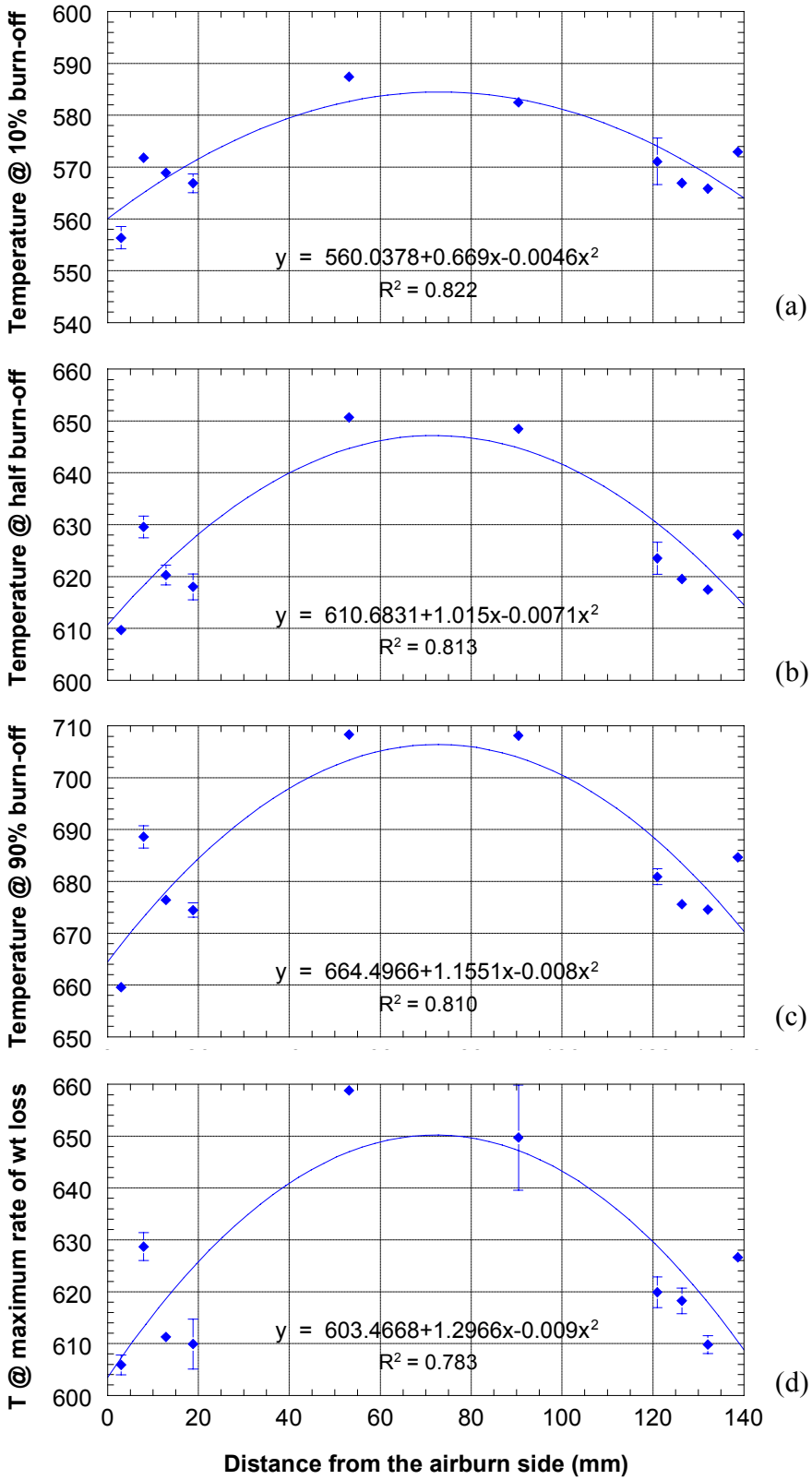

Figure 23 Non-isothermal air reactivity of BUTT-2 Core #5 at different distance from the airburn side: (a) Temperature @ 10% burn-off; (b) Temperature @ 50% burn-off; (c) Temperature @ 90% burn-off; and (d) Temperature @ maximum rate of weight loss. The solid lines show the polynomial relationship of the plots.

part (M1 and M3), whereas the rest are in between. The plots of temperatures at different burn-off (Figure 23) indicate that all samples show the same order of air reactivity for the whole range of air burn-off. These results are in agreement with the chemical analyses. T1 which exhibits the highest air reactivity also contains the highest concentration of inorganic contents. It is of interest to see that B2 (about 7.5 mm from the electrolytic end) shows higher air reactivity than B1, which was in contact with the cryolite in the bath (see Figure 23). This result also coincides with the chemical analyses shown in Figure 17(a) where the concentrations of fluoride, sodium, and aluminum in B2 are higher than those components in B1. Although B1 contains higher pore volume than B2 as shown in Figure 14(d), the porosity effect in this reactivity study can be neglected since the particle sizes in this TGA analysis were controlled, i.e. less than 75 μm (+200 mesh) and most pores were broken apart from the crushing process. Since there are two main factors that affect the air reactivity: the chemical compositions that act as catalysts and the porosity of the anode. As a result, this reactivity study eliminated the mass transfer effect and only the inorganic contents mainly influence the air reactivity.

It came up with a question why B1, which was in contact with the cryolite, contains such lower concentrations of inorganic matters as shown in Figure 17(a), i.e. B1 contains lower concentration of inorganic contents than B2, B3, and B4. This could possibly explained by the concept of carrying over of material from the bottom to the top. During the reactions in the bath, carbon was consumed and CO_2 was produced. As a result, when CO_2 rose up to the top of the anode, the molten inorganic matters would have been carried over from the bottom to a higher level. Since the porosity of the anode close to the working surface is higher, i.e. B1, than the inner part, these inorganic contents were not accumulated here and, instead, passed through the next layer. In contrast, B2, B3 and B4, which contain a fairly lower porosity than B1, had a potential to accumulate these inorganic matters and, hence, resulted in higher reactivity than B1.

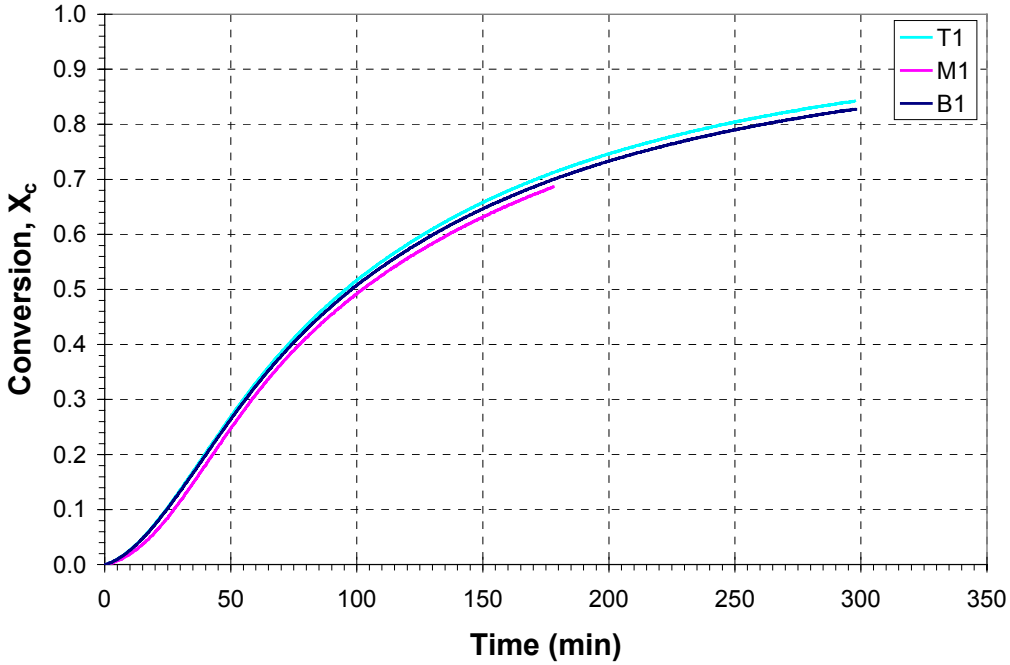

Figure 24 Conversion (daf) v.s. time curves for T1, M1, and B1 of BUTT-2 Core#5 in 1 atm air at 504±1°C.

3.2.4 Thermal Analyses: Isothermal Air Reactivity

There were three samples studied in the isothermal air reactivity at 504±1°C: T1, M1, and B1. These three samples represent the most top, the middle and the most bottom of the anode butt. From Figure 24 T1, M1, and B1 exhibit the same shape of the conversion versus time curves. Since the results of the isothermal air reactivity are not very different for all three samples, other samples were not studied. At the same conversion, T1 was oxidized faster than B1 and M1, respectively. This indicates that T1 is the most reactive and M1 is the least reactive to air. These results are in agreement with the non-isothermal air reactivity discussed in the previous part. Figure 25 and Figure 26 show the rate of conversion versus conversion and the normalized time ($t/t_{X_C=0.5}$), respectively. All three samples exhibit the same trends and magnitudes for the whole range of the x-axes. Hence, at about 500°C it can be said that all anode material has fairly uniform air reactivity throughout the core from the electrolytic to the airburn ends.

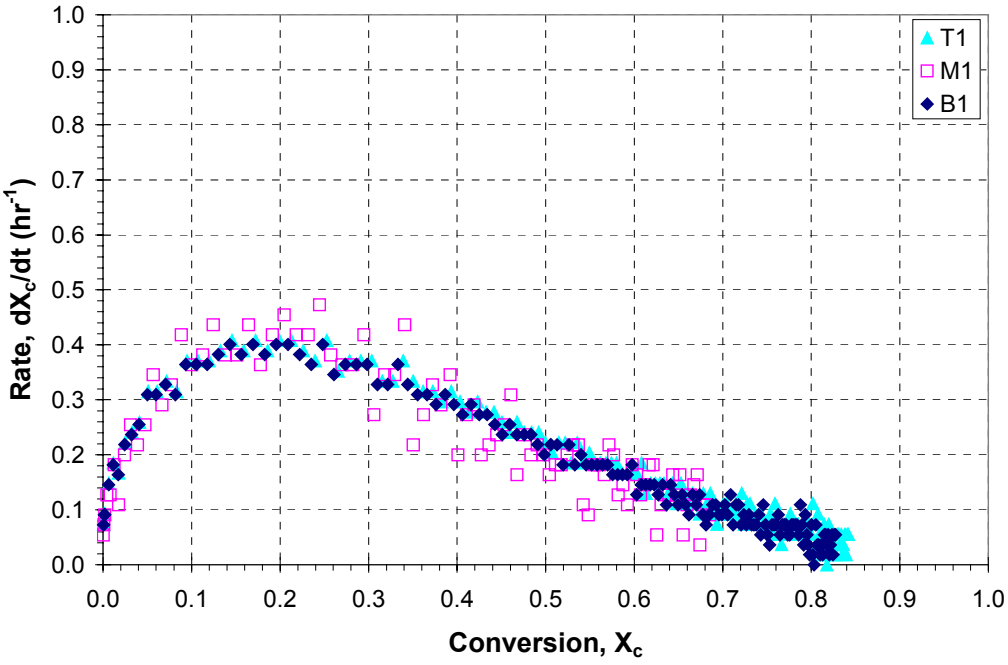

Figure 25 Rate v.s. conversion (daf) curves for T1, M1, and B1 of BUTT-2 Core#5 in 1 atm air at 504±1°C.

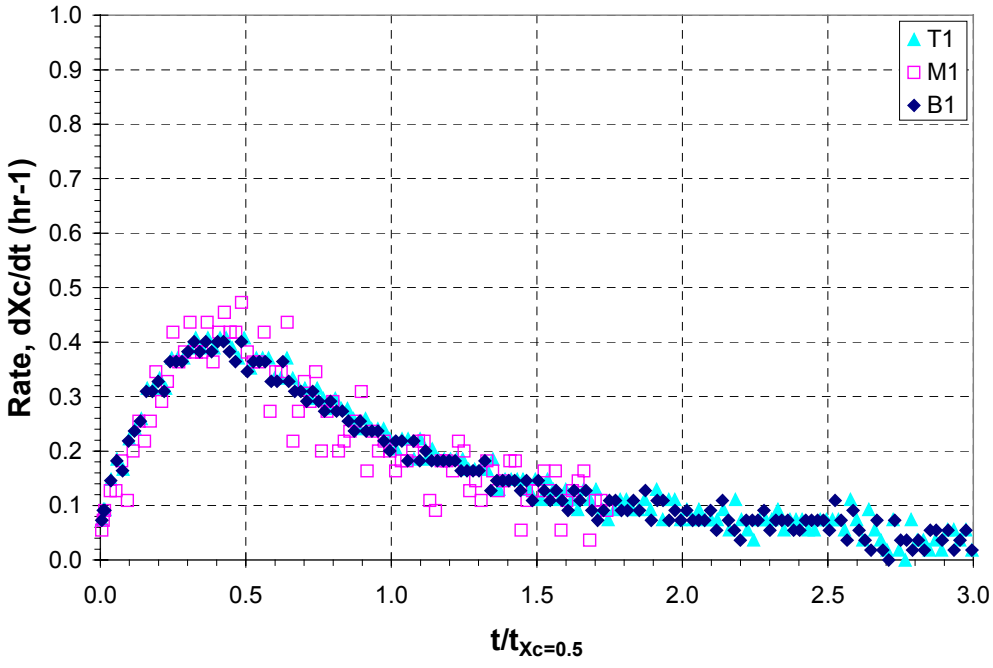

Figure 26 Rate v.s. normalized time curves for T1, M1, and B1 of BUTT-2 Core#5 in 1 atm air at 504±1°C.

3.2.5 Thermal Analyses: Isothermal CO_2 Reactivity

In the CO_2 isothermal reactivity experiment at 976±1°C, five samples were studied: T1, T2, M1, B2 and B1. The variation in CO_2 reactivity is shown in Figure 27. The reactivity of these samples is in the following order: T1 > B2 > T2 > B1 ≈ M1. The order of CO_2 reactivity at 976±1°C shows a very similar result to the non-isothermal air reactivity (see Figure 23 and Figure 27). Since the CO2 reactivity of the inner parts of the butt core approached the results obtained from the middle one (M1), other samples, e.g. B3, B4, T3, T4, etc., were presumably exhibited similar to those of M1 and were not included in this test.

Figure 28 and Figure 29 show the plots of rate versus conversion and normalized time, respectively. It can be seen that the reaction rate of CO_2 oxidation is very high at the initial stage. Especially, T1 is about twice more reactive than the butt material from the middle of the core. The reaction rate later decreases as the conversion increases (or time increases) and the reaction rates of all samples approach toward the middle of the core sample.

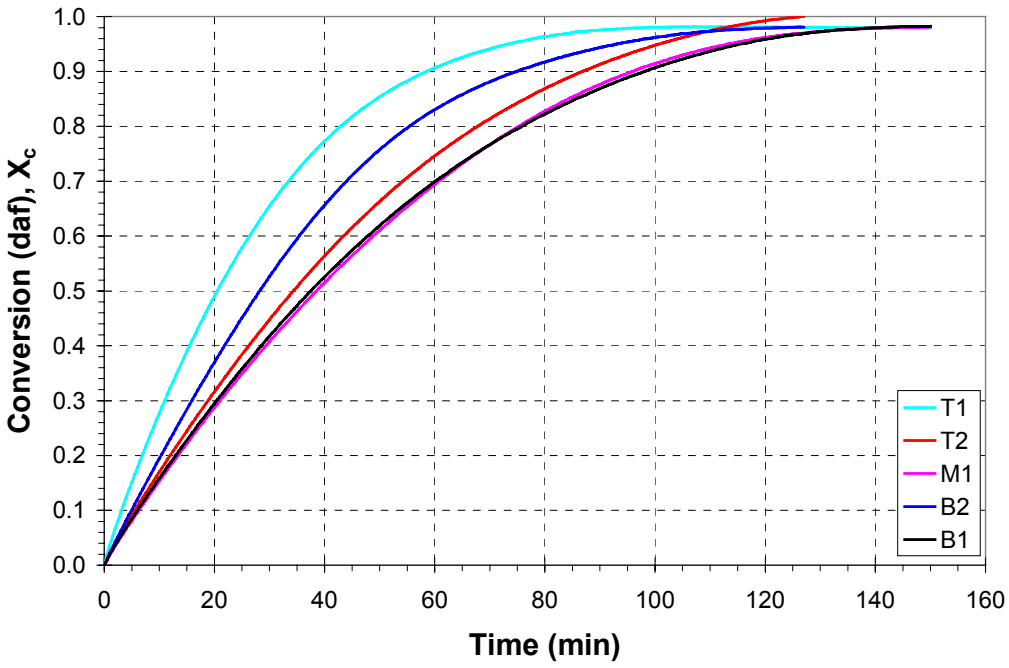

Figure 27 Conversion (daf) v.s. time curves for T1, T2, M1, B2, and B1 of BUTT-2 Core#5 in 1 atm CO_2 at 976±1°C.

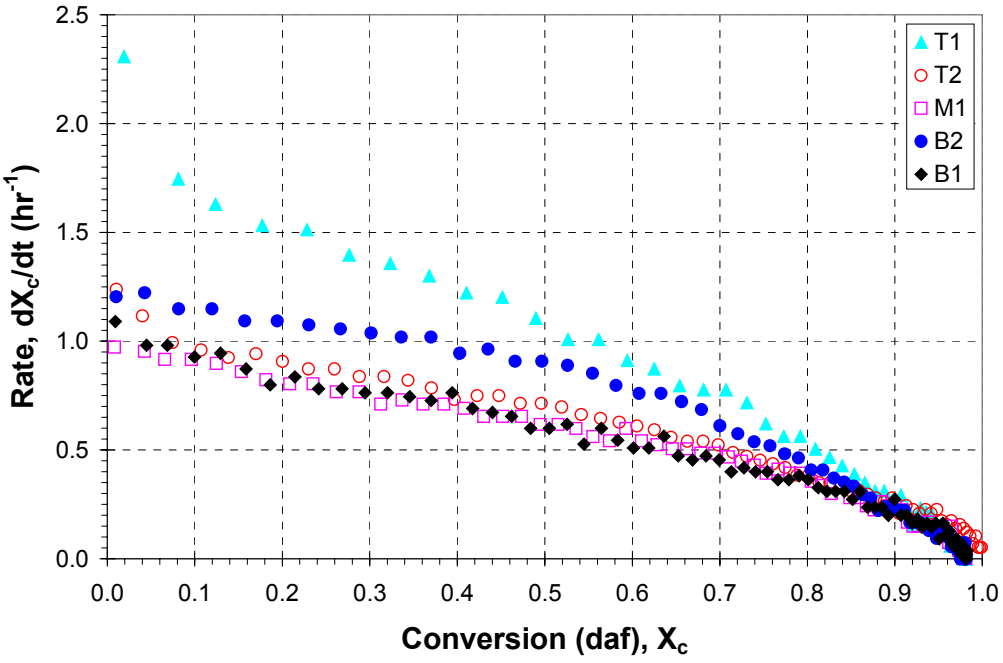

Figure 28 Rate v.s. conversion (daf) curves for T1, T2, M1, B2, and B1 of BUTT-2 Core#5 in 1 atm CO2 at 976±1°C.

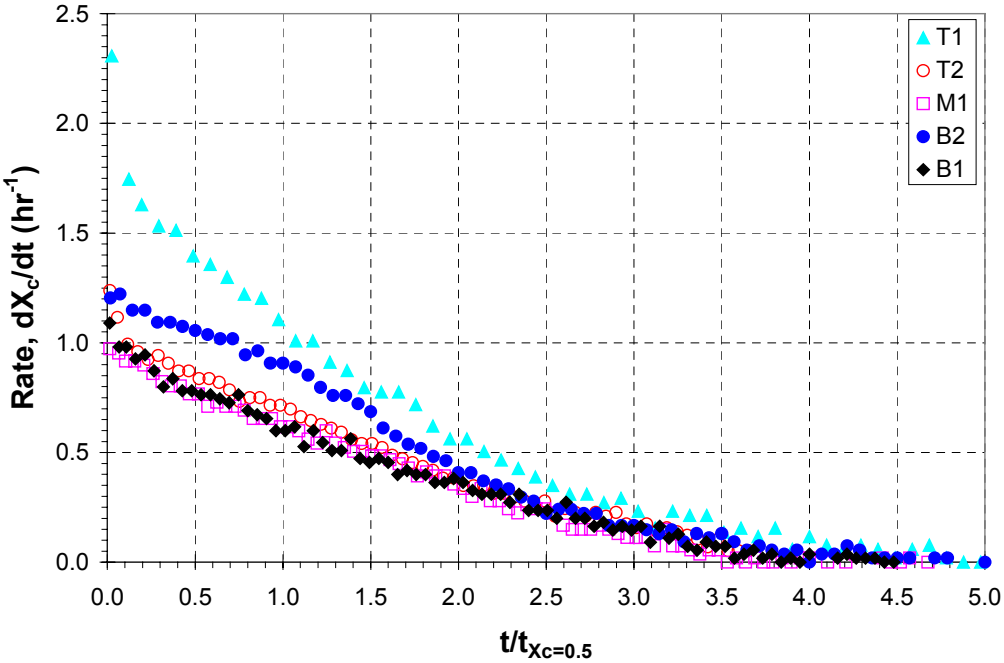

Figure 29 Rate v.s. normalized time curves for T1, T2, M1, B2, and B1 of BUTT-2 Core#5 in 1 atm CO_2 at 976±1°C.

3.2.6 Discussion of Anode Butt Chemistry

Since a lot of anode butts properties were measured, it is of interest to figure out if there is any relationship among them. Figure 30 show plots of inorganic contents (Al, Na and F) versus the apparent and absolute densities, specific pore volume and the ash content. It appears that the apparent and absolute densities and the specific pore volume are related to the inorganic contents as shown in Figures 30(a), (b), and (c), respectively. The ash content appears to have a slight relationship with the inorganic content as shown in Figure 30(d).

The air reactivities as represented by the temperatures at half burn-off were plotted with the Al, Na and F contents as shown in Figures 31(a), (b) and (c), respectively. The differences in the positions of the butt sample, i.e. top, middle and bottom, are also distinguished in these plots. The lower the temperature at half burn-off, the higher the air reactivity the butt material is exhibited. Higher inorganic contents are shown to have higher air reactivities. Hence, these inorganic matters performed as catalysts in the air oxidation. The effect of porosity is also important to the reactivity of a carbon material. The active surfaces, found primarily in micropores in the carbon material, must be well connected to the exterior surface of the particles by the feeder pores (transitional and macropores) [12]. Hence, reactant gas, e.g. air or CO_2, can rapidly diffuse otherwise these active surfaces will not be consumed. The effect of pore volume was added to the inorganic contents as shown in Figures 31(d), (e), and (f) by multiplying the inorganic concentration by the specific pore volume. The reason why the butt materials from the middle of the butt core exhibit significant lower air reactivity than the top and the bottom is clearer here. Not only the inorganic content of the butt materials from the middle butt core is relatively lower than the top and the bottom of the butt core, but the specific pore volume is also lower. These two effects help the air to react with the carbon materials slower in the middle butt core than the airburn and catalytic ends.

The temperature at half burn-ff were also plotted with the ash content, specific pore volume and the absolute density as shown in Figures 32(a), (b) and (c), respectively.

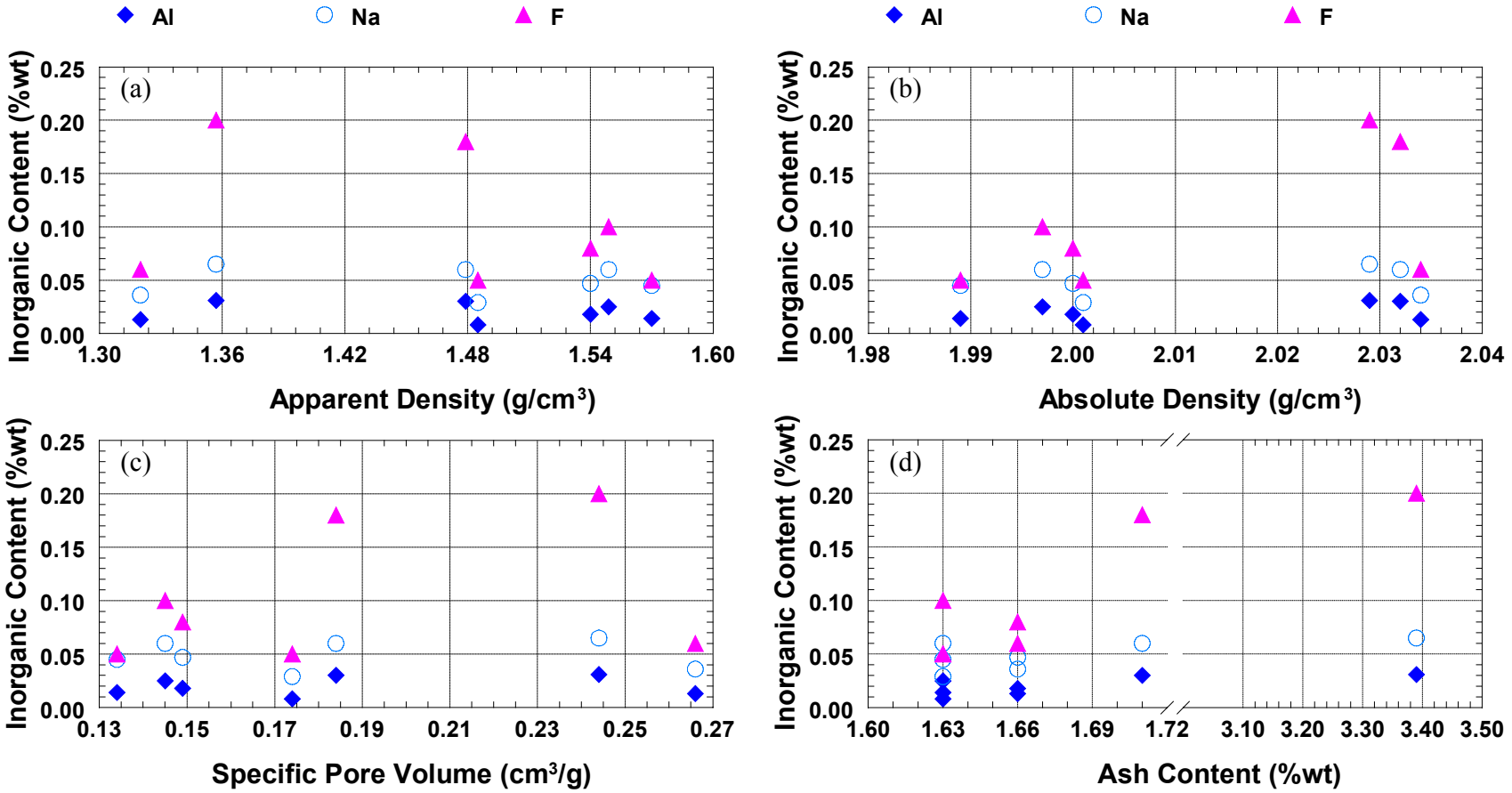

Figure 30 Inorganic contents v.s. (a) Apparent density; (b) Absolute density; (c) Specific pore volume; and (d) Ash content plots of BUTT-2 Core#5.

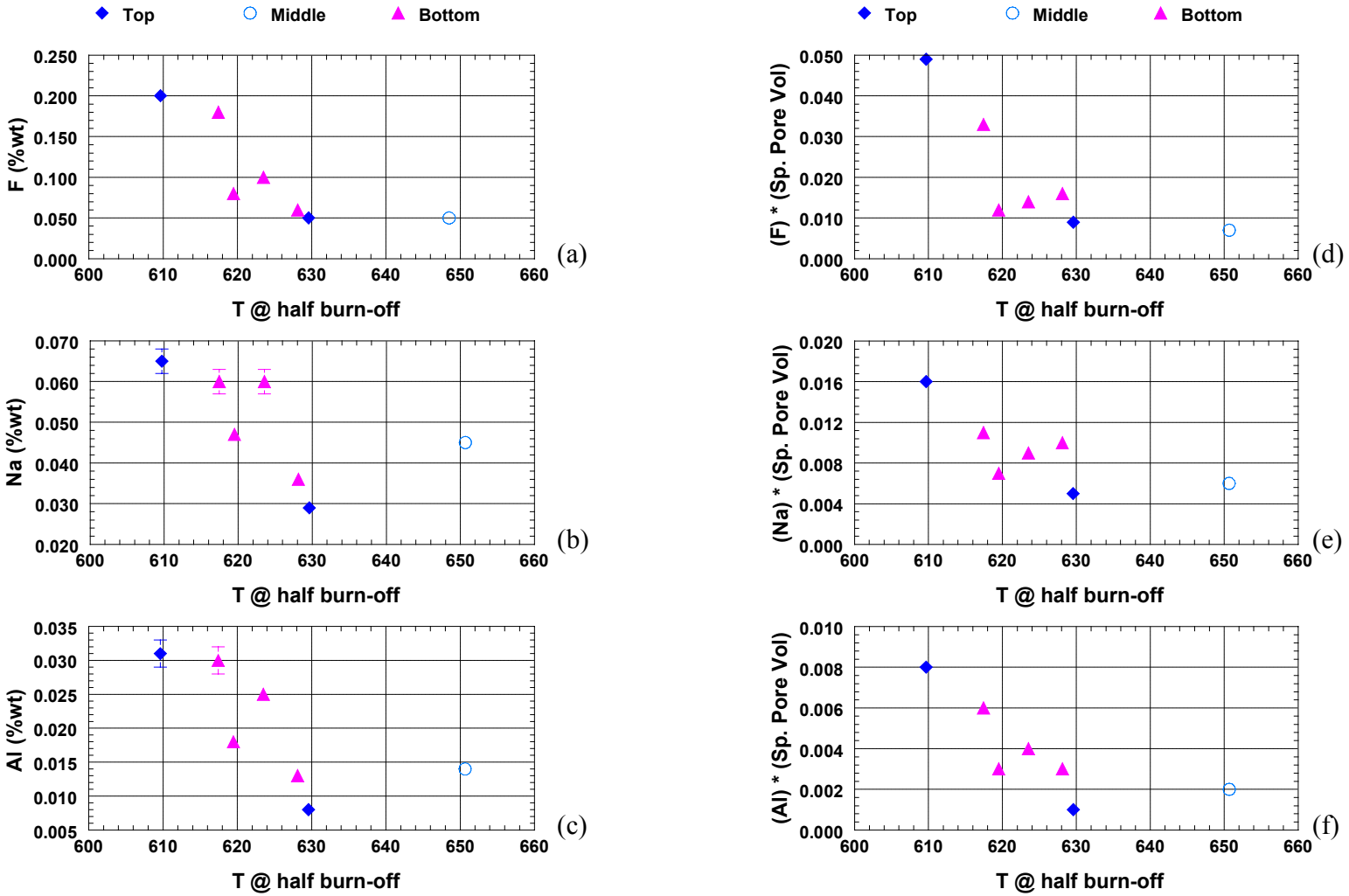

Figure 31 The effects of inorganic contents and (inorganic content ✕ specific pore volume) on air reactivities (represented by the temperature at half burn-off) of BUTT-2 Core#5.

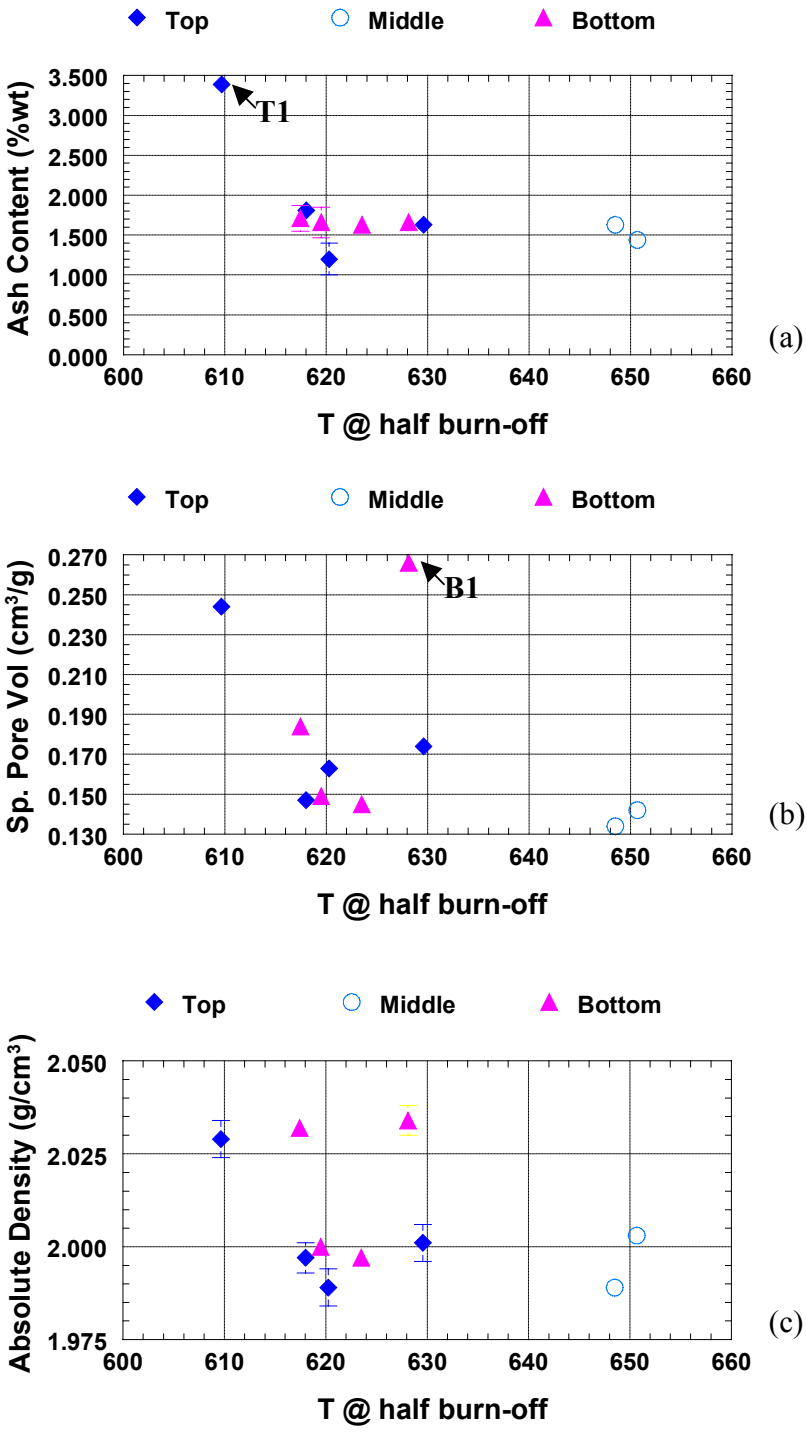

Figure 32 Effects of (a) Ash content, (b) specific pore volume, and (c) absolute density on the air reactivity (represented by the temperature at half burn-off) of BUTT-2 Core#5.

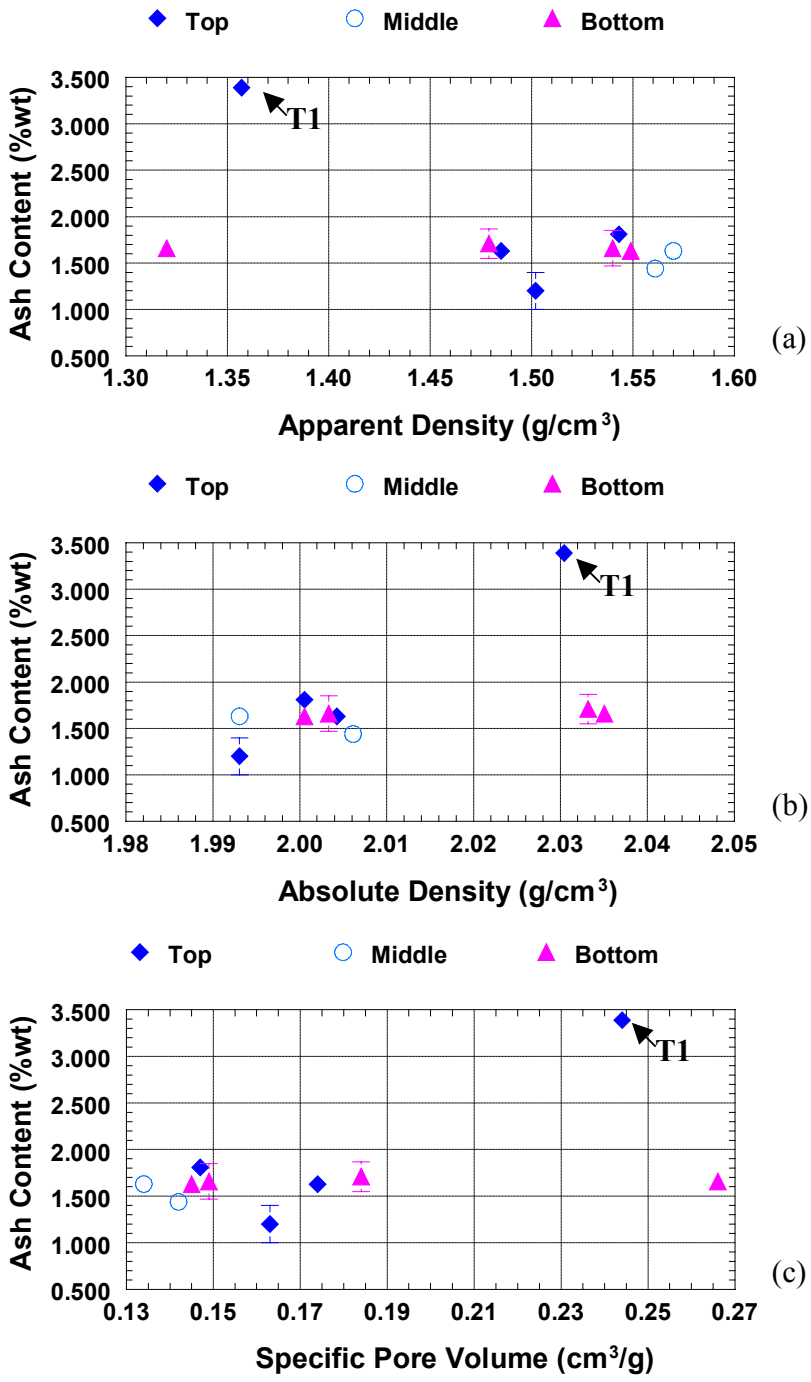

Figure 33 Relationship between physical properties and ash content of BUTT-2 Core#5: (a) Ash content v.s. apparent density; (b) Ash content v.s. absolute density; and (c) Ash content v.s. specific pore volume.

Figure 32 (a) shows no relationship between the air reactivity and the ash content. All samples contain about equal amount of ash except T1, which has about double amount of ash content than others. As mentioned earlier, the specific pore volume is very important to the reactivity of the carbon material. The air reactivity tends to have some relationship with the specific pore volume as shown in Figure 32(b). B1 seems not to follow this trend. This can be explained that B1 contains a lower concentration of reactive components, such as sodium, than the rest of the samples, as shown in Figure 19. A combined effect of inorganic contents and the specific pore volume was already explained previously. Figure 32(c) shows no relationship between the absolute density and the air reactivity.

Figures 33(a), (b) and (c) show the plots of the ash contents versus the apparent density, absolute density, and the specific pore volume, respectively. T1 contains fairly higher ash content than the other samples, which have comparable amount of ash. Apart from T1, the other samples do not have any relationship between the ash content and physical properties.

Figure 34 shows a plot of CO_2 reactivity versus distance from the airburn side. $(dX_c/dt)_{max}$ or R_{max}, which is the initial slope of the conversion versus time plot (Figure 28), is used to represent the isothermal reactivity of a material under a certain gas environment. All samples show a comparable value of reactivity except T1, which is about double as reactive as others. Hence, it can be concluded that no relationship was found between the CO_2 reactivity and the position of the butt material in the butt core. The relationship between the CO_2 reactivity and the ash content is not quite clear as shown in Figure 35(a). Although the ash content tends to slightly increase with the increase in CO_2 reactivity, these values are pretty similar and only T1 sample shows a significant higher in both reactivity and the ash content. Hence, it is presumed that there is no relationship between these two parameters. Figure 35(b) clearly shows that there is no relationship between the CO_2 reactivity and the absolute density. Similar to the air reactivity, CO_2 reactivity exhibits a relationship with the specific pore volume as shown in Figure 35(c). Although B1 which contains a high porosity has such a low reactivity as

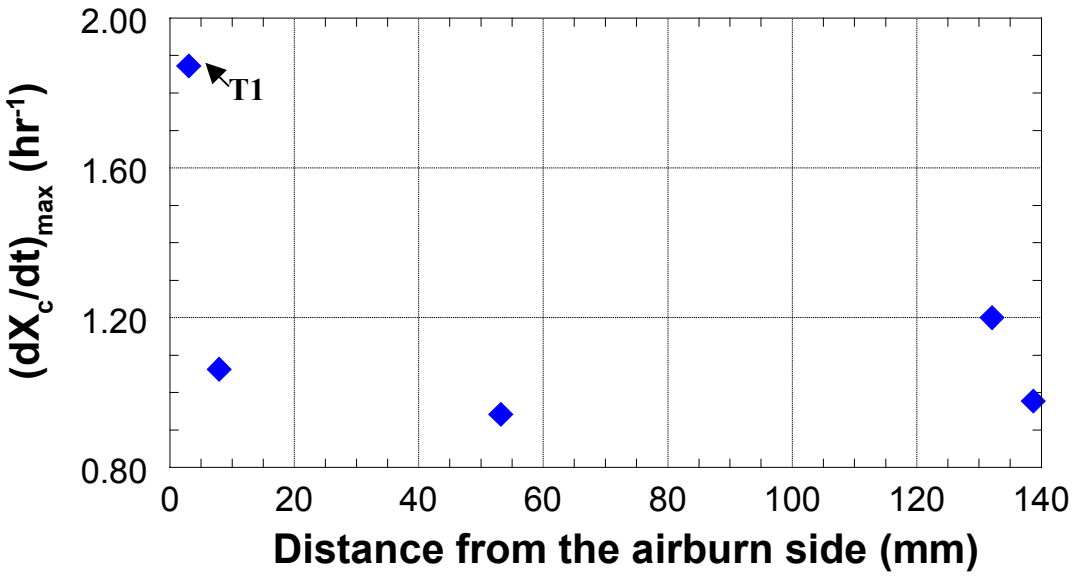

Figure 34 Reactivity (represented by $(dX_c/dt)_{max}$ or R_{max}) of Butt-2 Core #5 in 1 atm CO_2 at 976±1°C v.s. distance from the airbrun side.

compared as other butt materials from other positions, this result was derived from a low concentration of inorganic material in this specific sample. The inorganic contents and the combined effect between the inorganic content and the specific pore volume have similar effects to the CO_2 reactivity as previously shown in the air reactivity (see Figure 36(a) to (f) compared to Figure 31(a) to (f)). Either the specific pore volume or the inorganic content alone shows some relationships with the CO_2 reactivity and the combined effect between these two is even pronounced. Hence, among all parameters tested in this study, it can be concluded that only the specific pore volume and the inorganic contents are the most important factors that affect the reactivity of the anode butt materials.

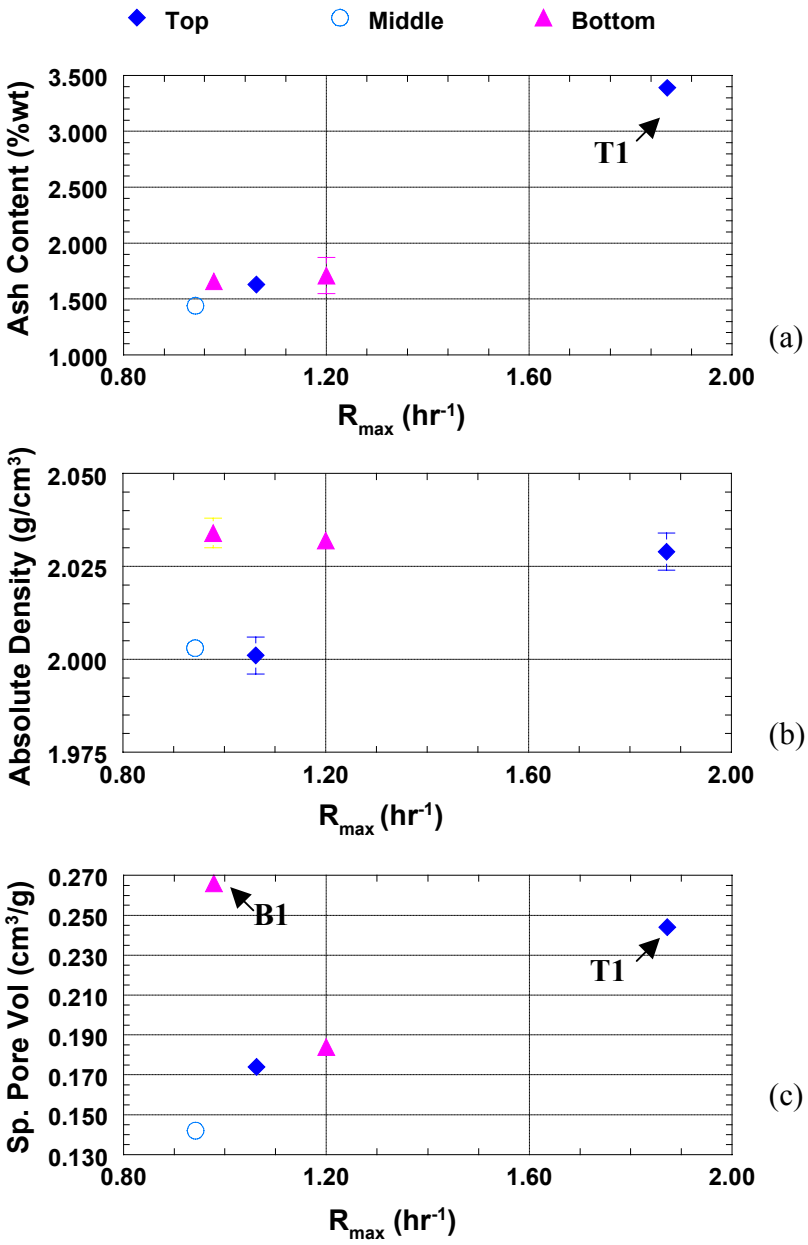

Figure 35 Effects of (a) Ash content, (b) Absolute density, and (c) Specific pore volume on the CO_2 reactivity (represented by (dXc/dt)max or Rmax) in 1 atm CO_2 at 976±1°C of BUTT-2 Core#5.

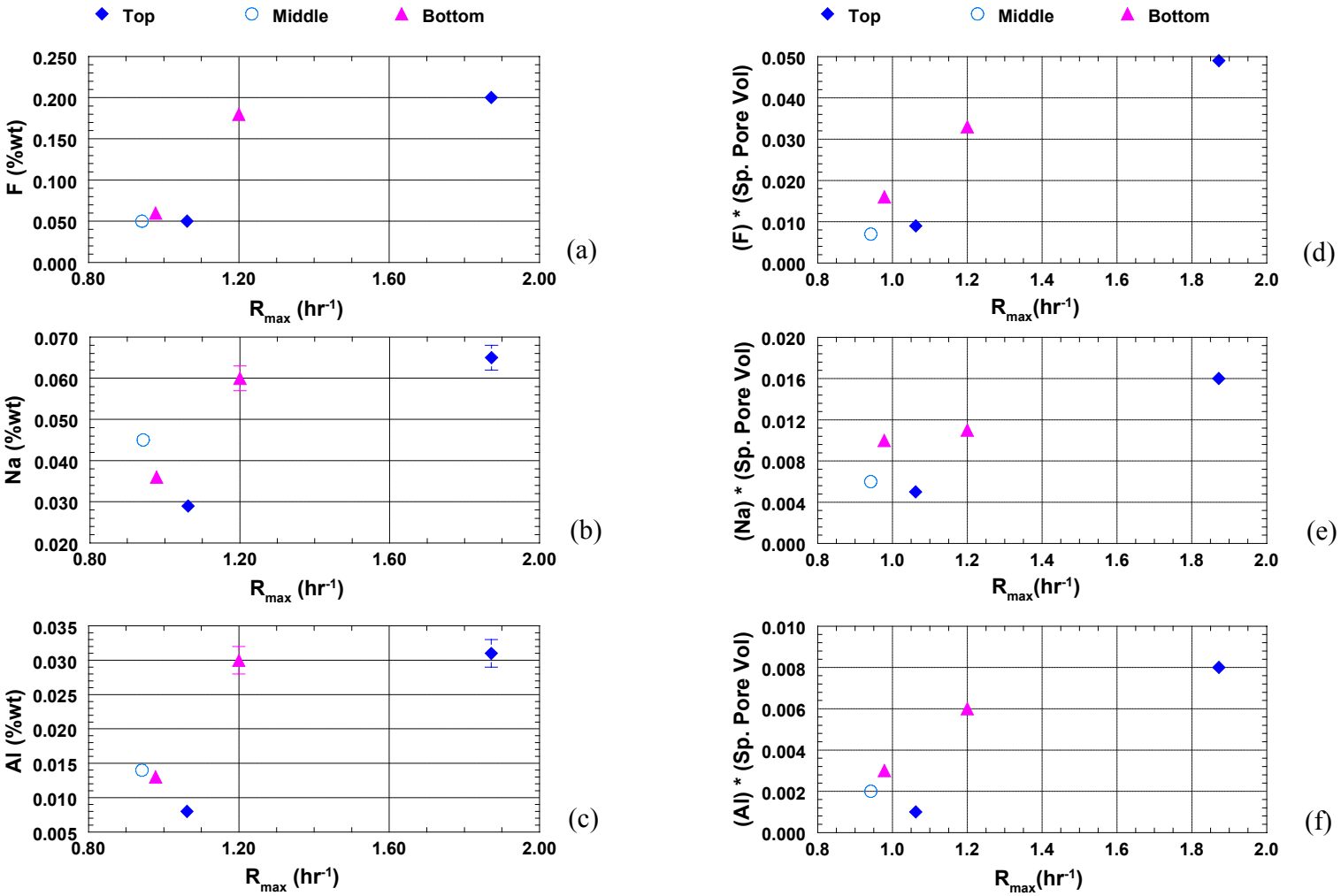

Figure 36 The effects of inorganic contents and (inorganic content ✕ specific pore volume) on the CO_2 reactivity (represented by $(dX_c/dt)_{max}$ or R_{max}) in 1 atm CO_2 at 976±1°C of BUTT-2 Core#5.

3.3 Pitches/Butts Study

In this part of the study, only the alternative pitches which have the softening point around 110-115°C were used to mix with the SCTP-2. The ratio of the alternative pitch to SCTP-2 was fixed to 20:80 and the properties of these pitch mixtures were compared to the experimental-scale anodes made from 100% SCTP-2. Three types of butt materials from the most top, middle, and the most bottom were used to study how different parts of the butt interact with each pitch. All results from this section were also compared to the results obtained in Section 3.1 where the mixed butt materials were used.

Different parts of the butt materials gave a significant difference in the green apparent density. Figure 37 shows the green apparent densities of the experimental-scale anodes made from the most top, middle, and the most bottom parts of the butt core. The middle part butt material gave a significant higher green apparent density than the top and the bottom parts for each pitch mixture. These results are directly due to the higher porosity of the top and bottom part than the middle one. It is of interest to observe that the experimental-scale anodes made from the Top + SCTP-2 and the Bottom + SCTP-2 gave lower green apparent densities than the Top + alternative pitch and the Bottom + alternative pitch. This may cause by the effect of QI in the SCTP-2, i.e. a lower QI pitch could penetrate into pores better than a higher QI pitch. The green apparent densities of the anodes made from the Top, Middle and Bottom parts are also compared with those made from the mixed butt materials. Only the anodes made from the middle part gave comparable results to the mixed anode butts while the anodes made from the top and bottom gave significantly lower green apparent densities.

Figure 38 shows the baked apparent densities of the experimental-scale anodes made from the Top, Middle, and the Bottom parts of the butt core. The SCTP-2 only gave slightly lower baked apparent densities of the anode made from the top and bottom parts than those made from the middle part. All other anodes made from the alternative pitch + SCTP-2 mixture gave slightly lower baked apparent densities of the anodes made from the top part, while the apparent densities of those made from the bottom and middle

are comparable. A comparison of the baked apparent densities of the anodes made from the Top, Middle, or Bottom to the anodes made from the mixed butt materials suggests that the SCTP-2 only (Figure 38(a)) and the pitch mixture of PP-1 + SCTP-2 (Figure 38(b)) gave comparable results to the anodes made from the mixed butt materials, while the pitch mixtures of WVU-5 + SCTP-2 (Figure 38(d)) gave quite lower results. In the case of GP-1 + SCTP-2, although the baked apparent densities are only slightly lower than those of the SCTP-2 only (Figure 38(c)) for all Top, Middle, and Bottom, these baked apparent densities are quite lower than the anodes made from the mixed butt materials. These results can be explained as follows. When the Top, Middle, or Bottom of the butt materials mixed with the GP-1 + SCTP-2 pitch mixture gave similar pitch loss to the anodes made from the mixed butt materials (Figure 39(c)). The lower baked apparent densities in this case were derived from the higher change in volume after baking as compared to the mixed butt materials (Figure 40(c)).

On the other hand, the low baked apparent densities of the WVU-5 + SCTP-2 pitch mixture mixed with the Top, Middle, or Bottom part of the anode butts were directly derived from a fairly high pitch loss as shown in Figure 39(d). Nevertheless, the pitch loss and the volume change of the Top, Middle or Bottom butt materials mixed with the SCTP-2 only or the PP-1 + SCTP-2 are similar to those of the mixed butt materials (Figure 39(a), (b) and Figure 40(a), (b)). However, the Middle butt material + SCTP-2 only gives a rather high in volume change than other samples of the same pitch mixture. This high volume change may derive from the low pitch loss of this anode (see Figure 39 (a)) and, hence, pitch was trapped inside the anode and underwent volume expansion during baking.

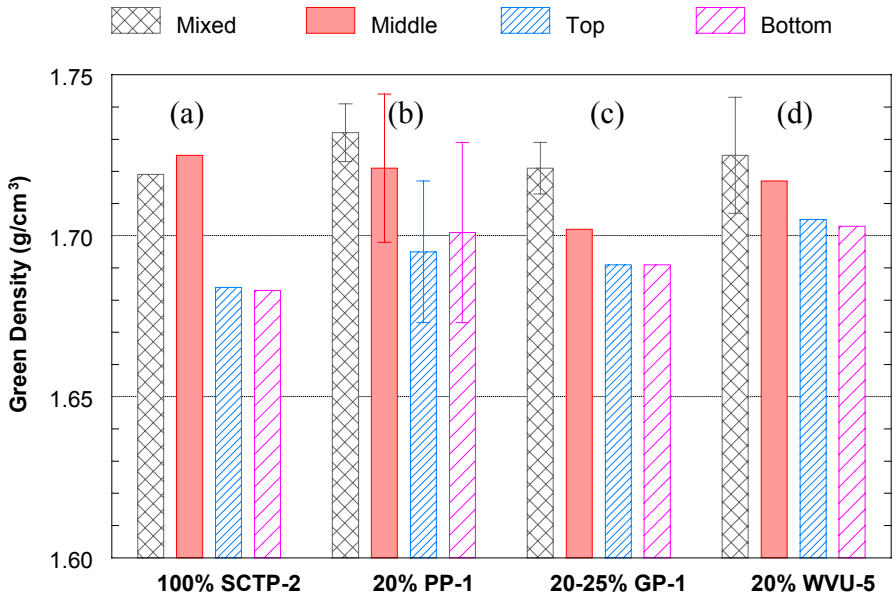

Figure 37 Green apparent densities of the anodes made from 49% petroleum coke, 29% butt materials (mixed, top, middle, or bottom parts), and 22% pitch mixture(s). (a) 100% SCTP-2; (b) 20% PP-1 and 80% SCTP-2; (c) 20% GP-1 and 80% SCTP-2; and (d) 20% WVU-5 and 80% SCTP-2.

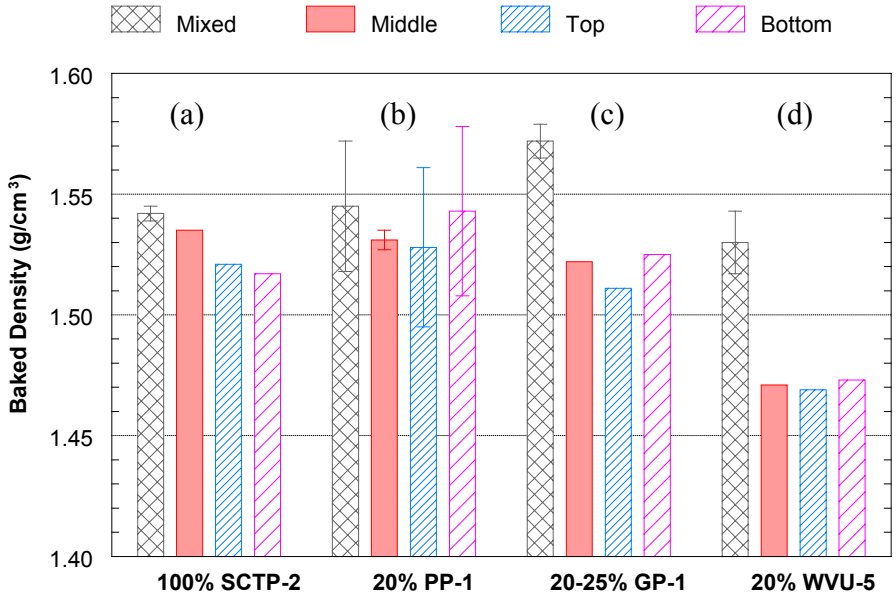

Figure 38 Baked apparent densities of the anodes made from 49% petroleum coke, 29% butt materials (mixed, top, middle, or bottom parts), and 22% pitch mixture(s). (a) 100% SCTP-2; (b) 20% PP-1 and 80% SCTP-2; (c) 20% GP-1 and 80% SCTP-2; and (d) 20% WVU-5 and 80% SCTP-2.

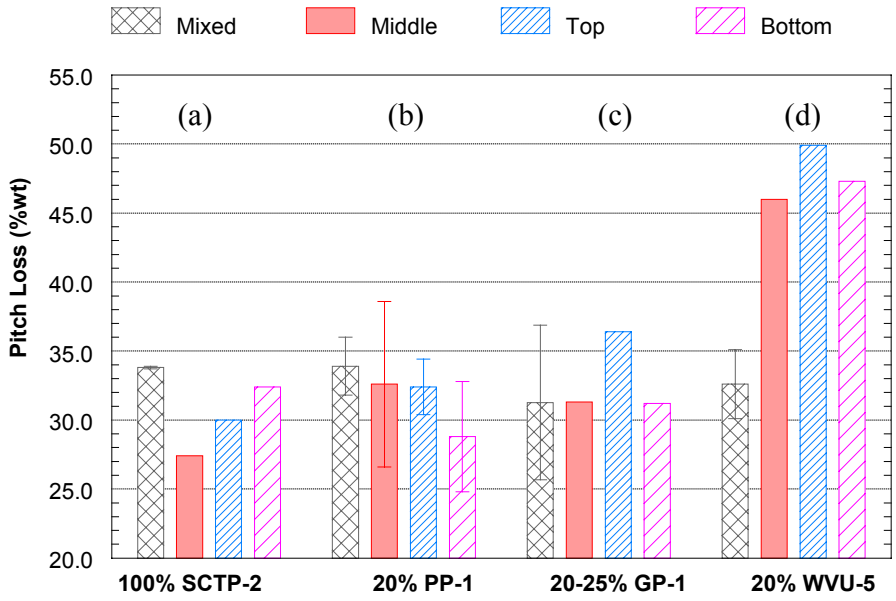

Figure 39 Percentages of pitch loss after baked of the anodes made from 49% petroleum coke, 29% butt materials (mixed, top, middle, or bottom parts), and 22% pitch mixture(s). (a) 100% SCTP-2; (b) 20% PP-1 and 80% SCTP-2; (c) 20% GP-1 and 80% SCTP-2; and (d) 20% WVU-5 and 80% SCTP-2.

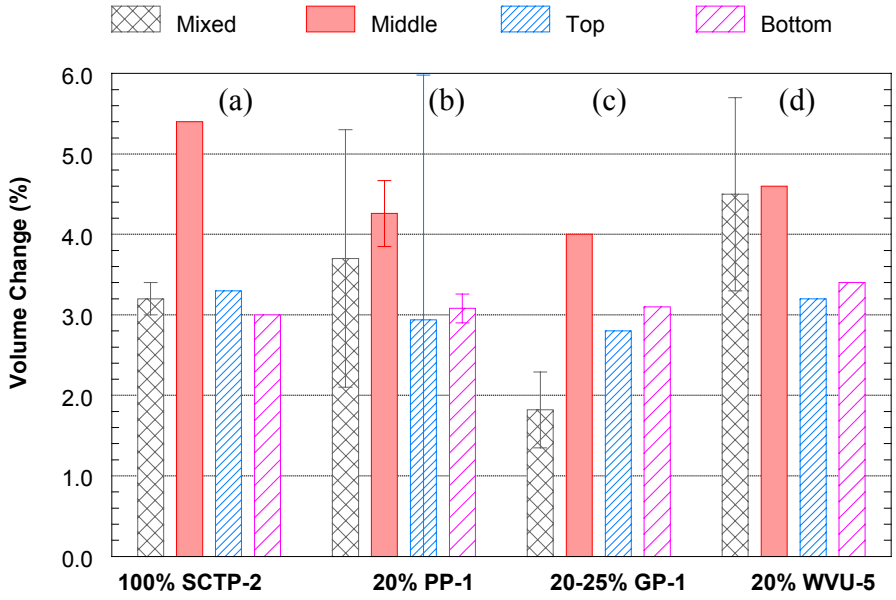

Figure 40 Percentages of volume change after baked of the anodes made from 49% petroleum coke, 29% butt materials (mixed, top, middle, or bottom parts), and 22% pitch mixture(s). (a) 100% SCTP-2; (b) 20% PP-1 and 80% SCTP-2; (c) 20% GP-1 and 80% SCTP-2; and (d) 20% WVU-5 and 80% SCTP-2.

4. Conclusion

4.1 Binder Pitches Study

The results of this study show that the petroleum pitch offers a potential to be used as additives to the standard coal-tar pitches for use as binders in the aluminum anode production, while the addition of coal-extracted pitch and gasification pitch give comparable anode properties when the ratio of standard coal tar pitch to the alternative pitch is greater than 50:50. Further work should be conducted to study the causes of improvement of adding alternative pitches to better understanding the roles of the binders from various types of pitches.

4.2 Anode Butts Study

Three industrial anode butts, with and without recycled butt material, were studied. Non-destructive X-Ray imaging was used to quantify the spatial distribution of density and porosity in the sample. Apparent and absolute densities were measured and the specific pore volumes were calculated as a function of the distance from the airburn side. The results from the X-Ray CT and the densities and pore volume measurement showed a decrease in apparent density, and an increase in absolute density and specific pore volume from the center of the core to the surfaces. The anode butt that did not contain recycled butt material in the original formulation showed a higher reactivity with air at the airburn side while it had lower reactivity with CO_2 at the electrolytic side. It can be confirmed from this work that the main factors that derived the change in air and CO_2 reactivities of the anodes along the electrolytic surface to the airburn surface were the concentration of the inorganic contents, e.g. sodium, calcium, etc., and the porosity of the carbon material.

4.3 Pitches/Butts Study

The experimental-scale anodes made from the top and bottom of the butt materials gave quite lower green apparent densities than the anodes made from the

middle part of the butt materials. These results were linked with high porosity of the top and bottom of the butt materials that inhibited the pitch to penetrate well into the pores. However the effect of porosity was weakened in the baked apparent density. Anodes that made from the pitch mixture that contained 20% PP and 20%GP gave comparable baked density to the anodes made from SCTP only. Whereas the anodes that were made from the pitch mixture that contained 20% WVU gave somewhat lower baked densities than the SCTP only and these results were caused by a high pitch loss of this pitch after baking.

5. References

[1] CRU International, Carbon Products – Aluminum Raw Materials, London, U.K., May 2002.

[2] Rusinko, F., Andresen, J. M., Adams, A., Chapter 13 in Great Lakes Carbon Corp. 6th Carbon Conference (Houston. USA), 2000.

[3] Schmidt-Hatting, W., Kooijman, A. A., Perruchoud, R., Investigation of the Quality of Recycled Anode Butts, Light Metals, 705-720, 1991.

[4] Gray, R. J.., and Krupinski, K. C., In Introduction to Carbon Technologies; Marsh H, Heintz EA., and Rodriguez-Reinoso F, Ed.; Secretariado de Publicaciones, 1997, pp 329-424.

[5] Grjotheim, K. and Welch, B. J., In Aluminum Smelter Technology; 2nd ed.; Aluminum-Verlag: Dusseldorf, 1988, pp 75-118.

[6] Jenkins, R.G., Nandi, S. P., and Walker, P. L. Jr., Reactivity of Heat-Treated Coals in Air at 500 [Deg]C, Fuel, 52, 288-93, 1973.

[7] Mahajan, O. P., and Walker, P. L., Jr. "Porosity of Coals and Coal Products." In Analytical Methods for Coal and Coal Products, edited by C. Karr, Jr., 125-62. New York: Academic Press, 1978.

[8] The Energy Institute Penn State University, Binding Efficiency of Coal-Derived Binders Towards Anode Butts: 1st Quarterly Technical Progress Report, June 2003.

[9] Cutshall, E. R., and Bullough, V. L., Influence of baking temperature and anode effects upon carbon sloughing, Light Metals,1039-1076, 1985.

[10] Perruchoud, R. C., Meier, M. W. and Fischer, W. K. Bath impregnation of carbon anodes. Light Metals, 543-549, 1996.

[11] Sadler, B. A. and Salisbury, C. Impact of recycled anode waste materials on anode quality. Light Metals, 609-614, 1994.

[12] Walker, P. L. Jr., Matsumoto, S., et al., Catalysis of gasification of coal-derived cokes and chars, Fuel, 62(2), 140-149, 1983

"Processing and Reuse of Activated Carbon Used to Adsorb Mercury from Power Plant Flue Gases"

Final Report

Dale L. Nickels
Dr. Thomas Weyand

Contract #: 2477-PMET-DOE-0350

Pittsburgh Mineral & Environmental Technology
700 Fifth Ave.
New Brighton, PA 15066

June 24, 2004

ABSTRACT

The Environmental Protection Agency (EPA) has decided to regulate mercury emissions from coal fired power plants. The regulations will be developed and finalized, with full compliance anticipated by 2007. Test work performed by others has identified a system by which the mercury in flue gases can be captured onto Powdered Activated Carbon (PAC) to control mercury emissions. However, the existing production capacity for PAC is only 10% of the capacity required for full implementation.

The process envisioned and defined in this project enables the reuse of PAC after its injection and collection from a flue gas stream in which the PAC injection point is after the electrostatic precipitators but prior to a baghouse. Once collected, the PAC is thermally treated in an inert atmosphere to desorb the contained mercury allowing the PAC to be returned to the injection system for reuse. The desorbed mercury is sequestered and concentrated for recovery into saleable product.

Compared to single-pass PAC that is injected once, collected and disposed of; this process offers significant operating cost savings, reduced PAC consumption to stretch the existing supply, and mercury emissions that are recyclable.

A bid package was prepared for the construction of a demonstration plant suitable for processing mercury laden PAC (or other sorbents) for a 270MW power plant.

TABLE OF CONTENTS

TABLES, FIGURES AND DRAWINGS

TABLES

FIGURES

DRAWINGS

INTRODUCTION

This project addresses the removal and recovery of mercury that is sorbed to Powdered Activated Carbon (PAC) to remove mercury from coal combustion power plant flue gas streams.

Previous work performed by ADA ES and others for the US DOE has demonstrated the effectiveness of injecting PAC into flue gas streams for mercury removal. This approach has been highly successful in removing up to 80% of the mercury from the flue gas when the PAC is injected ahead of a COHPAC facility.

To date, the PAC with sorbed mercury is assumed to be disposed after use. This will result in a significant expense for the mercury removal, since the most effective PAC employed to date is DARCO FGD manufactured by Norit Americas is estimated to cost approximately $0.50/ pound delivered to the power plant. In addition to the purchase expense, the disposal of this material may potentially fall under regulations requiring its disposal in "special" or hazardous waste landfills.

The proposed approach dramatically reduces the need for ongoing PAC purchases and provides for a thousand fold concentration of mercury in a specially formulated carbon that can subsequently be treated for mercury recovery as a salable metal, thus avoiding any disposal of potentially toxic waste streams. The estimated operating cost for this process is ~$0.05/lb of treated PAC compared with a purchase price of $0.50/lb PAC and an unknown but potentially significant disposal cost.

The process is shown in schematic in Figure 1.

FIGURE 1
Mercury Control System

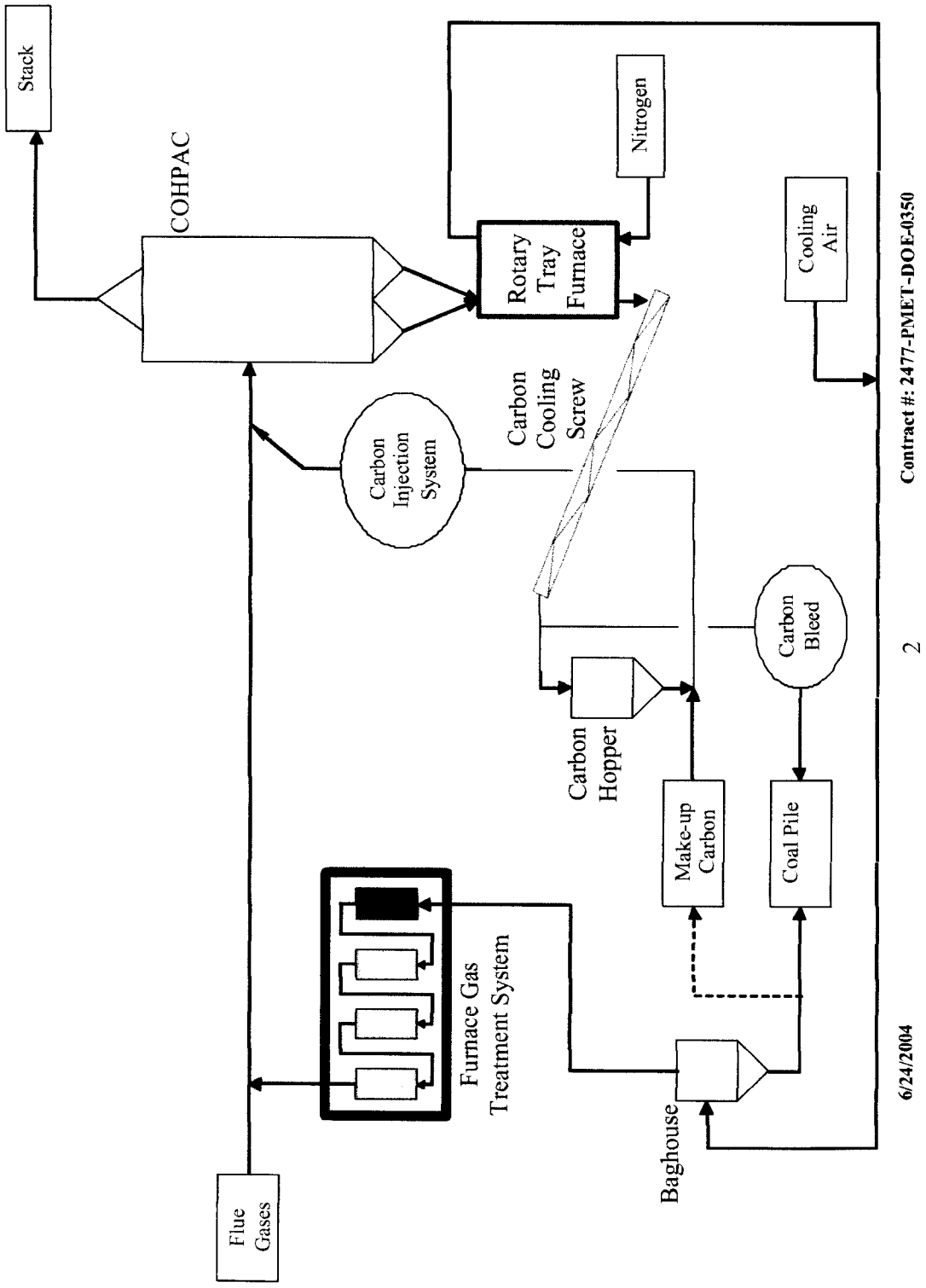

PAC is injected into the flue gas stream ahead of the COHPAC bag filter. Mercury contained in the flue gas is removed from the gas stream as gas passes thru the carbon layer on the COHPAC bags and exits the facility via the plant stack. PAC in the COHPAC is periodically removed from the filter bags and fed to a rotary tray furnace for mercury removal from the PAC. This furnace is sealed and operates under an inert counter flowing nitrogen atmosphere. Mercury vapor exits the rotary tray furnace with the nitrogen process gas and is directed to a multiple column gas treatment system which utilizes packed beds of sulfur impregnated carbon to remove the gaseous mercury from the cooled process gas stream. After passing thru the sulfur impregnated carbon columns, the carrier gas is injected into the flue gas stream ahead of the carbon injection site.

Carbon exits from the rotary tray furnace via an air lock to a water-cooled screw conveyor. The cooled carbon is returned to the carbon hopper supplying the PAC injection system. Depending upon the amount of ash recovered in the COHPAC, a bleed stream of carbon will be required to maintain a material balance in the system. The bleed stream will take a portion of the desorbed carbon from the screw discharge. This material can be combusted in the coal-fired boiler.

The focus of this project is two fold:

1. Perform bench scale feasibility testing is to determine if the process envisioned in Figure 1 is technically viable.

2. Prepare a bid package for the construction of a demonstration plant based upon the process in Figure 1 that is suitable for processing mercury laden PAC (or other sorbents) for a 270MW power plant.

EXECUTIVE SUMMARY

The Environmental Protection Agency (EPA) has decided to regulate mercury emissions from coal fired power plants. The regulations will be developed and finalized, with full compliance anticipated by 2007. Test work performed by others has identified a system by which the mercury in flue gases can be captured onto Powdered Activated Carbon (PAC) to control mercury emissions. However, the existing production capacity for PAC is only 10% of the capacity required for full implementation.

The process envisioned and defined in this project enables the reuse of PAC after its injection and collection from a flue gas stream in which the PAC injection point is after the electrostatic precipitators but prior to a baghouse. Once collected, the PAC is thermally treated in an inert atmosphere to desorb the contained mercury allowing the PAC to be returned to the injection system for reuse. The desorbed mercury is sequestered and concentrated for recovery into saleable product.

Based upon the results from the bench-scale feasibility testing in this report, the envisioned process is technically viable when the thermal desorption operation occurs under the following parameters:

- Inert atmosphere during elevated temperature processing;
- 550°C desorption temperature; and
- 30 minutes of retention at temperature

Using this process, PAC can be recycled at least 10 times without any degradation of the sorption characteristics.

Based upon the operating parameters established above, a bid package was prepared for the construction of a demonstration plant suitable for processing mercury laden PAC (or other sorbents) for a 270MW power plant.

Use of the PAC desorption/recycling system will decrease the yearly operating costs by at least $216,200 resulting in a return-on-investment (uninstalled capital basis) of 28.14%.

Compared to single-pass PAC that is injected once, collected and disposed of; this process offers:

- Significant yearly operating cost savings,
- Reduced PAC consumption to stretch the existing supply,
- Mercury emissions that are recyclable, and
- Eliminated environmental liability from landfilled mercury laden PAC.

SECTION 1
BENCH SCALE FEASIBILITY TESTING

PURPOSE AND SCOPE

The purpose of bench scale feasibility testing is to determine if the process envisioned in Figure 1 is technically viable. The criteria for this determination are:

- Will the PAC physically degrade when exposed to air at elevated temperatures?
- Will the PAC retain its sorptive properties when exposed to several desorption cycles?
- Can mercury be desorbed from the loaded PAC?

In order to answer these questions the following scope of work was carried out:

- Acquisition of a virgin PAC from Norit Americas (DARCO FGD).
- Acquisition of a mercury laden PAC that was produced from an operating mercury control system. The virgin PAC used in this control system was also Norit's DARCO FGD.
- Generate a synthetically mercury loaded PAC for testing.
- Generate temperature versus loss in mass data for PAC in air.
- Produce thermally cycled model PAC for sorptive properties testing.
- Perform mercury desorption on the synthetically loaded sample.
- Perform mercury desorption on the field sample of mercury loaded PAC.
- Perform sorption characteristic testing on the starting and thermally cycled PAC for comparison.

SAMPLE ACQUISITION

Two PAC samples (supplied by ADA-ES) were acquired from a coal fired power plant operating a mercury control system in which the PAC is injected into the flue gas down stream of the ESP's and prior to a baghouse. Referred to as SITE hereinafter.

- PMET RFA# 4444-1
  - 10 gallon sample: Received on 9/23/03
- PMET RFA# 4444-3
  - 5 gallon sample: Received on 12/29/03

GENERATION OF SYNTHETICALLY LOADED PAC

Prior to the arrival of the SITE sample material, a synthetically loaded PAC (DARCO FGD, the same grade of PAC used at SITE) was generated.

One gram of $HgCl_2$ and Hg were blended into coarse sand. This material and PAC were introduced into an apparatus to transfer the mercury compounds from the sand to the PAC. One 24 hour transfer test generated 250g of PAC that contained 6.4 ppm of total mercury, which is similar to what is expected at the SITE. The transfer apparatus is depicted in Figure 2.

FIGURE 2

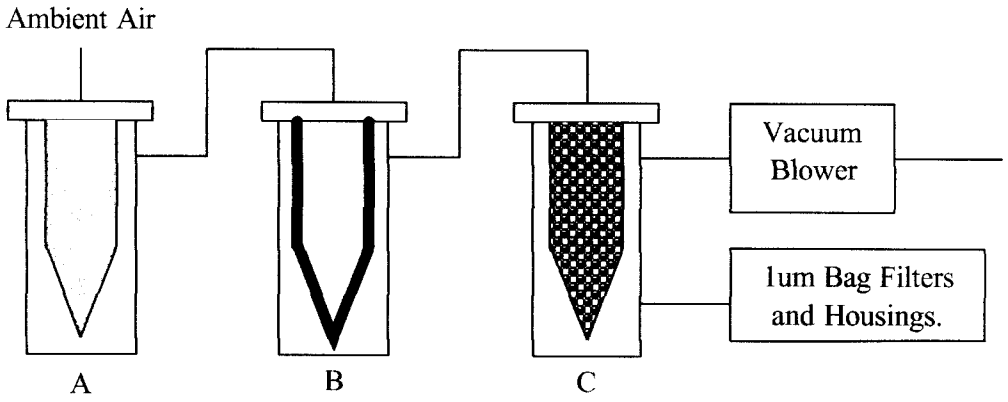

A: Mercury laden sand.
B: PAC ¼" thick.
C: Sulfur impregnated carbon for mercury exhaust control.

TESTING OF THE MODEL PAC

Two series of thermal treatments of the model PAC were performed. Both of these treatments were performed in air rather than nitrogen to study the reactivity of the carbon at various temperatures. The oxidation of the carbon was tracked by the loss in weight of the sample when the material was subjected to air at temperature for 60 minutes. The results of these tests are shown in Figure 3.

FIGURE 3

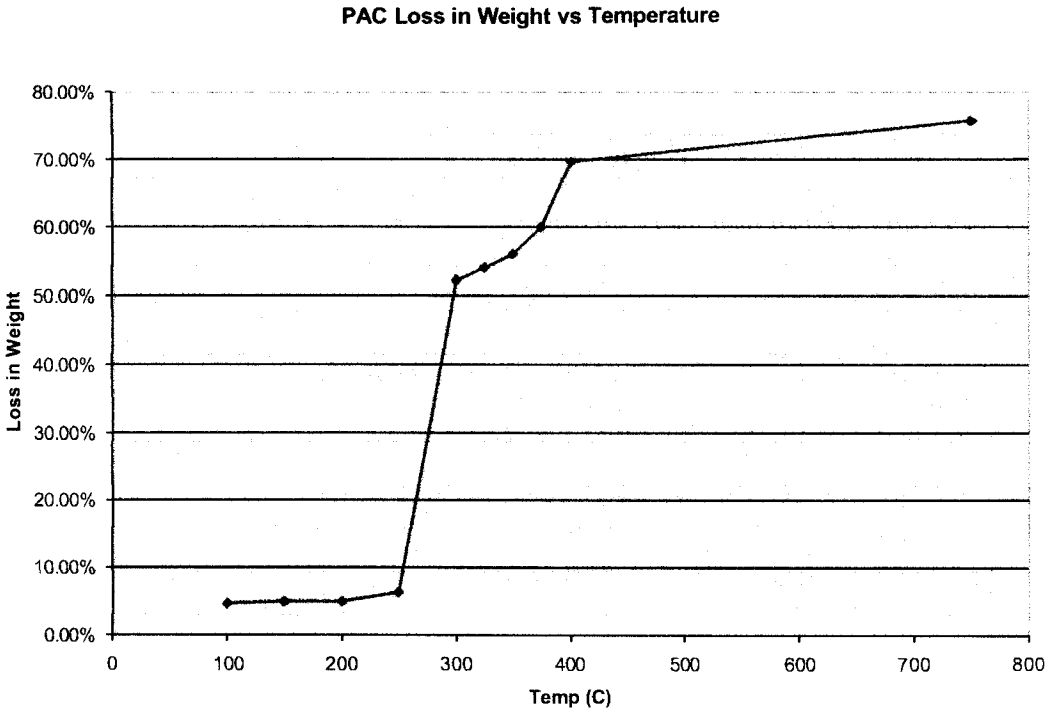

Some loss in weight (~5%) occurs at temperatures up to 200°C, and above 250°C the carbon reacts vigorously with essentially all of the available carbon being oxidized. This particular PAC sample (DARCO FGD) has an ash content of approximately 25%.

Figure 4 shows the loss in weight for a PAC sample exposed to air at 250°C.

FIGURE 4

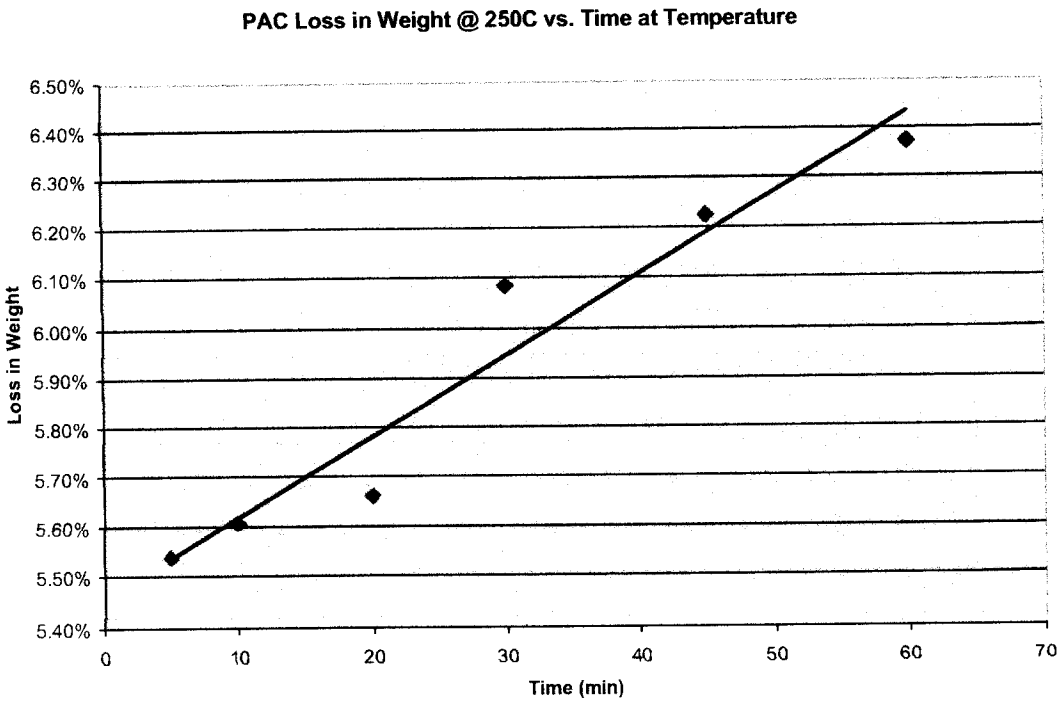

Figure 4 shows that even at a modest temperature of 250°C; the sample material undergoes oxidation of the carbon at a fairly constant rate of 0.016% Loss in Weight per minute exposed.

Clearly this testing indicates that an inert atmosphere is required for the tray desorption furnace to avoid significant losses of the PAC material during mercury desorption.

One thermal desorption test was performed using an inert atmosphere (nitrogen) in which the model PAC was cycled from ambient to 450°C ten times to simulate multiple recycles in the commercial system.

Figure 5 shows the change in carbon sorption capacity and surface area over the ten cycles.

FIGURE 5

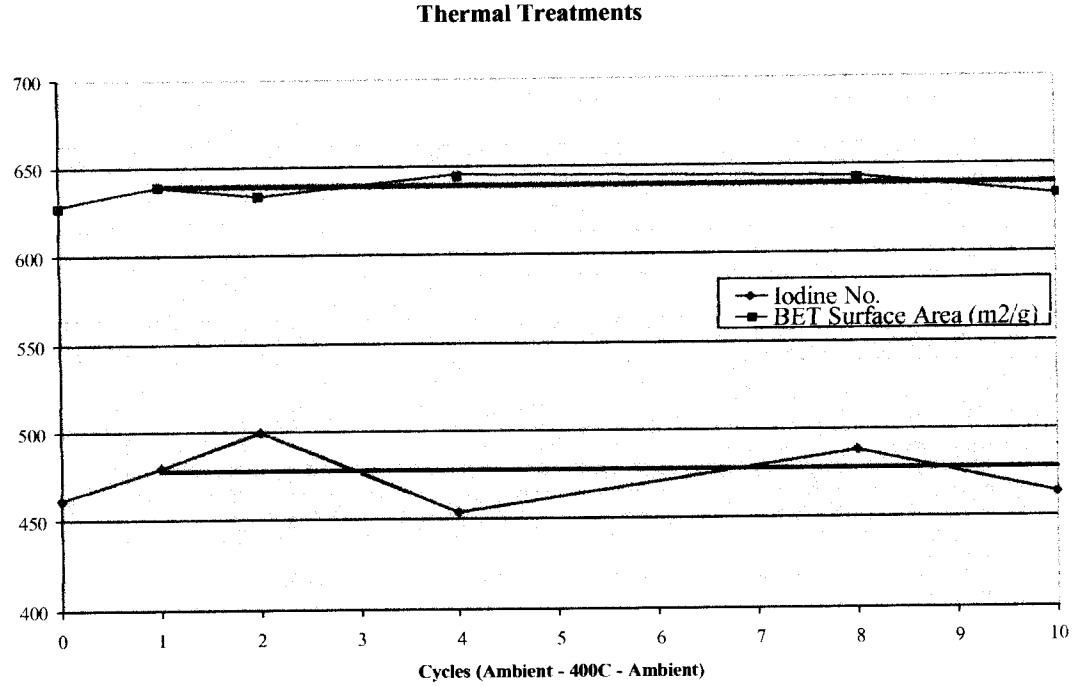

The weight loss of the model PAC over the ten cycles was less than 0.1%.

Figure 6 shows the nitrogen isotherm comparison of the model PAC and cycled PAC (10 thermal desorption cycles).

FIGURE 6

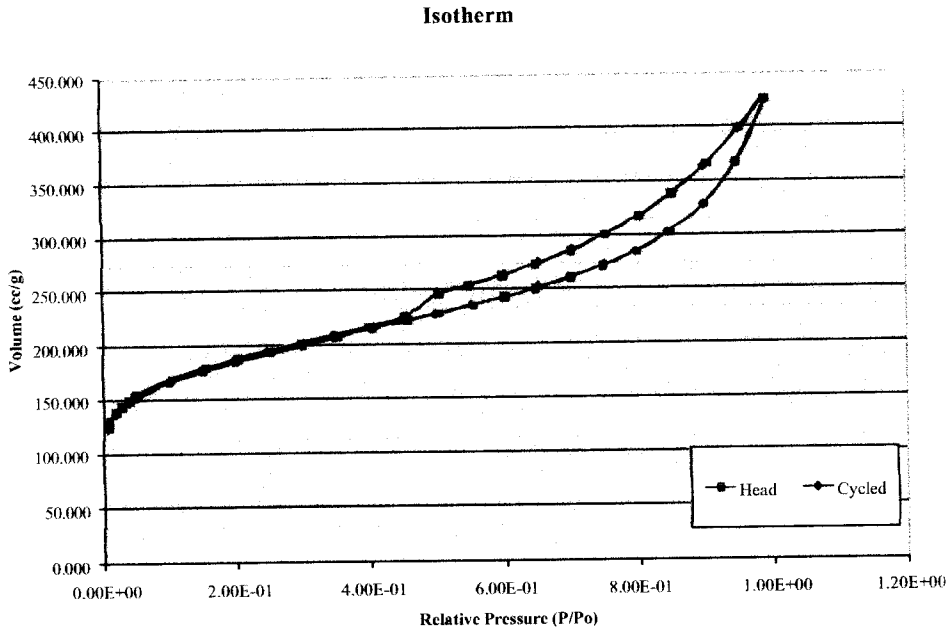

Figure 7 shows the pore size distribution comparison of the model PAC and cycled PAC (10 thermal desorption cycles).

FIGURE 7

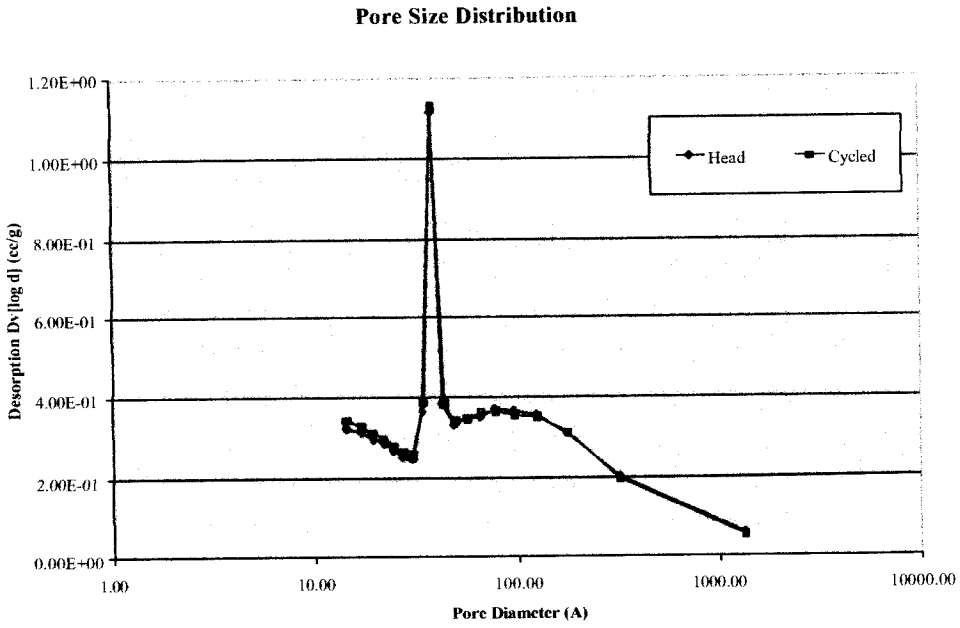

Comparison of the "Area-Volume-Pore Size" Data

Analysis	Head PAC	Recycled PAC
Multipoint BET	605.9 m^2/g	603.7 m^2/g
Single Point BET	616.3 m^2/g	613.6 m^2/g
t-Method External Surface Area	257.9 m^2/g	257.9 m^2/g
t-Method Micro Pore Surface Area	348.0 m^2/g	345.8 m^2/g
Total Pore Volume for pores with dia. < 390Å @ P/Po = 0.9475	0.5689 cc/g	0.5676 cc/g
t-Method Micro Pore Volume	0.1750 cc/g	0.1734 cc/g
Average Pore Diameter	37.56 Å	37.61 Å

Another thermal desorption test was run, in which the synthetically loaded PAC was subjected to conditions that would mimic a commercial rotary tray furnace.

- The loaded model PAC was placed into a tray to a depth of ½".
- This tray was placed into a retort oven and the nitrogen purge was started.
- The sample was ramped to 400°C in 15 minutes and held at temperature for 15 minutes.
- The sample was allowed to cool to 200°C over 60 minutes.
- The sample was then removed and agitated.
- This thermal desorption cycle was repeated 4 times using the same PAC sample.

After 15 minutes thermal desorption the total mercury was reduced to 0.38 ppm, and after 30 minutes the total mercury was reduced to <0.1 ppm.

SITE SAMPLE TESTING

The as received PAC was assayed for mercury and LOI (Loss On Ignition).

Sample ID	Mercury Content (ppm)	LOI (%)
4444-1	37.9	24.5
4444-3	35.3	19.0
Virgin PAC	0.1	75.7

The SITE PAC is loaded with mercury; however it also contained a large amount of ash. This must be fine ash that was not collected by the ESPs and allowed to pass to the COHPAC where it is collected with the injected PAC. Fine ash escaping from the ESPs must be minimized in order for the PAC to be recycled.

The mercury laden PAC was thermally desorbed at 450°C, 550°C, 650°C and 750°C in an inert atmosphere to simulate a commercial furnace.

Sample 4444-1 Mercury Desorption Data

Elapsed Time in Furnace (min)	Mercury Concentration (ppm)			
	450°C	550°C	650°C	750°C
0	37.9	37.9	37.9	37.9
30	9.54	BDL	BDL	BDL
60	8.24	BDL	BDL	BDL

BDL < 0.01 ppm Hg

Sample 4444-3 Mercury Desorption Data

Elapsed Time in Furnace (min)	Mercury Concentration (ppm)			
	450°C	550°C	650°C	750°C
0	35.3	35.3	35.3	35.3
30	14.4	BDL	BDL	BDL
60	12.3	BDL	BDL	BDL

BDL < 0.01 ppm Hg

Mercury was successfully stripped from both samples at 550°C and higher. However, the mercury was not completely removed from the PAC at 450°C.

CONCLUSIONS

When PAC is exposed to air at elevated temperatures, it clearly starts to physically degrade. This degradation occurs by the partial oxidation of the carbon structure. In order for the proposed process to function properly, the mercury desorption operation must occur in an inert atmosphere such as nitrogen, argon or helium.

As evidenced by the testing performed on virgin PAC and PAC that was thermally cycled 10 times to simulate multiple passes through the mercury desorption operation, the sorption characteristics of the cycled PAC remained unchanged in comparison the virgin PAC.

Whether it was the synthetically loaded PAC or the SITE sample, the attached mercury is able to be desorbed from the PAC to levels less than 0.01ppm. The SITE sample required temperatures in excess of 500°C for 30 minutes during the desorption operation. Since the boiling points of mercury and mercury chloride are below 450°C, it can be surmised that an active binding agent exists in the SITE PAC. This could occur if other halogens (such as Fluorine) existed in the flue gas.

The envisioned process is technically viable when the thermal desorption operation occurs under the following parameters:

- Inert atmosphere during elevated temperature processing;
- 550°C desorption temperature; and
- 30 minutes of retention at temperature.

SECTION 2
BID PACKAGE

PURPOSE AND SCOPE

The purpose of this section is to generate a bid package that would enable a reputable engineering firm to cost out the procurement and installation of a pilot-plant within 20% of the actual cost.

The following items were produced as part of the bid package:

- Mass Balance
- Process Flow Diagram (PFD)
- Equipment List
- General Arrangement Drawing
- Elevation Drawing
- Process and Instrumentation Diagrams (P&IDs)

A budgetary economic evaluation was also produced to compare this process to single-pass injection, collection and disposal options.

MASS BALANCE

The mercury control system that is installed at Alabama Power E.C. Gaston[1] was used as the baseline case for the mass balance. Other criteria used as the basis for the mass balance include:

- 270 MW boiler
- 80% boiler capacity factor
- 1,000,000 acfm of flue gas to the COHPAC (baghouse)
- 80% mercury removal efficiency
- 1.5 lbs of PAC per MMacf of flue gas
- 6,700 operating hours per year
- $0.50 per pound of virgin PAC
- 20% PAC bleed rate
- 1.15 COHPAC loading factor

The mass balance and PFD was produced using the data produced in SECTION 1 along with the baseline case and basis points.

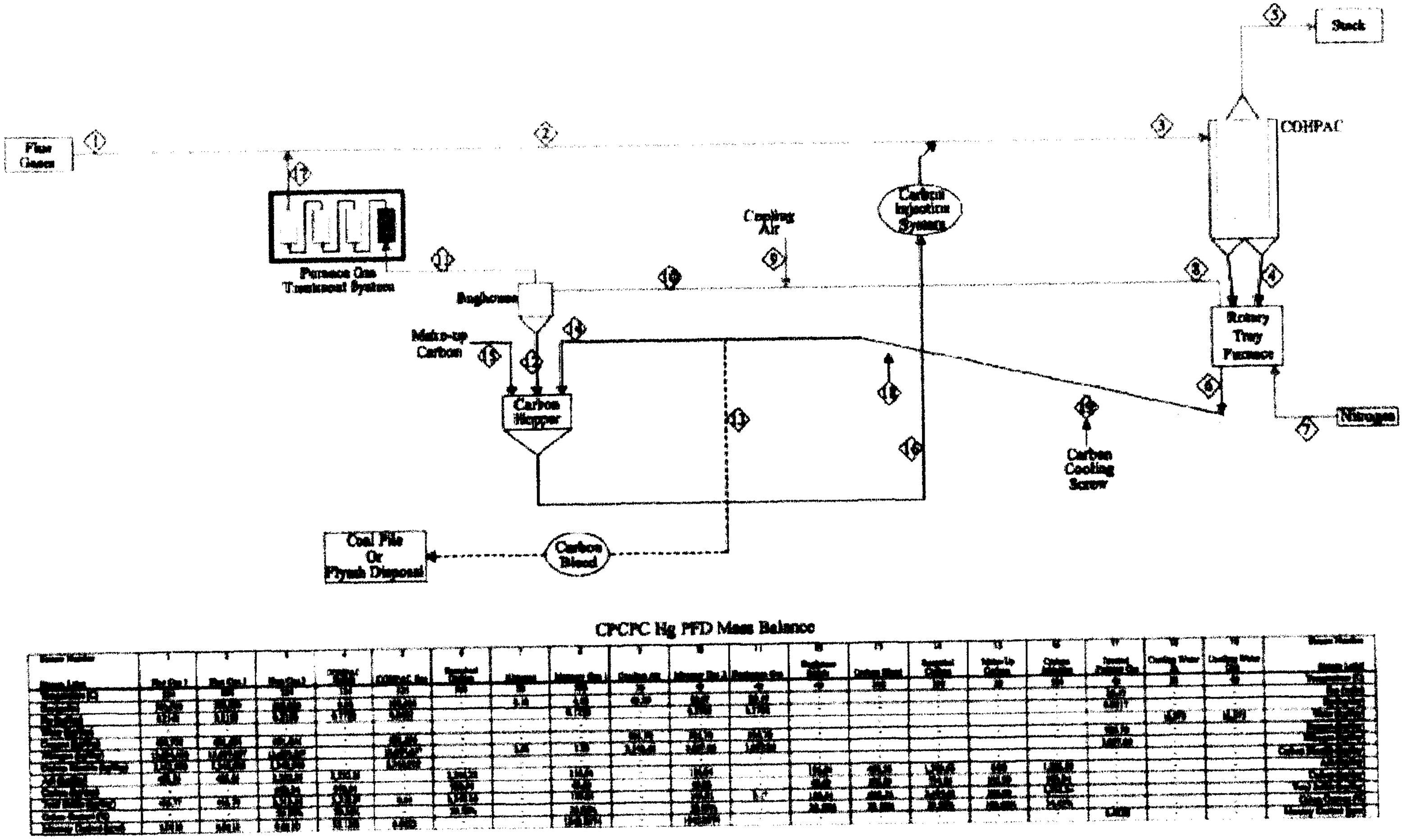

PITTSBURGH MINERAL AND ENVIRONMENTAL TECHNOLOGY	DWG NO.
PROJECT: CPCPC Hg PFD	05
DATE: MARCH 10, 2004 REVISION: DRAWN BY: MRP	

To aid in the viewing of this document, the following enlargement of the mass balance is included.

Stream Number Stream Label	1 Flue Gas 1	2 Flue Gas 2	3 Flue Gas 3	4 COHPAC Solids	5 COHPAC Gas	6 Desorbed Carbon
Temperature (C)	124	124	124	124	124	550
Gas (acfm)	500,000	500,089	500,089	0.00	500,089	-
Hg (kg/day)	0.2142	0.2160	0.2160	0.1728	0.0432	-
Water (kg/day)	-	-	-	-	-	-
Oxygen (kg/day)	600,730	601,656	601,656	-	601,656	-
Nitrogen (kg/day)	13,604,000	13,607,057	13,607,057	-	13,607,057	-
Carbon Dioxide (kg/day)	5,342,900	5,342,900	5,342,900	-	5,342,900	-
Ash (kg/day)	466.56	466.56	2,332.86	2,332.86	-	2,216.22
Carbon (kg/day)	-	-	979.94	979.94	-	930.94
Total Solids (kg/day)	466.77	466.78	3,313.02	3,312.97	0.04	3,147.16
Carbon Content (%)	-	-	29.58%	29.58%	-	29.58%
Mercury Content (ppm)	0.0110	0.0110	0.0110	52.1526	0.0022	-

Stream Number Stream Label	7 Nitrogen	8 Mercury Gas 1	9 Cooling Air	10 Mercury Gas 2	11 Baghouse Gas	12 Baghouse Solids
Temperature (C)	20	550	20	49	49	49
Gas (acfm)	0.18	0.18	89.29	89.47	89.47	-
Hg (kg/day)	-	0.1728	-	0.1728	0.1728	-
Water (kg/day)	-	-	-	-	-	-
Oxygen (kg/day)	-	-	925.70	925.70	925.70	-
Nitrogen (kg/day)	8.38	8.38	3,048.62	3,057.00	3,057.00	-
Carbon Dioxide (kg/day)	-	-	-	-	-	-
Ash (kg/day)	-	116.64	-	116.64	-	116.64
Carbon (kg/day)	-	49.00	-	49.00	-	49.00
Total Solids (kg/day)	-	165.81	-	165.81	0.17	165.64
Carbon Content (%)	-	29.55%	-	29.55%	-	29.58%
Mercury Content (ppm)	-	1042.0374	-	1042.0374	-	-

Stream Number Stream Label	13 Carbon Bleed	14 Recycled Carbon	15 Make-Up Carbon	16 Carbon Injection	17 Treated Furnace Gas	18 Cooling Water In	19 Cooling Water Out
Temperature (C)	200	200	20	184	49	20	40
Gas (acfm)	-	-	-	-	89.47	-	-
Hg (kg/day)	-	-	-	-	0.0017	-	-
Water (kg/day)	-	-	-	-	-	16,376	16,376
Oxygen (kg/day)	-	-	-	-	925.70	-	-
Nitrogen (kg/day)	-	-	-	-	3,057.00	-	-
Carbon Dioxide (kg/day)	-	-	-	-	-	-	-
Ash (kg/day)	466.56	1,749.66	0.00	1,866.30	-	-	-
Carbon (kg/day)	195.99	734.95	195.99	979.94	-	-	-
Total Solids (kg/day)	662.55	2,484.61	195.99	2,846.24	-	-	-
Carbon Content (%)	29.58%	29.58%	100.00%	34.43%	-	-	-
Mercury Content (ppm)	-	-	-	-	0.4338	-	-

EQUIPMENT LIST

Based upon the PFD and mass balance, the following equipment list was generated. It includes all the primary pieces of process equipment.

Description	Utility Requirements	Size	Cost
Rotary Tray Furnace	20 kW, 480V, 3Ø, 100A	Size L	$100,000
Nitrogen Supply System		4 Dewer Manifold	$2,000
Mercury Laden PAC Feeder – Furnace Inlet	2 HP, 480V, 3Ø		$5,000
Rotary Air Lock – Furnace Discharge	2 HP, 480V, 3Ø	6" dia.	$2,500
Desorbed Carbon Cooling Screw Conveyor	5 HP, 480V, 3Ø 3 gpm 20°C water	6" dia., 40 rpm	$5,000
Desorbed Carbon Hopper		300 ft^3	$4,000
Virgin PAC Feeder	2 HP, 480V, 3Ø	2 ft^3	$5,000
Pneumatic Conveying System	30 HP, 480V, 3Ø	3" w/ 250' max run 275 cfm @ 10 psi	$4,000
Blower	3 HP, 480V, 3Ø	2" w/ 300' max run 100 cfm @ 5 psi	$1,500
Baghouse	1 cfm Compressed Air @ 125 psi	50 ft^2	$3,000
Carbon Columns		15 ft3 8.5 sec. of contact time	$5,000
Sub-Total			**$137,000**
Instrumentation			$30,000
Utility Hookups			$20,000
Uninstalled Total			**$187,000**

Since this bid package envisions a pilot-plant with limited life, the equipment is priced based upon used/refurbished equipment. The pricing was obtained from several used equipment dealers across the US.

Pricing for a new rotary tray furnace was provided by Wyssmont (Appendix A). This was obtained to provide the unit specifications for the primary piece of equipment.

GENERAL ARRANGEMENT DRAWING

Once the equipment was specified, it was laid out as if the pilot-plant site had a large (40' x 40') and level plot for installation.

The original CAD drawing is to scale however, to make it fit within the 8.5" by 11" size format the drawing was compressed and is no longer to scale.

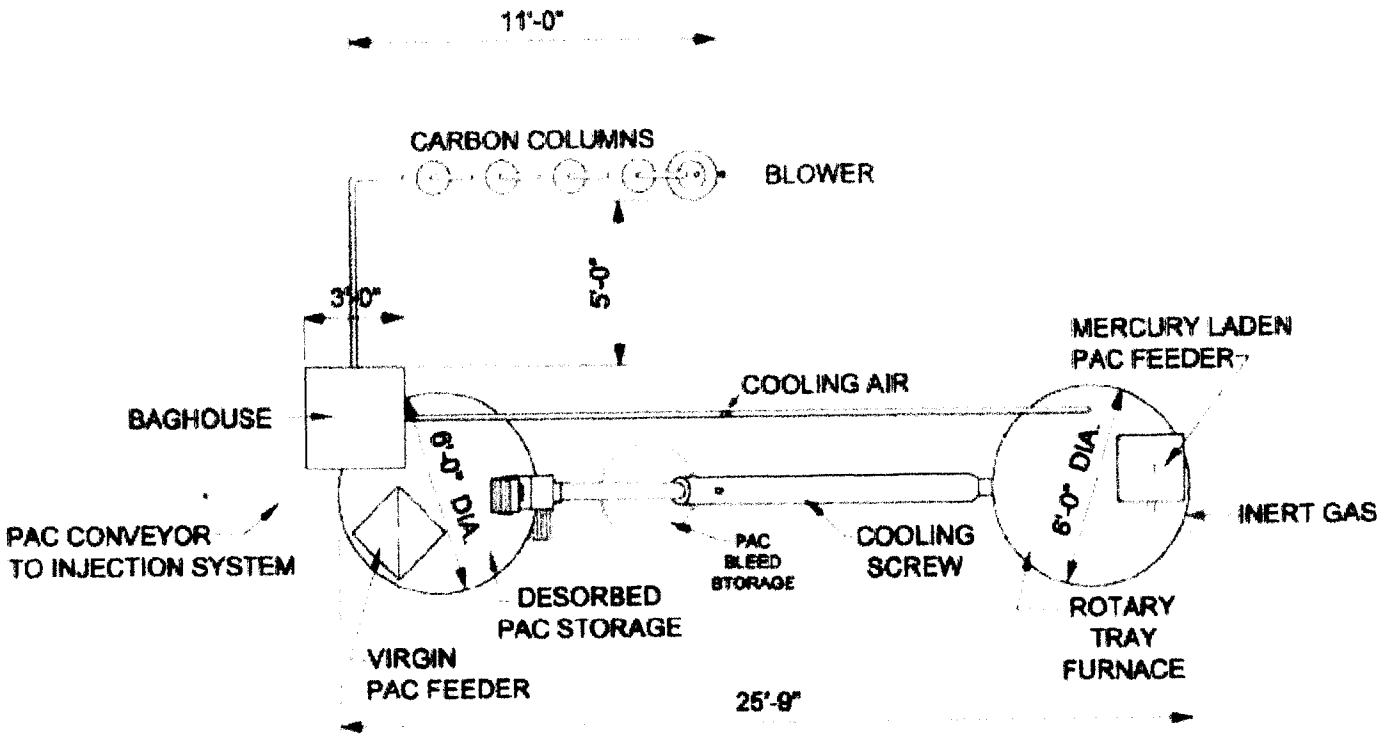

PLAN - PAC DESORPTION / RECYCLING PLANT

SCALE: 1/2" = 1'-0"

PITTSBURGH MINERAL AND ENVIRONMENTAL TECHNOLOGY

DWG NO. 02

PROJECT NO: 03V64

DATE: APRIL 22, 2004

REVISION:

DRAWN BY: MRP

ELEVATION DRAWING

In order to show the elevations of all the pieces of equipment, the elevation drawing arrangement does not match the general arrangement drawing.

The original CAD drawing is to scale however, to make it fit within the 8.5" by 11" size format the drawing was compressed and is no longer to scale.

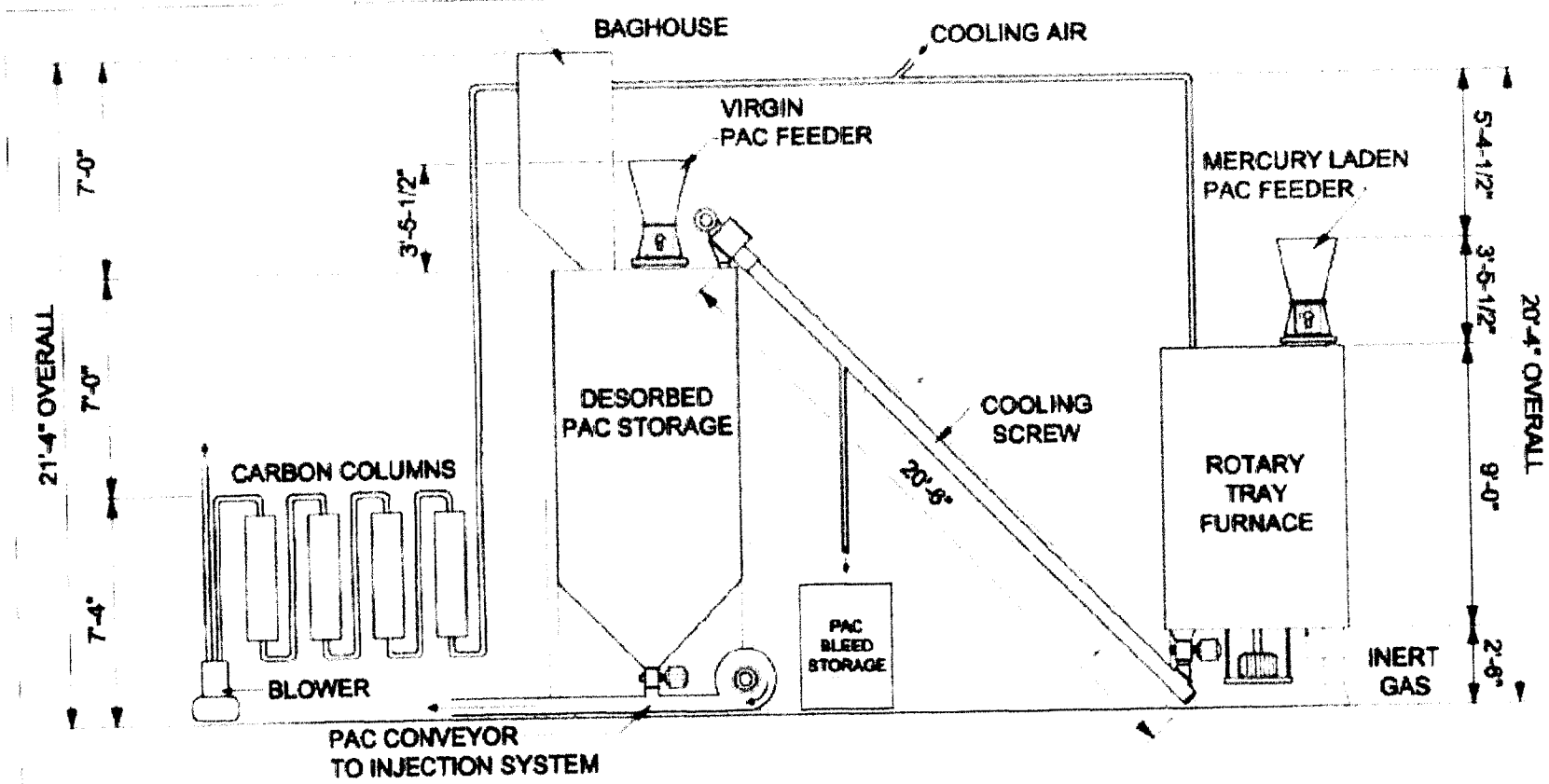

ELEVATION - PAC DESORPTION / RECYCLING PLANT

SCALE: 1/4" = 1'-0"

PITTSBURGH MINERAL AND ENVIRONMENTAL TECHNOLOGY

PROJECT NO: 03V64

DATE: APRIL 12, 2004

REVISION: APRIL 22, 2004 DRAWN BY: MRP

DWG NO. 01

PROCESS AND INSTRUMENTATION DIAGRAMS

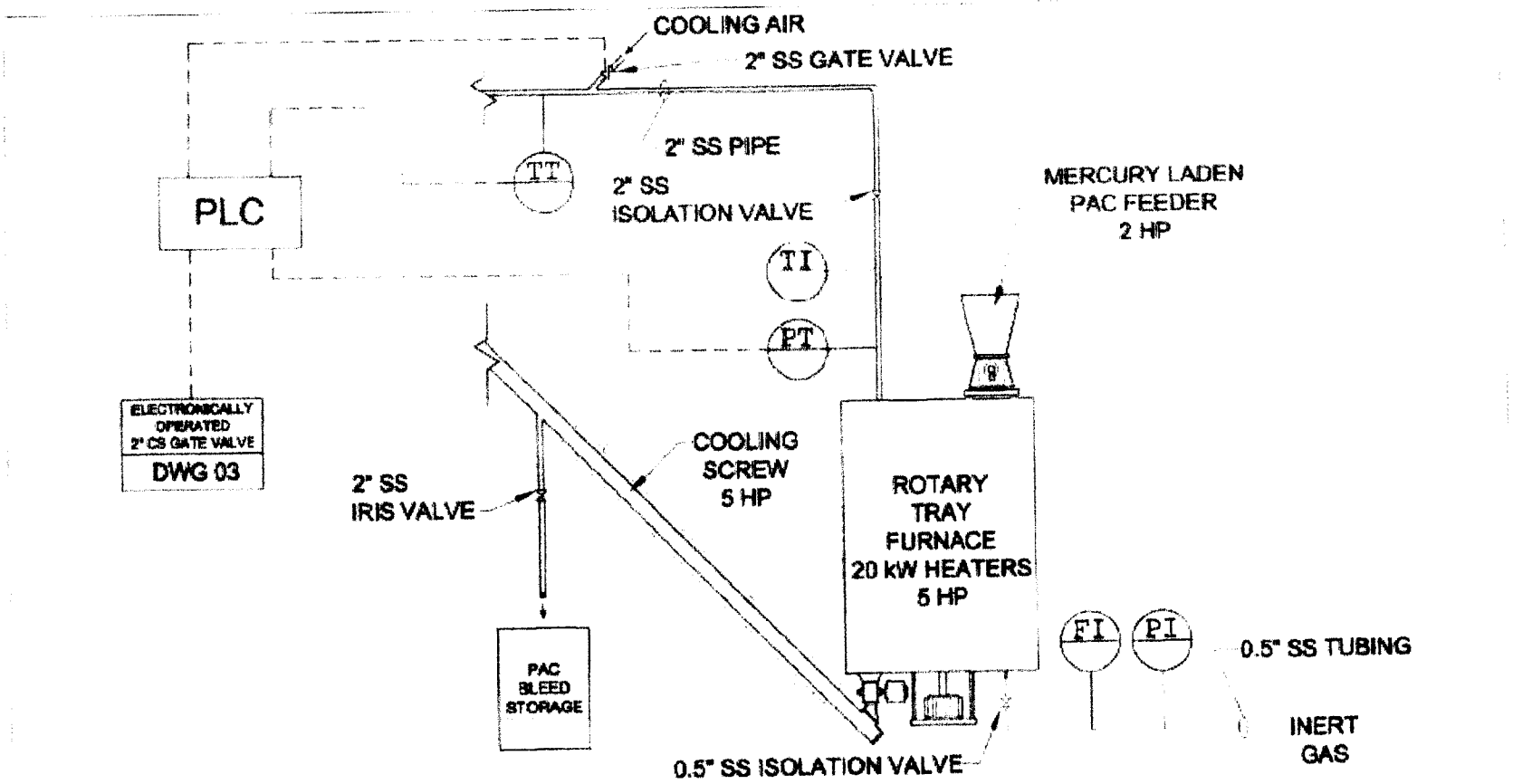

ELEVATION - PAC DESORPTION / RECYCLING PLANT

SCALE: N.T.S.

PITTSBURGH MINERAL AND ENVIRONMENTAL TECHNOLOGY

DWG NO. 04

PROJECT NO: 03V64

DATE: MAY 10, 2004

REVISION: MAY 12, 2004 DRAWN BY: MRP

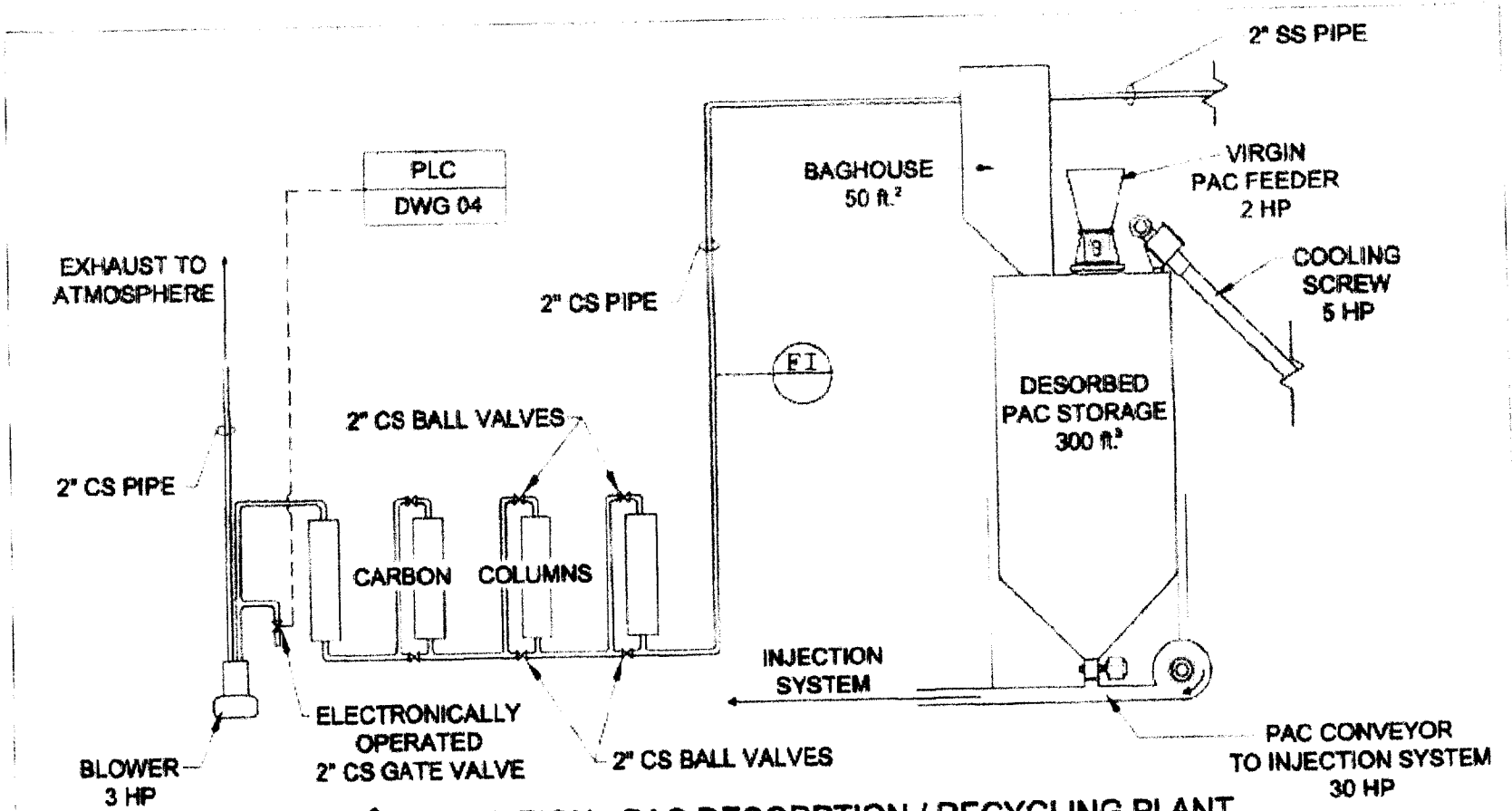

ELEVATION - PAC DESORPTION / RECYCLING PLANT

SCALE: N.T.S.

PITTSBURGH MINERAL AND ENVIRONMENTAL TECHNOLOGY

DWG NO. 03

PROJECT NO: 03V64

DATE: MAY 06, 2004

REVISION: MAY 12, 2004 DRAWN BY: MRP

Based upon the bid package presented in this section and data taken from the Gaston testing final report[1], the following yearly operating costs were derived.

	Dust Carry Over from ESP to COHPAC (gr/acf)	
	0.04	0.01
	Standard ADA System	ADA System With Recycling System
Capital Costs		
COHPAC	$1,000,000	$1,150,000
Injection System	$500,000	$575,000
Carbon Recycling System		$187,000
Sub-Total	$1,500,000	$1,912,000
Yearly Amortization (5 yrs @ 8%)	**$364,975**	**$465,222**
Operating Costs		
PAC	$301,500	$60,300
Labor	$100,500	$100,500
Utilities & Consumables	$25,000	*$50,000*
Consumed PAC Disposal	???	$0
Sub-Total	**$427,000**	**$210,800**
Total (Yearly Costs)	**$791,975**	**$676,022**
	ROI (uninstalled basis)	28.14%

The COHPAC capital cost was estimated utilizing engineering capital cost estimating data. The capital cost of the injection system was taken from the Gaston testing final report[1].

The 1.15 loading factor that was applied to COHPAC and injection system costs. This reflects a 1.15X increase in size of equipment due to the additional volume of carbon and ash that is carried into the COHPAC as a result of an 80% recycle stream.

In order to minimize the loading factor, the dust carry over value was deceased to the lowest value achieved during testing of the Gaston COHPAC (0.01 gr/acf). Normal operations require the dust carry over value to be <0.04 gr/acf.

It is assumed that with a sufficient level of automation, the same manpower could run both systems as easily as one.

Return On Investment (ROI) was calculated using the following method:

Savings in Yearly Operating Costs / Increase in Capital Required

This cost analysis does not include any installation costs, as the Gaston testing final report[1] did not include any installation costs for the injection or COHPAC systems.

It should be noted that this budgetary economic evaluation does not include any cost to dispose of the consumed PAC from the standard ADA mercury control system. This cost could range from $12/ton[2] (fly ash) to $1,200/ton[2] (mercury containing hazardous waste). This could result in an additional $360,000 in yearly operating costs. 181

In utilizing the PAC recycling system, the mercury is removed from the PAC prior to the bleed point which allows the spent PAC to be used for fuel value in the boiler avoiding all disposal costs.

CONCLUSIONS

The loading factor value is very sensitive to the fine ash carry over. It is extremely important that the ESP's are operating at maximum capacity so that the COHPAC, injection system and PAC desroption/recycling systems are not over loaded with material. Ultimately this will affect the process economics as the loading factor increases the size and cost of the systems.

Use of the PAC desorption/recycling system will decrease the yearly operating costs by $216,200. The capital required to install the PAC desorption/recycling system will be paid for in less than four years.

If mercury contaminated PAC is disposed of as hazardous waste, there is some future concern with regard to liability. There are numerous examples of instances when mercury containing materials were disposed of using the guidelines for that period of time; however as time passed the guidelines changed resulting in landfills that are now tagged as "Superfund" sites. Some of the parties responsible for the generation of the material that resides in those landfills are now liable for damages and/or cleanup costs. Use of the PAC desorption/recycling system removes all mercury liability from the spent PAC.

1. C. Bustard, S. Sjostrom, S. Renninger, L. Monroe Ph.D., R. Miller, R. Chang Ph.D. "Full-Scale Evaluation of Mercury Control with Sorbent Injection and COHPAC at Alabama Power E.C. Gaston". www.adaes.com/publications/Gaston Paper Final 2001-30-02.pdf, January 30, 2002.

2. L. Monroe, J. Cichaniwicz, G. Offen. "UARG Comments on Process Inputs for EPA's Planned IPM Modeling Runs". www.epa.gov/ttnatw01/combust/utiltox/uarg ipm comments.doc, April 19, 2002.

APPENDIX A

Wyssmont ™ Company, Inc.

Process Engineers: drying, sublimation, cooling, calcining, gas-solids reaction.

1470 Bergen Boulevard
Fort Lee, NJ 07024-2197

Phone: (201) 947-4600
Fax: (201) 947-0324
E-mail:sales@wyssmont.com
www.wyssmont.com

February 19, 2004

PMET
700 Fifth Avenue
New Brighton, PA 15066

Attention: Mr. Dale Nickels
e-mail: dale@pmet-inc.com

Reference: Heat-Treating Activated Carbon
in the Wyssmont System
Our Reference Number B02206

Dear Dale:

Thank you for your interest in our equipment.

This is and ideal application for our equipment. Our TURBO-HEAT-TREATER• can uniformly vaporize the Mercury in the feed material.

The Wyssmont TURBO-DRYER operates continuously and almost always gives the lowest operating cost per pound of product when all costs are considered. Please refer to the attached letter of additional benefits of the TURBO-DRYER.

The benefits of the TURBO-HEAT-TREATER for this application include:

- **Excellent product quality and uniformity**. The material bed is turned over gently after each transfer. This continuous mixing and levelling, along with the close temperature control and controlled residence time assure the highest product quality and uniformity.

- **Gentle handling and low exhaust velocities minimize particle attrition and dust carryover.** This is one of the many advantages of the TURBO-HEAT-TREATER compared to high air flow units such as flash, fluid or rotary units.

- **Flexibility.** The unit can handle materials with a wide range of handling characteristics – from sludges and pastes through filter and centrifuge cakes to pellets and powders. For even the wettest material, backfeed is seldom required. Easily adjustable drying parameters allow for handling different moisture levels. Upstream upsets that can cause heat transfer surfaces to foul, hot spots, and consequent process problems are eliminated with a TURBO-HEAT-TREATER.

- **Easy automatic operation.** It is self-compensating for variations in the feed rate. The system can be operated at 20-25% of capacity up to the maximum without requiring changes by the operator – the heat-treater automatically adjusts for this amount of change and produces the same product quality – unlike other dryers. Most users say they "turn it on and forget it."

Mechanically, the unit offers the following advantages:

1. **Reliable, continuous and automatic operation.** Our units are famous for extended periods of operation without shutdown for maintenance.

2. **Low Maintenance Costs**. Usually the annual maintenance costs are less than 1% of the initial capital cost.

3. **Low Horsepower Requirements**. The unit has low horsepower requirements. This further reduces operating costs.

We are pleased to submit our preliminary design based on the information you provided.

Product Rate	140 kg/hr
Mercury in Feed	0.004%
Retention Time, minutes	30

TURBO-HEAT TREATER Size L

Dimensions	
Diameter, ft.	6
Height, ft.	9
Horsepower Requirements	
TURBO-TURBO-Fans	½
Tray System	½
Approximate Price*	$275,000. - $300,000.

*Type 316 stainless steel for all interior parts, designed for operation at 550°C.

We have included an internal electrical heating system with a small (5-10cfm) of inert gas to remove the mercury vapor from the system. This small exhaust stream can then be processed in your mercury recovery system.

PMET
New Brighton, PA

February 19, 2004

Control instrumentation which includes two-station temperature control and local panelboard will cost approximately $25,000. We have not included a PLC in this control package. Generally our system does not require a separate PLC. If you can incorporate our system in another PLC most of the items in our control package can be eliminated. We can then provide temperature sensors, damper operators and SCR controller.

A Multiple Screw Feeder→ Model MSF-836 can be provided to meter the feed into the dryer and spread the feed across the top shelf. In type 316 Stainless Steel construction with variable speed drive the cost is approximately $18,000.

We can also recommend a discharge airlock to seal the product discharge. In type 316 Stainless Steel with drive the cost is approximately $8,000.

We are very proud of our excellent reputation throughout the industry. Over the last twenty (20) years in CHEMICAL ENGINEERING MAGAZINE Research Reports, in which thousands of chemical engineers were polled, Wyssmont was cited as the most preferred supplier of dryers by more than a 2:1 margin.

We look forward to working with you on this project. If you have any questions please do not hesitate to contact us or our local representative, Mr. Kirk Marker.

Very truly yours,

WYSSMONT COMPANY, INC.
Joseph Bevacqua

Joseph Bevacqua
Vice President – Sales

JB/jt
Enc: Process Letter

cc:Daco Technical Sales
P. O. Box 527
Morgan, PA 15064-0527
412-257-1810

FINAL TECHNICAL PROGRESS REPORT

SUBMITTED TO

CONSORTIUM FOR PREMIUM CARBON PRODUCTS FROM COAL

The Pennsylvania State University
407 Academic Activities building
University Park, PA 16802-2398

NOVEL ANTHRACITE SORBENTS FOR CO_2 CAPTURE

Reporting Period Start Date: *March 1, 2003*
Reporting Period End Date: *February 29, 2004*
Principal Authors: *Dr. M. Mercedes Maroto-Valer, PI*
Dr. Zhong Tang

Report Issued Date: *July 15, 2004*

DOE Award number: *DE-FC26-98FT40350*

Internal Agreement Number: *2484-TPSU-DOE-0350*

Submitting Organization: *The Energy Institute*
The Pennsylvania State University
405 Academic Activities Building
University Park, PA 16802-2398
Phone: (814) 863 8265

DISCLAIMER

FINAL TECHNICAL PROGRESS REPORT

March 1, 2003 – February 29, 2004

Table of contents

Abstract

Anthracites have inherent chemical properties, fine pore structure and relatively low price that makes them excellent raw materials for the production of premium carbon products, such as for the synthesis of CO_2 sorbents. The President's Global Climate Change Initiative commits to reduce greenhouse gas intensity by 18% over the next ten years. However, the costs of current CO_2 separation and capture technologies are estimated to be about 75% of the total cost of ocean or geological sequestration. Furthermore, the demand to develop revolutionary direct capture technologies has also been identified by the U.S. DOE. Accordingly, the objective of this project was to synthesize high-surface-area powdered anthracites and impregnate them with amine compounds. The feasibility of using these materials for CO_2 capture was investigated.

Three Pennsylvania anthracites (PSOC-1468, AFM 800 and AFM 2600) were selected for this work. PSOC-1468 was obtained from the Penn State Coal Bank, and AFM 800 and AFM 2600 were provided by FB Leopold. A parametric study was conducted to ascertain the effect of time and temperature on the porous structure of activated carbons produced from anthracite. A lab scale fluidized bed reactor was used for the activation. The N_2-77K isotherms show that the activated anthracites have highly developed microporosity and a small amount of mesopores. The surface area can get up to 792m^2/g with 3 hours activation time. However, extending the activation time beyond 3 hours decreases the surface area. Regarding the activation temperature effect, it has been shown here that the surface area and pore volume of the activated anthracite increased first going from 800 to 850°C, where the sample activated at 850°C has a surface area and volume of 927.9m^2/g and 0.442mL/g, respectively. However, when increasing the activation time to 890°C resulted in a decrease of both surface area and pore volume. Moreover, the anthracite activated at the lowest temperature (800°C0 has the largest CO_2 adsorption capacity, probably due to its narrow pore structure. The surface areas go through a maximum with increasing solid yields.

The adsorption capacity of the activated anthracites decreases rapidly with increasing adsorption temperature, probably due to the adsorption being a physisorption process. The anthracite with the highest CO_2 adsorption capacity was the sample activated at 800°C for 2 hours, whose surface area was only 540m^2/g, and the adsorbed amount of CO_2 was 65.7mg-CO_2/g-adsorbent. This is probably due to a relationship between microporosity and CO_2 physisorption processes. Several surface treatment methods, including NH_3 heat treatment, HNO_3 oxidization and polyethylenimine (PEI) impregnation, were used to modify the surface properties of the activated anthracites in an attempt to increase their CO_2 capture capacity at higher temperatures. The surface treatment methods investigated changed the porous structure and surface chemistry of the anthracites, and therefore, affected their CO_2 capacities. No significant difference was observed between the adsorption capacities of the three anthracites (PSOC-1468, AFM 800 and AFM 2600) investigated in this work.

List of tables

List of figures

1. INTRODUCTION

1.1. Rationale

Anthropogenic emissions have increased the CO_2 concentration on the atmosphere with over 30% compared to pre-industrial levels [1]. Most of these anthropogenic emissions are caused by fossil fuel utilization, where around one-third is due to electricity generation from fossil fuel combustion, mainly coal-fired units. Furthermore, fossil fuel electricity generation units rank as the first target to reduce anthropogenic emissions due to their stationary nature. However, the costs of current CO_2 separation and capture technologies are estimated to be about 75% of the total cost of ocean or geological sequestration, including the costs for compression to the required pressure for subsequent sequestration [2]. For instance, for a pulverized coal power plant, the estimated capture costs are \$35-\$264/ton of CO_2 with a power cost increase of 25-215 mills/kWh. Consequently, there is a demand to develop revolutionary "direct capture" technologies. New solid-based sorbents are being investigated, where the amine groups are bonded to a solid surface, resulting in an easier regeneration step [3, 4]. The supports used thus far, including commercial molecular sieves and activated carbons, are very expensive and hinder the economical viability of the process. Accordingly, there is a need to find low-cost precursors that can compete with the expensive commercial supports, and develop effective solid sorbents that can be easily regenerated, and therefore, have an overall lower cost over their lifetime performance.

Anthracites contain mostly carbon (92–98%) present in large polycyclic aromatic sheets, resulting in a highly ordered structures with a high ultra-microporosity [5]. Due to their

inherent chemical properties, fine porosity and relatively low price, significant opportunities exist for the non-fuel uses of anthracites, especially as sorbents precursors. Furthermore, previous studies have shown that being able to produce an activated carbon with high surface area and pore volume, while maintaining the pore volume in a narrow pore range, may prove to make the best activated carbons, as it is the case for anthracites.

Activated carbons are sorbents with a highly developed porosity, especially micro- and mesopores, that are used in a wide range of household, medical, industrial, military and scientific applications, including gas-phase and liquid-phase processes [6]. The activation process together with the intrinsic nature of the precursors strongly determines the characteristics of the resulting activated carbons. Activated carbons can be produced from different precursors, including coals of different rank, and lignocellulosic materials, by physical or chemical activation processes [7-12]. Recently, increasing attention has been focused on using anthracites as feedstock for activated carbons, due to their inherent chemical properties, fine structure and relatively low price that make them excellent raw materials for the production of activated carbons with highly developed microporosity [13-18].

The porous structure (surface area and pore size distribution) and surface chemistry control the adsorption properties of the activated carbons in traditional applications like water filtration and air purification [6]. Similarly, the CO_2 adsorption capacity of activated carbons is a function of their pore structure and surface chemistry properties. It has been reported that the CO_2 adsorption capacities of activated carbons decrease with increasing adsorption

temperature due to the physical nature of the adsorption process [4]. Therefore, different surface treatments have been developed to improve the CO_2 adsorption capacity of activated carbons. For example, it has been shown that the CO_2 capture capacity can be increased by introducing nitrogen functional groups on the surface either by NH_3 heat treatment or chemical impregnation [19, 20, 21]. Previous work has focused on applying these treatments to high surface area materials, like commercially available activated carbons and zeolites, and to a lesser extent fly ash carbons [19, 20, 21]. The authors have previously shown that high surface area activated carbons can be produced from anthracite by steam activation [15, 18]. Unfortunately, the use of anthracites as precursors for adsorbent materials is being under-exploited, probably due to the limited number of studies assessing the possible routes for their conversion into activated carbons.

1.2. Program objectives

The overall objective of this research program is to develop low-cost, high-surface- area, amine impregnated powdered anthracites and test their possible use for CO_2 capture. The sorbents developed here will satisfy the need to develop revolutionary "direct capture" technologies, as identified by the U.S. Department of Energy. The outlook for the activated carbon market is for continued growth, as increasing stringent environmental requirements drive both developed and developing regions to incorporate activated carbons into water and air treatment systems. One of the applications that could increase dramatically the market volume is for CO_2 capture, due to the large volumes that need to be adsorbed. Therefore, this project could open a huge market for the anthracite industry. It is anticipated that the proposed sorbents will have significant performance and cost savings benefits over other

solid sorbents used for CO_2 capture. Furthermore, the anthracite precursors selected for this study are lower cost materials than other proposed sorbent supports, like zeolites.

1.3. Research design and tasks

This research program can be divided into the following three tasks described below.

- Task 1: Procurement and characterization of anthracites. In this task, a series of Pennsylvania anthracites provided by F.B. Leopold Co. Inc., were procured. It is anticipated that around 4 samples from different Pennsylvania coal seams will be included in this study. The sample selection will be conducted on basis of the chemical properties, including ash and volatile matter. The samples were prepared by F.B. Leopold Co. Inc to different particle sizes. The anthracites were then characterized by Penn State University using a customary suite of coal analyses.

- Task 2: Development of anthracite based sorbents. The samples were activated using the protocol previously developed by the authors [15, 18]. This protocol includes a one-step activation process using a system that consists of a stainless steel tube reactor and a vertical tube furnace. The anthracite samples were activated under a wide range of controlled operating variables in order to establish the optimum route for the generation of activated anthracites with properties similar to commercial zeolites and activated carbons (i.e. surface area >1,000m^2/g). The porous structure (micro-, and mesopores) was characterized using N_2 adsorption isotherms. The activated anthracite samples were then amine impregnated using alcohol amines by immersing them in an amine solution.

- Task 3: Capture of CO_2 by anthracite-derived sorbents. The samples prepared under Task 2 were tested as possible sorbents for CO_2 capture. The sorbents performance was

determined for CO_2 adsorption and desorption using a TGA analyzer. The adsorption was reported as mg CO_2/g sorbent. The CO_2 sorption/desorption capacities of the prepared activated sorbents were compared to those of commercial sorbents.

2. EXPERIMENTAL

2.1. Task 1: Procurement and characterization of anthracites

F.B. Leopold and Penn State University initially identified eight Pennsylvania anthracite samples for this work. These samples were selected from a suite of seventeen Pennsylvania anthracite samples. The selection criteria included ash and volatile matter content and rank. The samples present ash contents between 7.45 to 16.27, and volatile matters (daf) between 4.0 to 10.1. Furthermore, the suite selected includes four anthracites (HS, JED, LCN, CC and COL) and three semi-anthracites (7300, MB and 8800). The characterization analyses included proximate and porous texture analysis (Section 2.2.3).

2.2. Task 2: Development of anthracite-based CO_2 sorbents

2.2.1. Steam activation

Three Pennsylvania anthracites (PSOC-1468, AFM 800 and AFM 2600) were selected for the activation studies. PSOC-1468 was obtained from the Penn State Coal Bank and AFM

800 and AFM 2600 were provided by FB Leopold. For the activation experiments, the anthracite was first grounded and screened, and the sample with particle size between 150-250μm was used for steam activation.

A fluidized bed reactor was used for the activation experiments, as shown in Figure 1. The activation temperature was between 700-850^{o}C, and the steam concentration was 65.8% in the feeding gas stream. The stainless steel reactor was the most important part of the system, which was heated by a vertical furnace that has a 3.5" inside diameter. The reactor was designed to withstand temperatures up to 1100ºC. The versatility of the design allowed the use of different particle size, activating agent, heat treatment, residence time, flow rate of activation agent and amount of sample.

2.2.2. CO_2 sorbent preparation

Several surface treatment methods, including NH_3 heat treatment, HNO_3 oxidization and PEI impregnating, were selected to modify the surface properties of the activated anthracite produced from PSOC-1468. The effect of the surface treatment on the CO_2 capture capacity of the activated anthracites was investigated. The activated anthracite samples used for this study include: AC-850-3 (PSOC-1468 activated at 850^{o}C for 3 hours), AC-850-2 (PSOC-1468 activated at 850^{o}C for 2 hours) and AC-890-3 (PSOC-1468 activated at 890^{o}C for 3 hours).

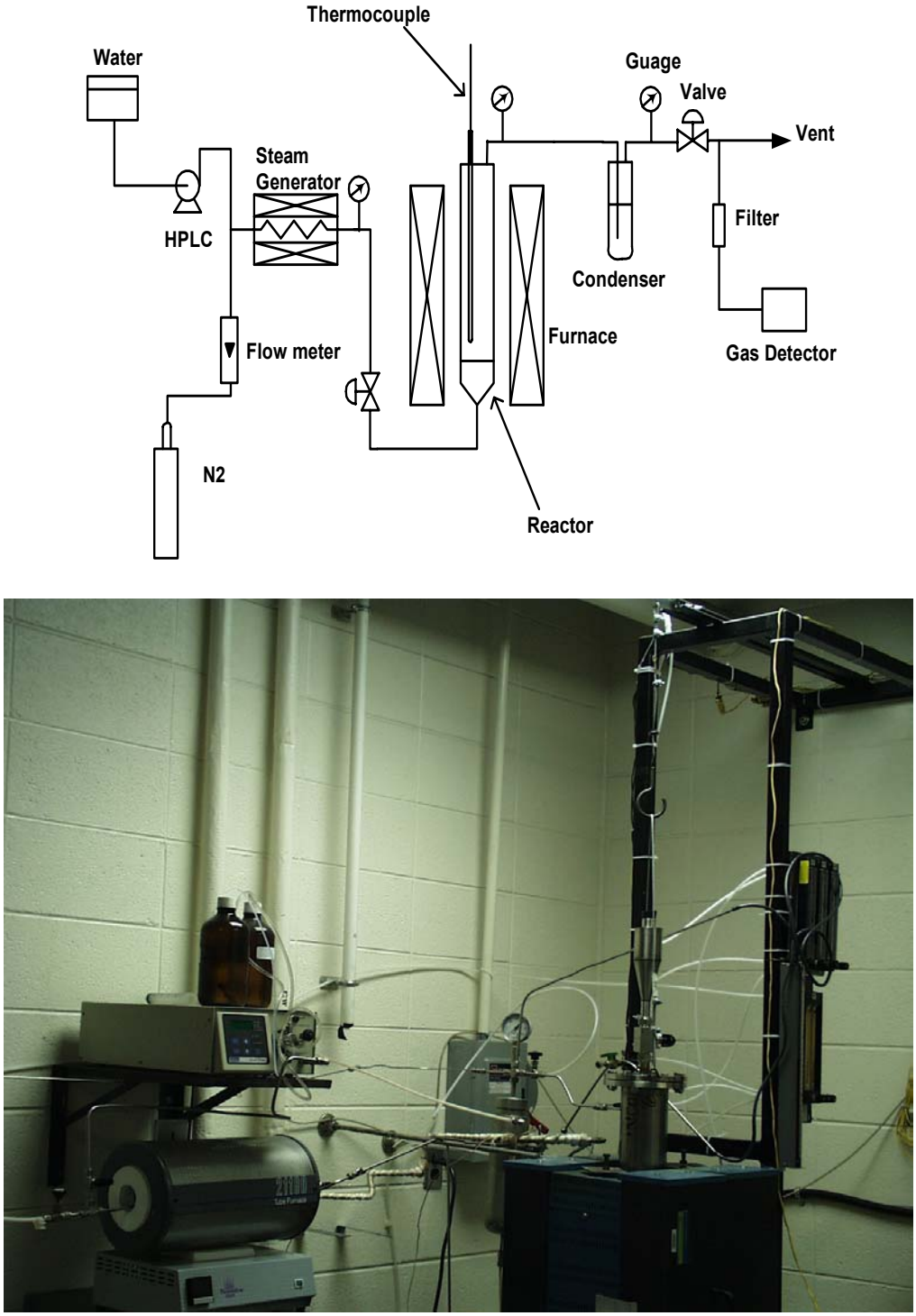

Figure 1. Diagram and picture of the activation system used for this work.

2.2.2.1 NH_3 treatment

AC-850-3 was used for this treatment. A known amount of AC-850-3 was put into a quartz boat that was placed in the middle of a horizontal tube furnace. NH_3 gas was then introduced, while the furnace was heated up to desired treatment temperature. After the furnace was held at the set temperature for 90 minutes, the NH_3 gas was switched to argon and the furnace was cooled down. The sample was removed from the reactor tube at room temperature. The produced samples were labeled as AC-850-3-NH_3-xxx, where the last three digits of the sample name indicate the treatment temperature.

2.2.2.2 HNO_3 treatment

For this treatment, 3 g of AC-850-2 was put into 100mL 5N HNO_3 solution. The sample was oxidized in boiling nitric acid for 5 hours, and then filtered and washed with de-ionized water till the pH of the filtrate was around 7. The treated sample was dried at 110^{o}C for overnight, and labeled as AC-850-2-HNO_3.

2.2.2.3 Amine impregnation

The AC-850-3 and AC-890-3 samples were impregnated with a PEI (polyethylenimine) in methanol solution (30wt%) and then dried in a vacuum oven at 75^{o}C overnight. The resultant samples were labeled as AC-850-3-PEI and AC-890-3-PEI.

2.2.3. Sorbent characterization

The porosity of the samples was characterized by conducting N_2 adsorption isotherms at 77K using a Quantachrome adsorption apparatus, Autosorb-1 Model ASIT (Figure 2). The total pore volume, V_t was calculated from the amount of vapor adsorbed at relative pressure of 0.95, and the total surface area S_t was calculated using multi-point BET equation in the relative pressure range 0.05-0.35. The pore sizes 2nm and 50nm were taken as the limits between micro- and mesopores and meso- and macropores, respectively, following the IUPAC nomenclature [22]. The mesopore size distribution was calculated by the Barrett-Joyner-Halenda (BJH) method. The micropore size distribution was calculated by density functional theory (DFT) method.

Figure 2. Quantachrome adsorption apparatus, Autosorb-1 Model ASIT.

A Kratos Analytical Axis Ultra XPS was used to study the surface chemistry of the modified activated anthracites. XPS quantification was performed by applying the appropriate relative sensitivity factors (RSFs) for the Kratos instrument to the integrated peak areas. These RSFs take into consideration the X-ray cross section and the transmission function of the spectrometer. The X-ray source is monochromatic aluminum (1486.6 eV) and the X-ray power is 280 Watts. The approximate sampling depth under these conditions is 25Å. The C-C in carbon 1s at 284.4eV was selected for the charge correction.

2.3. Capture of CO_2 by anthracite sorbents

The adsorption and desorption performance of the produced activated anthracites was conducted using a PE-TGA 7 thermogravimetric analyzer, shown in Figure 3. The weight change of the adsorbent was followed to determine the adsorption and the desorption performance of the activated anthracites. In a typical adsorption/desorption process, about 20-25mg of the sample was placed in a small platinum pan, heated to 100^{o}C in N_2 atmosphere at a flow rate of 100mL/min, and held at that temperature for 30 minutes. The temperature was then adjusted to the desired adsorption temperature and 99.8% bone-dry CO_2 adsorbate was introduced at a flow rate of 100mL/min. After adsorption, the gas was switched to 99.995% pure N_2 at a flow rate of 100mL/min to perform desorption at the same temperature. Adsorption capacity in mg-adsorbate/g-adsorbent and desorption capacity in

percentage were used to evaluate the adsorbent, where these values are calculated from the weight change of the sample in the TGA adsorption/desorption process.

Figure 3. Picture of the PE-7A TGA apparatus used for the CO_2 studies.

3. RESULTS AND DISCUSSION

3.1. Task 1: Procurement and characterization of anthracites

Table 1 shows the proximate analysis result of the three samples investigated. AS expected for anthracites, the volatile mater content is low (<5%). These samples were also selected due to their low ash content.

Table 1. Proximate analyses of the anthracite samples studied

Name	Moisture	Ash	Volatile	Fixed carbon daf*
PSOC-1468	4.51	6.83	3.65	96.9
AFM 800	5.04	6.43	3.36	97.0
AFM 2600	4.58	9.73	4.64	95.9

* Calculated based on ASTM D 388-99

3.2. Task 2: Development of anthracite-based CO_2 sorbents

It is known that the activation conditions, time and temperature, as well as the properties and structure of the precursor affect the porous structure of the resultant activated carbons [13, 23, 24]. Accordingly, a parametric study was conducted to ascertain the effect of time and temperature on the porous structure of activated carbons produced from anthracite.

3.2.1 Effect of activation time on the porosity of the activated anthracites

For this study, the anthracite PSOC-1468 was selected. The activation temperature was first selected at 850^{o}C according to previous studies conducted by the authors [15]. The typical isotherms of the resultant activated carbon with different activation time are shown in Figure 4. For comparison, the isotherm of the raw sample (PSOC-1468) is also presented in Figure 4.

Figure 4 shows that the activation dramatically increases the surface area and pore volume of the anthracite. All the isotherms of ACs are Type I according to the BDDT (Brunauer, Deming, Deming, Teller) Classification [25]. This indicates that the AC made from anthracite has many micropores and only a few mesopores. With increasing activation time, the isotherm shows a more open knee at lower relative pressure of the isotherm, indicating a broader pore size distribution with larger micropores and increasing mesoporosity.

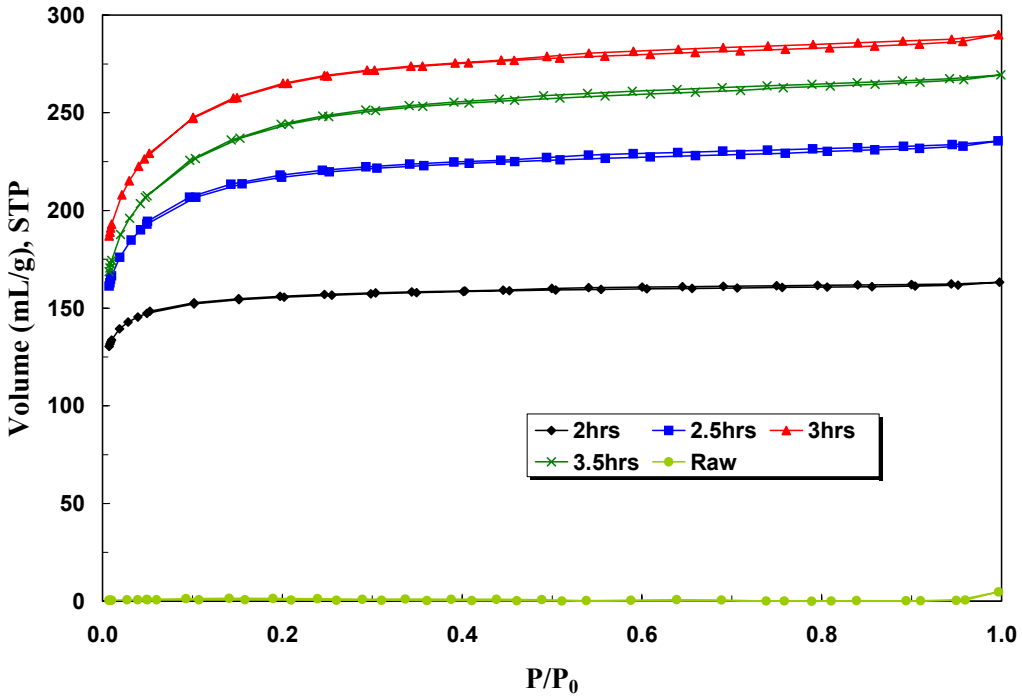

Figure 4. N_2-77K isotherms of the raw anthracite (PSOC-1468) and its steam activated carbons produced at 850°C

Figures 5 and 6 show the micropore and mesopore size distribution of the activated anthracites that were activated at 850°C with different activation time, respectively. It can be seen that there are no micropores and few mesopores for the raw anthracite. In contrast, after activation, there is a significant amount of mesopores in the activated anthracites (Figure 5 and Figure 6). For the activated anthracite after 2 hours activation time, there is a large peak between 0.4-1.0nm. For the anthracites produced after 2.5 and 3.0 hours activation time, the peak between 0.4-1.0nm is still there, and there are some additional peaks at 1.6 and 2.0 nm, and also a peak at 2.4nm for the anthracite sample produced after 3 hours steam activation. Furthermore, for the sample produced after 3 hours activation time, the largest peak moves to 1.2nm, and the height of the peaks at 1.6, 2.0 and 2.4nm increases. Due to technical

limitations of the instrument, it is not possible to get adsorption data at very low relative pressure, and therefore the pore size distribution < 0.4nm cannot be calculated by the DFT method. However, the results indicate that the pore development during activation includes pore opening followed by pore enlargement.

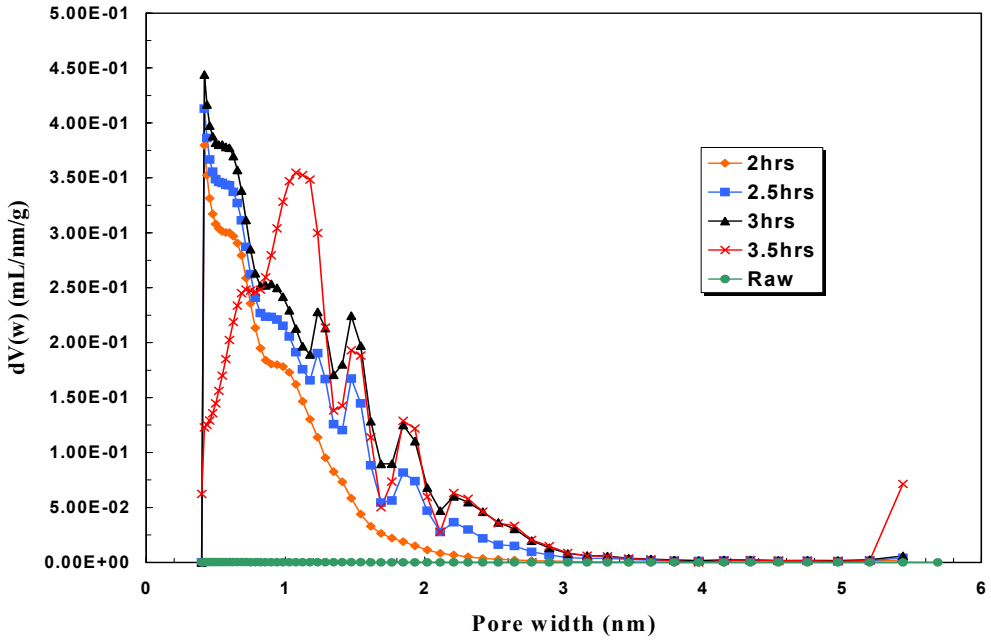

Figure 5. Micropore size distribution by DFT method of the raw anthracite (PSOC-1468) and its steam activated carbons produced at 850°C

Figure 6 shows that all the activated anthracites with different activation time have the same mesopore distribution profile. This indicates that the anthracites activated at 850°C have similar mesoporous structure.

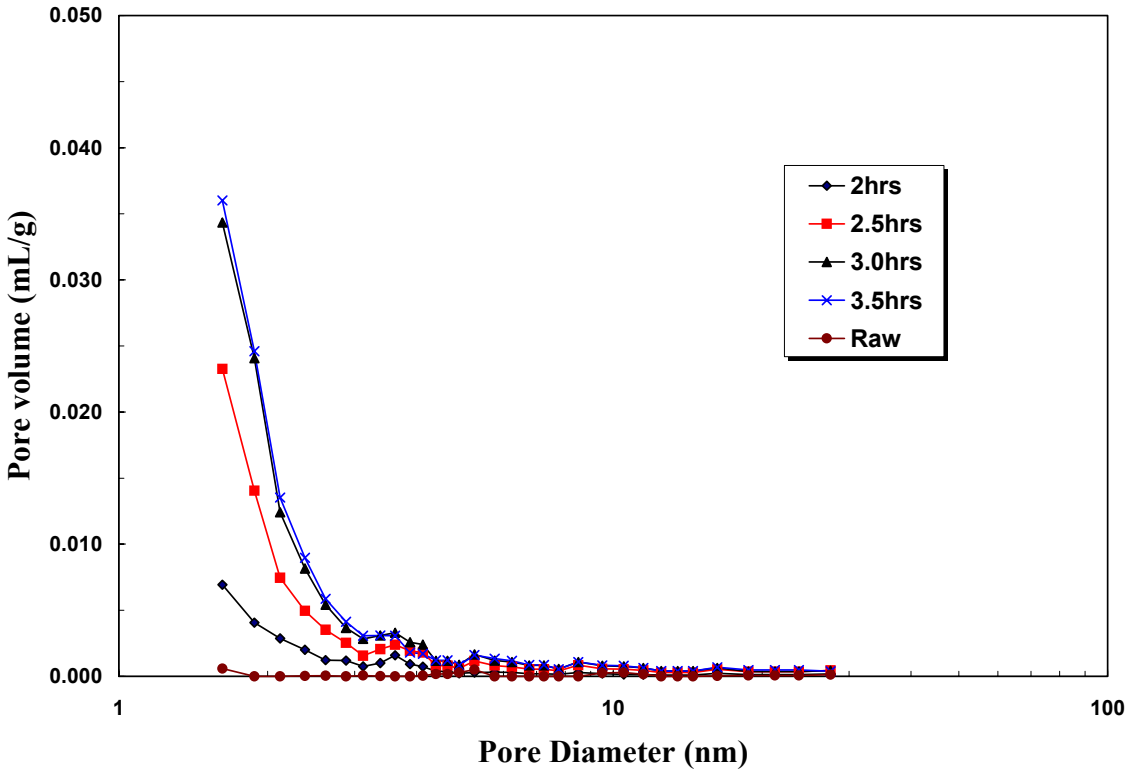

Figure 6. Mesopore size distribution by BJH method of the raw anthracite (PSOC-1468) and its steam activated carbons produced at 850^{o}C

The surface areas and pore volumes for the activated carbons produced by steam activation at 850^{o}C of the PSOC-1468 anthracite are presented in Table 2. The surface and pore volume first increase with increasing activation time and get to a maximum value after 3.0 hours activation (928m^2/g and 0.442mL/g), and then decrease with increasing activation time (855m^2/g and 0.412mL/g for AC for 3.5 hours activation time). However, the ratio of micropore surface area over total surface area and the ratio of micropore volume over total pore volume keep decreasing with increasing activation time. For instance, the ratio of micropore surface area decreases from 99% to 97%, when increasing the activation time from 2 to 3.5 hours. Similarly, the ratio of micropore volume to total pore volume decreases

from 92% to 84% when increasing the activation time from 2 to 3.5 hours. This indicates that larger pores were produced with increasing activation time.

Table 2. Surface areas and pore volumes of the raw anthracite (PSOC-1468) and its steam activated carbons produced at 850°C

Sample number	Activation time, hr	S_t m^2/g	S_m m^2/g	V_t mL/g	V_m mL/g
Raw		1.29			
1	2.0	452.4	437.6	0.2502	0.2314
2	2.5	636.6	600.2	0.3604	0.3128
3	3.0	793.0	742.0	0.4434	0.3774
4	3.5	732.0	681.1	0.4131	0.3460

S_t : Total surface area, S_m: Micropore surface area

V_t : Total surface area, V_m: Micropore surface area

3.2.2. Effect of activation temperature on the porous structure of the activated anthracites

In the previous section, the effect of the activation time on the porous structure of the PSOC-1468 anthracite activated at 850°C was investigated. The study showed that the surface area was as high as 928 m^2/g after 3 hours activation. However, extending the activation time beyond three hours decreases the surface area. Therefore, for this study three hours activation time was selected to investigate the effect of the activation temperature on the pore structure

of the produced activated anthracites. It should be noted that the optimum activation time may vary as a function of the activation temperature.

Figures 7 and 8 shows the surface area and pore volume (micropores and mesopores) of the the PSOC-1468 anthracite activated for 3 hours at 800, 850 and 890°C. It can be seen that the surface area and pore volume of the activated anthracite increased first going from 800 to 850°C, where the sample activated at 850°C has a surface area and volume of 928m^2/g and 0.442mL/g, respectively. However, increasing the activation time to 890°C resulted in a decrease of both surface area and pore volume.

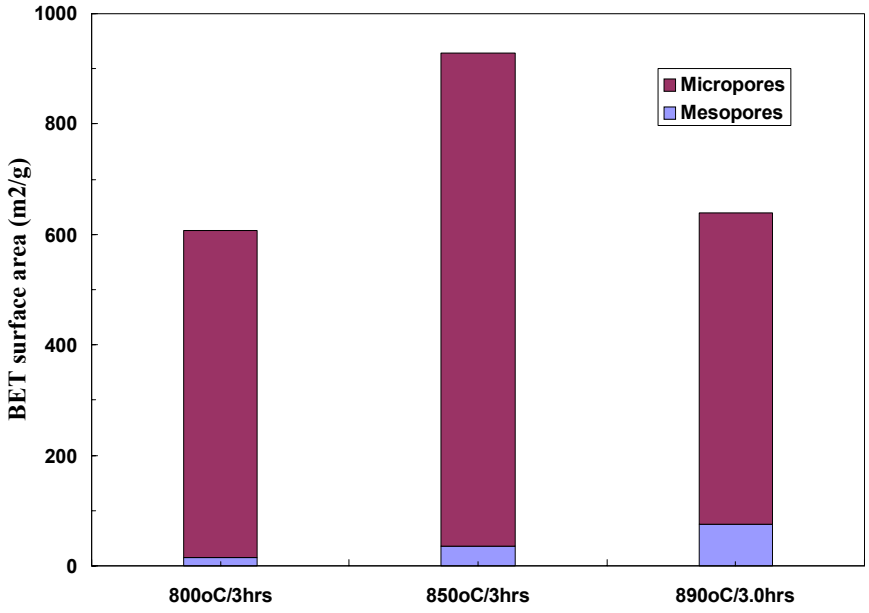

Figure 7. Surface area of the PSOC-1468 anthracite activated for 3 hours at 800, 850 and 890°C

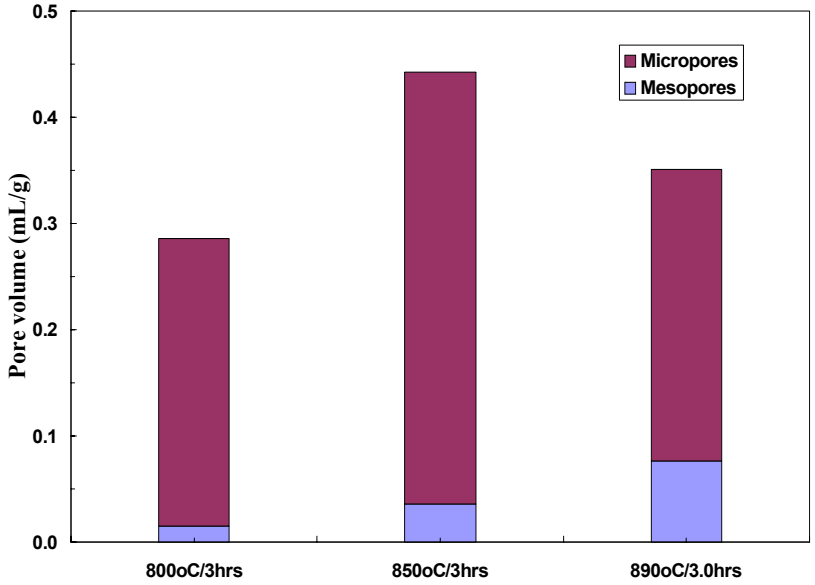

Figure 8. Pore volume of the PSOC-1468 anthracite activated for 3 hours at 800, 850 and 890°C.

On the other hand, the mesopore surface area and mesopore volume kept increasing with increasing activation temperature from 800 to 890°C, where the mesopore surface area was 15.6, 36.5 and 74.4m^2/g for the anthracites activated at 800, 850 and 890^{o}C, respectively (Figure 7). However, all the activated carbons produced are mainly microporous. This indicates that the lower activation temperature (800 and 850°C) helped to produce highly microporous activated carbon from anthracite, while higher temperatures (890°C) developed more mesopores in the activated carbon.

Figure 9 shows the mesopore size distribution, as determined by the BJH method, of the PSOC-1468 anthracite activated at different temperatures for 3 hours. It can be seen clearly that the mesopore size of the activated anthracites increased with increasing activated

temperature. This is consistent with the trends observed for the surface area and pore volumes (Figures 7 and 8).

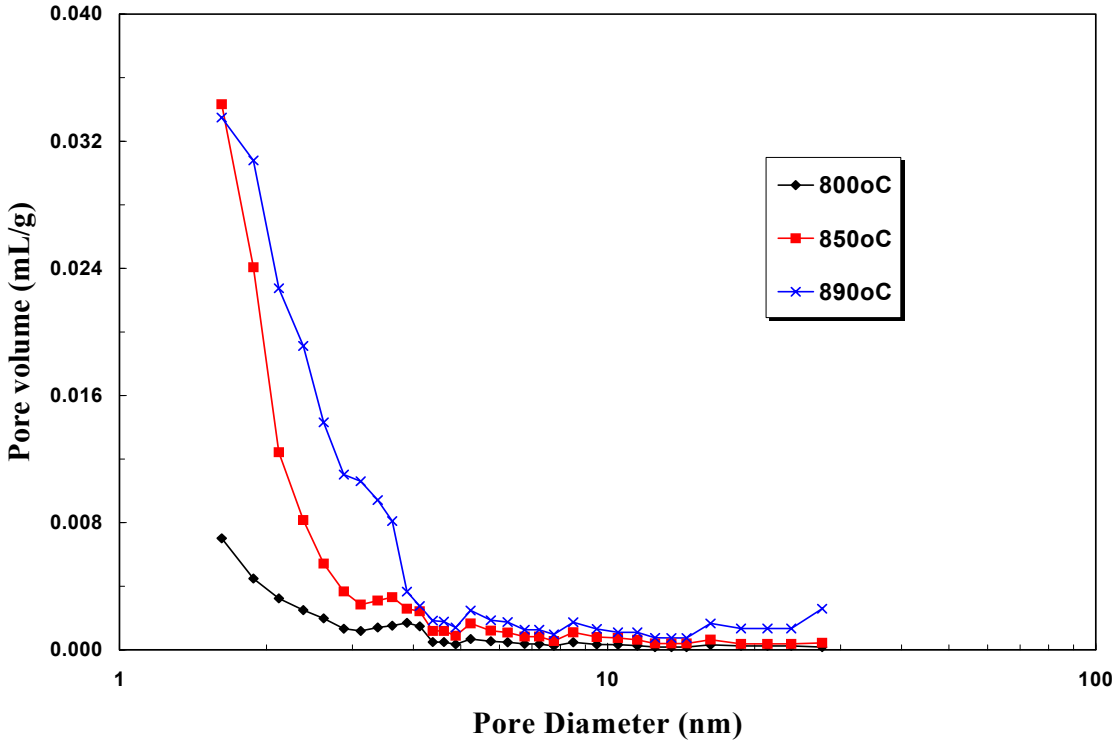

Figure 9. Mesopore size distribution by BJH method of the PSOC-1468 anthracite activated at different temperatures for 3 hours

In order to understand the effect of both the activation time and temperature on the porous structure of the activated anthracites, a series of activation experiments were conducted for different times (2.0 –3.5 hours) and temperatures (800 - 890^{o}C). In addition, a sample was activated at 700^{o}C for 2 hours. Figures 10 and 11 show the variation of the surface area and pore volume of the PSOC-1468 activated anthracites. The sample activated at 890^{o}C for 2

hours has the highest surface area and pore volume (1071m^2/g and 0.553mL/g, respectively). In contrast, the surface area and pore volume of the anthracite activated at 700^{o}C for 2 hours were only 22m^2/g and 0.015mL/g, respectively. Therefore, this low temperature activation (700^{o}C) did not develop significantly the pore structure of the anthracite. This is probably because of the low reactivity of the anthracite at this activation temperature that is not effective to even to open the closed porosity of the anthracite.

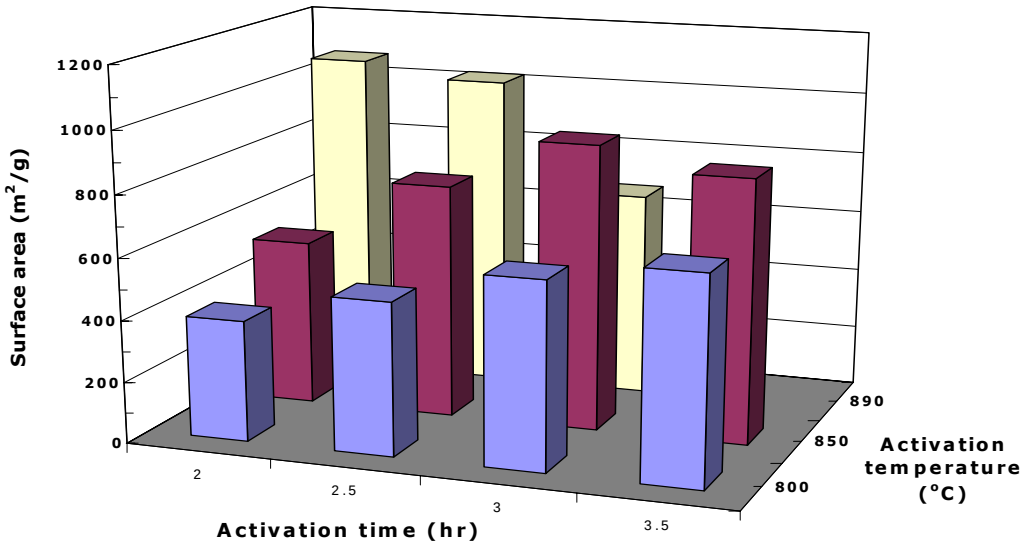

Figure 10. Surface area of the PSOC-1468 anthracite activated under different temperature and time conditions

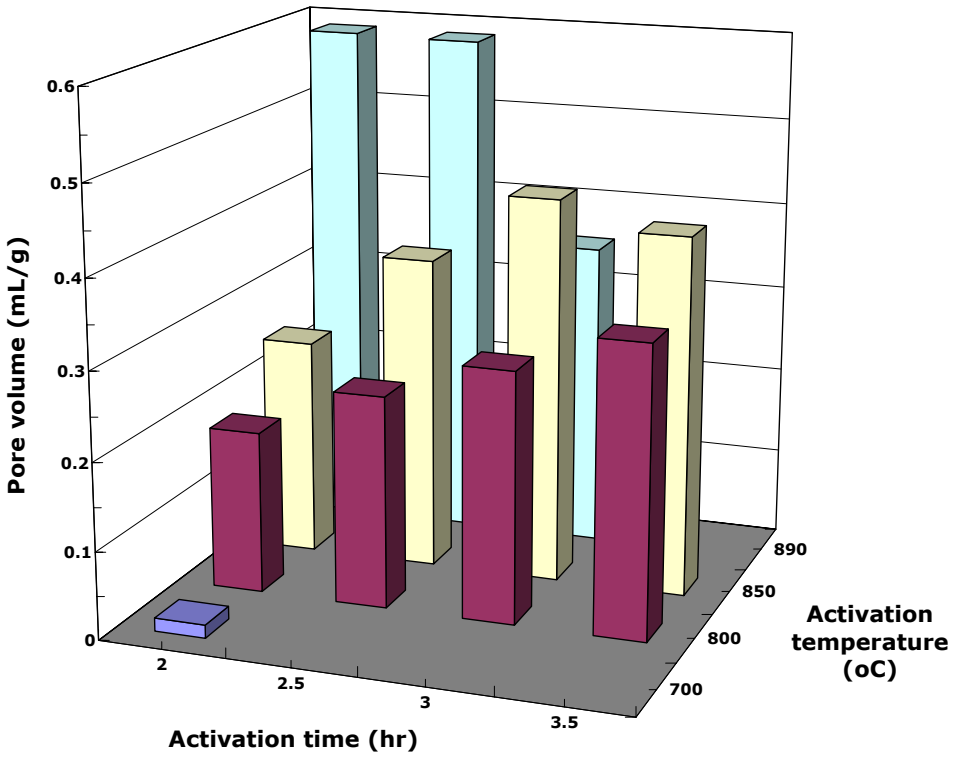

Figure 11. Pore volume of the PSOC-1468 anthracite activated under different temperature and time conditions

Table 3 lists the solid yield of the anthracite activated under different conditions (time and temperature). Figure 12 shows the relationship between surface area and the solid yield of the activated anthracites. As expected, the solid yields decrease with increasing activation time and temperature. For example, for the anthracite activated for 2 hours, the solid yield goes from 81% for the 800°C activation down to 24% at 890°C. Similarly, for a given activation temperature, the solid yield decreases with activation time. For example, for the anthracite activated at 850°C, the solid yields were 61 and 17% for the 2 and 3.5 hours activation, respectively. As described when increasing the activation time at a given temperature, the

surface area does not increase continuously with decreasing solid yields (or conversely, higher burn–off levels).

Table 3. Solid yield (wt.%) of anthracites activated under different conditions (time and temperature)

	2 hours	2.5 hours	3 hours	3.5 hours
800°C	81	78	68	56
850°C	61	47	36	17
890°C	24	20	5	n.d.

n.d.: not determined

Figure 12 shows that the surface areas go through a maximum with increasing solid yields. For example, for the activation at 850°C, the surface area first increases with decreasing solid yield and reaches a maximum value at around 40% solid yield, after which the surface area decreases. This behavior has been previously reported for anthracites activated using steam and CO_2 , although the solid yield value at which the surface area peaks varies within these studies, probably due to the different activation conditions used [13, 16]. The initial increase in surface area is probably due to opening of porosity and formation of micropores, while the decrease in surface area for lower solid yields (<40%) is due to the enlargement of micropores and and pore wall removal. This is also consistent with the variations reported for surface area and pore volume as a function of activation conditions (Figures 7-8 and 10-

11) that indicated a widening of the porosity with extended times and temperatures, and consequently, lower solid yields.

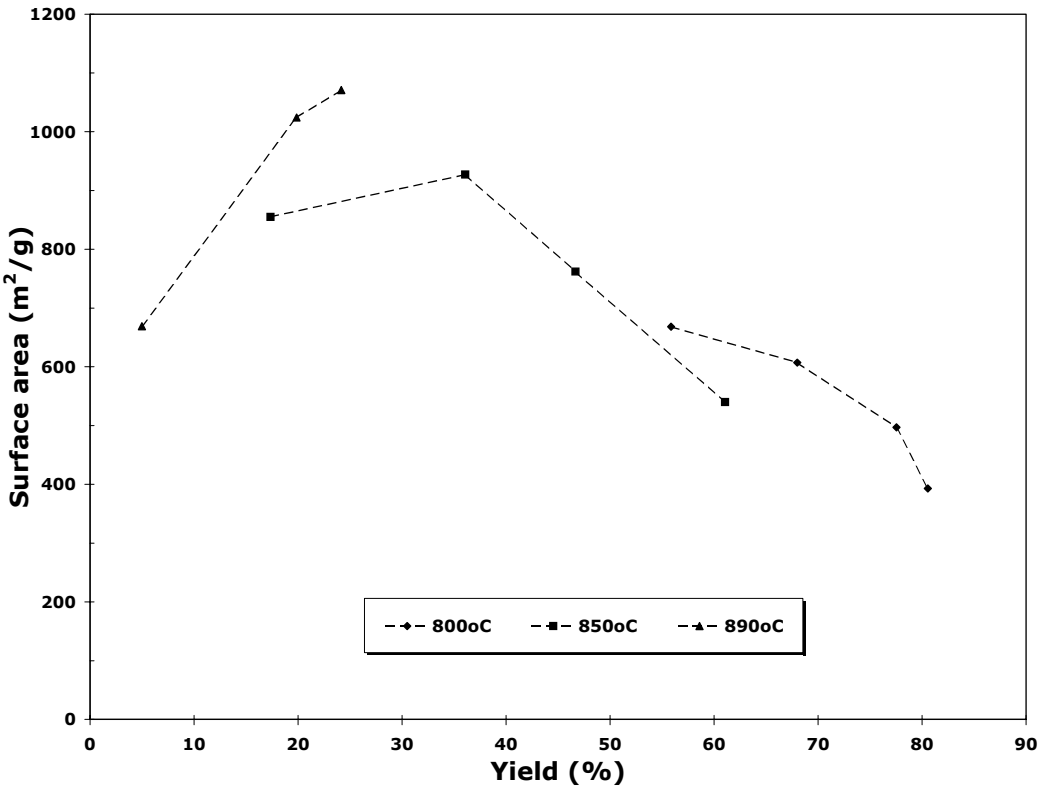

Figure 12. Variation of the surface area as a function of solid yield

3.2.3. Characterization of surface treated activated anthracites

The porous texture properties, as determined from the 77K N_2-isotherms, of the parent activated carbons and their counterparts treated with NH_3 and HNO_3 are shown in Table 4. The NH_3 treatment increased the surface area of the activated samples, especially at lower temperatures (650°C), while the HNO_3 treatment decreased the surface area of the activated

anthracites. For example, the surface area of the NH_3 treated activated anthracites increased from 928 to 1052 and 952 m^2/g at 650 and 800^oC, respectively.

Most of the pores of the activated anthracites AC-850-3 and AC-850-2, which were produced from anthracite by steam activation at 850°C using different activation times, are mainly micropores (>92%). The low temperature NH_3 treatment (650°C) can increase the surface area while keeping the sample microporosity (92%). In contrast, the high temperature NH_3 treatment (800°C) increases slightly the surface area of the anthracite, but increases significantly its pore diameter from 1.91 to 1.97 nm. The surface area of the activated anthracite decreased for the HNO_3 treatment, due the formation of mesopores, resulting in an increase of the average pore size from 1.85nm to 2.21nm.

Table 4. Porous texture of the parent activated anthracites and their counterparts treated with NH_3 and HNO_3

Sample	BET surface area m^2/g	Pore volume ml/g	Microporosity ratio, %	Average pore diameter, nm
AC-850-3	928	0.442	92	1.91
AC-850-3-NH_3-650	1052	0.523	92	1.91
AC-850-3-NH_3-800	952	0.469	88	1.97
AC-850-2	540	0.250	96	1.85
AC-850-2-HNO_3	195	0.108	86	2.21

Table 5 shows the porous structure varaitions of the activated anthracites that were impregnated with PEI. The chemical impregnation results in a dramatic decrease of the surface area of the activated anthracite, where the surface area and pore volume of the impregnated anthracites are very small ($1 m^2/g$ and 0.005ml/g). This is probably due to pore blockage and surface coverage by PEI, as previously reported for MCM-41 materials impregnated with PEI [20].

Table 5. Porous structure properties of the activated anthracites and their impregnated counterparts

	Before treatment		After treatment	
	S_{BET}, m^2/g	V_t, ml/g	S_{BET}, m^2/g	V_t, ml/g
AC-850-3	928	0.442	<1	<0.01
AC-890-3	636	0.351	<1	<0.01

3.2.4. Characterization of activated anthracites produced from different parent anthracites

Figure 13 shows the surface area and pore volume of the activated anthracite from different parent anthracites (PSOC-1468, AFM –800 and AFM-2600), which were activated at 800°C for 3 hours. The surface area and pore volume values of the activated PSOC-1468 sample

were higher than those reported for the activated AFM-800 and AFM-2600 samples. This may indicate that the reactivity of PSOC-1468 was higher than that of AFM-800 and AFM-2600.

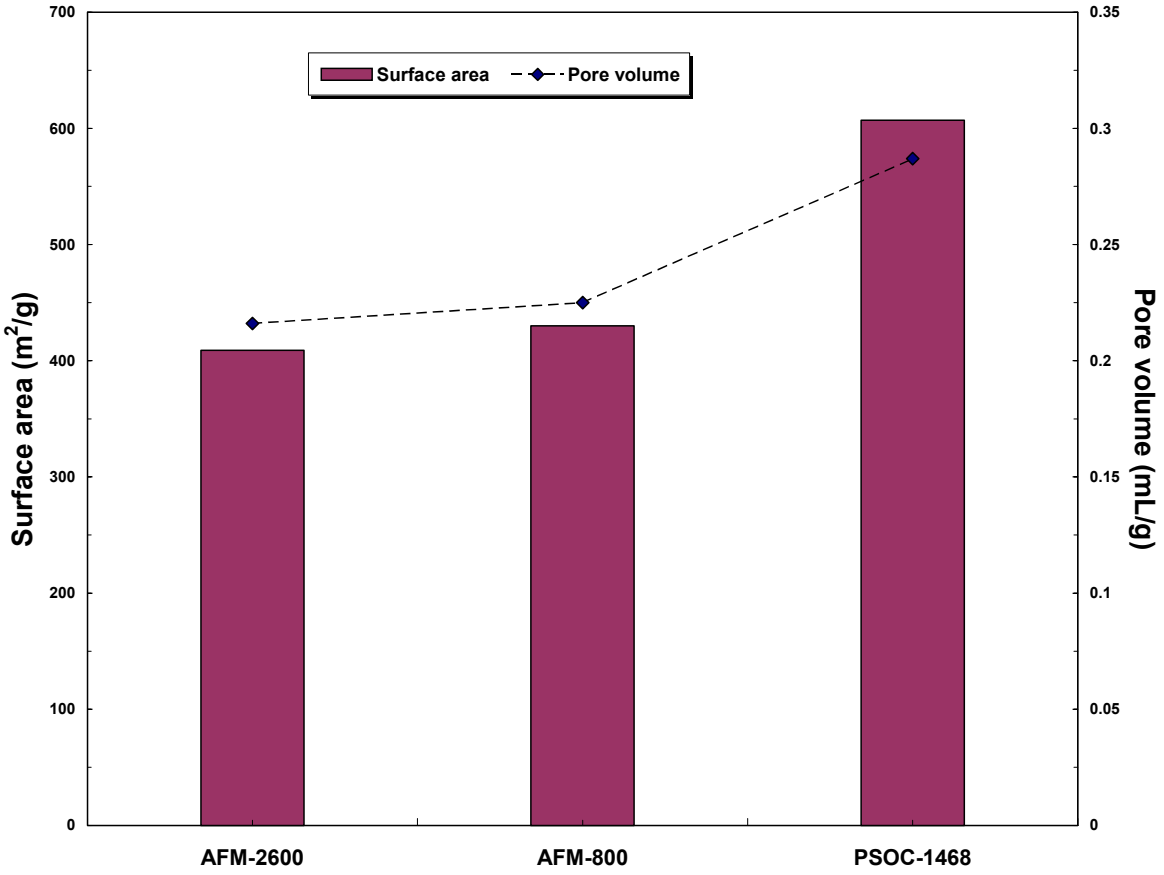

Figure 13. Surface area and pore volume of activated anthracites from different parent anthracites activated at 800°C for 3hours

3.3. Task 3: Capture of CO_2 by anthracite sorbents

Figure 14 shows a typical adsorption and desorption profiles of the activated samples made from anthracite using TGA. It can be seen that the adsorption process takes longer time than the desorption. For instance, at 30°C, for the sample after 2.0 hours activation time, it takes about 300 minutes for the sample to get saturated in CO_2, while it needs only about 100 minutes to complete the desorption. The small fluctuations observed at the beginning of the adsorption and desorption processes are due to the change of the gas environment from N_2 to CO_2 or from CO_2 to N_2.

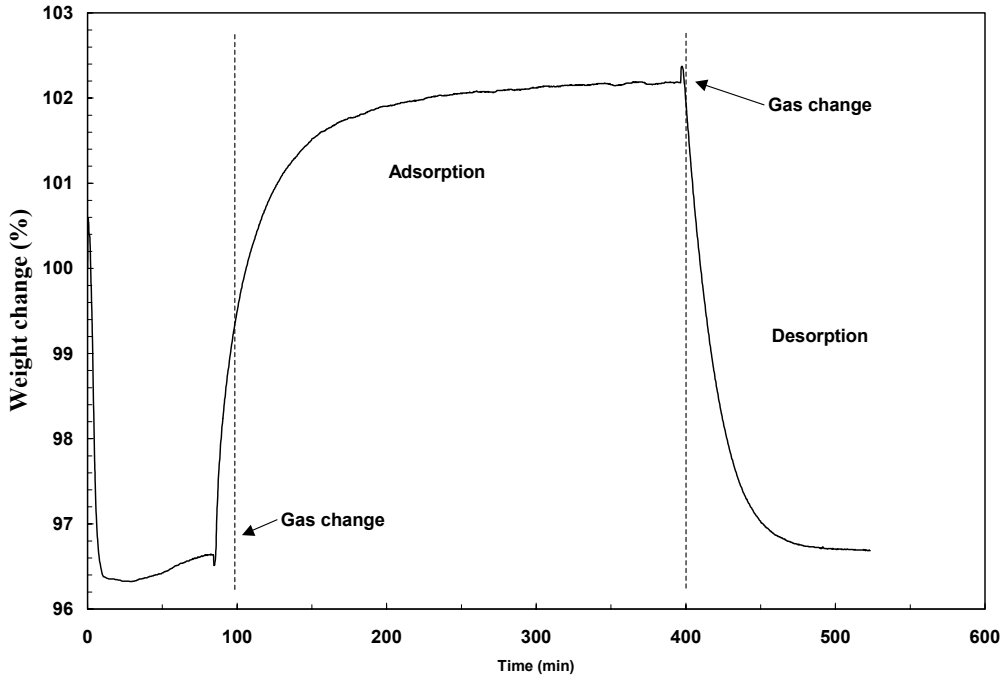

Figure 14. Typical adsorption/desorption profile at 30°C for the activated anthracite AC-850-3

3.3.1. Effect of adsorption temperature

Table 6 lists the CO_2 adsorption and desorption results at 30 and 75°C of the PSOC-1468 anthracite that was activated at 850°C. Because the CO_2 adsorption of activated anthracites is mainly a physical process, the adsorption capacity decreases with increasing adsorption temperature. For example, the CO_2 capture capacity of the activated anthracites at 75°C is about half to one-third to that at 30°C. At 75°C, the anthracite after 2.0 hours activation has the highest CO_2 capture value (26.3mg-CO_2/g-AC), and the CO_2 capture capacity decreased with increasing surface area or pore volume. In contrast, at 30°C, the anthracite after 3.5 hours activation has the highest CO_2 capture value (60.9mg-CO_2/g-AC). However, it was expected that the sample with the highest surface area would give the highest CO_2 capture value. Finally, Table 6 shows that for all the samples the desorption is higher than 97%, indicating that these samples can readily desorb the CO_2 and be reused.

Table 6. CO_2 capacities at 30 and 75°C for the anthracites activated at 850°C.

AC sample	30°C		75°C	
	Adsorption mg-CO_2/g-sorbent	Desorption %	Adsorption Mg-CO_2/g-sorbent	Desorption %
2.0hrs	58.5	97	26.3	97
2.5hrs	58.5	97	24.2	98
3.0hrs	60.6	99	21.6	99
3.5hrs	60.9	99	21.7	99

3.3.2. Effect of activation conditions on the CO_2 adsorption capacities

Figure 15 shows the CO_2 capacity values at 30°C for all the activated anthracites (PSOC-1468) produced under different conditions. For the purposes of comparison, the raw anthracite and one commercial activated carbon are also included. F-400.

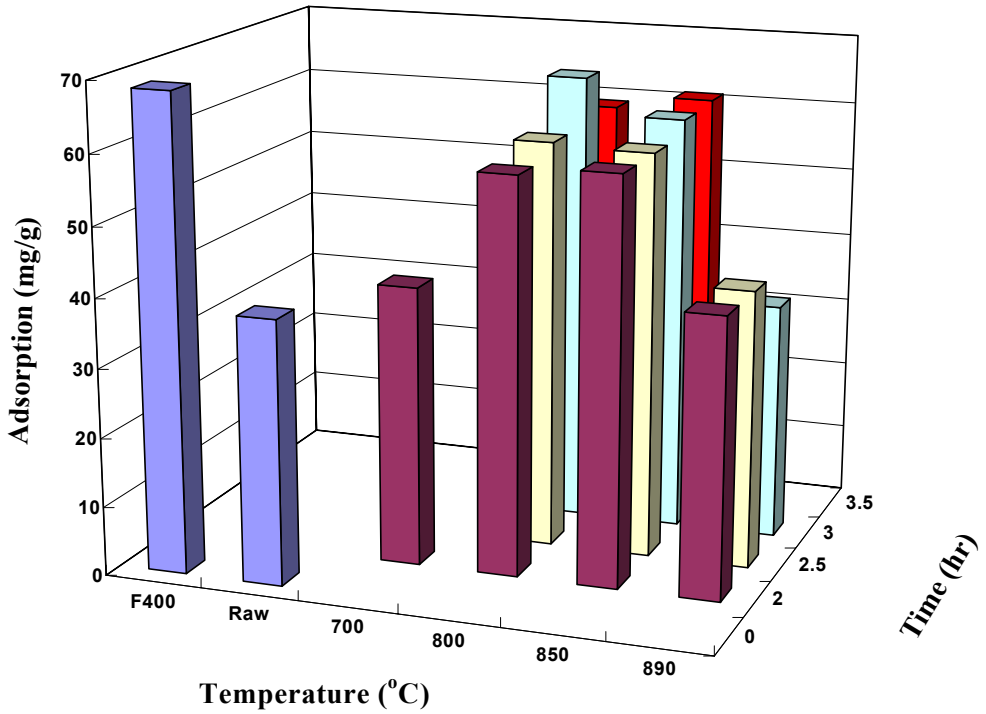

Figure 15. CO_2 adsorption capacities at 30°C of the activated samples produced from PSOC-1468 and the commercial F400 carbon

The CO_2 adsorption capacity decreased with increasing activation temperature for all the adsorption temperatures studied here, where the anthracite activated at 800°C for 3 hours has the highest CO_2 capacity (65.7mg-CO_2/g-adsorbent). Moreover, this value is very similar to

that of the commercial activated carbon F-400 (68.5mg-CO_2/g-adsorbent). The CO_2 capture capacity of the anthracite activated at 890°C for 2 hours is around 40mg-CO_2/g-adsorbent, although this sample has the highest surface area and pore volume. Figure 15 also shows that the raw anthracite together with the anthracites activated at lower temperatures (700°C) for 2 hours have surprisingly high CO_2 adsorption capacities (38 and 40mg-CO_2/g-adsorbent, respectively), despite of their low porosity. For example, the surface area of the activated anthracite at 700°C for 2 hours was only 22.4m^2/g. This is presumably due to the fine pore structure of the parent anthracite and the low temperature activated samples, which is discussed in more detail in section 3.3.3.

Since the CO_2 adsorption results show that the anthracite activated at 800°C has the largest CO_2 adsorption capacity, this temperature was selected to further investigate the effect of parent anthracite on the CO_2 adsorption, as shown in Figure 16.

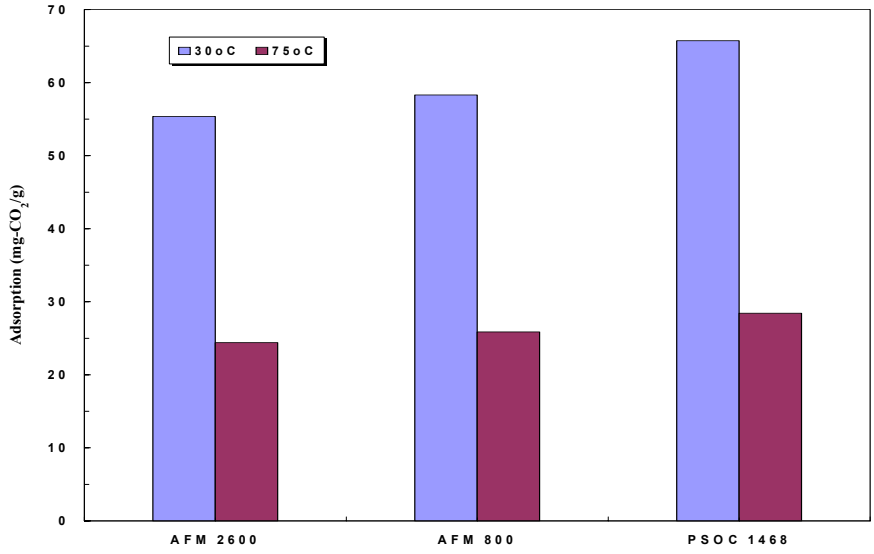

Figure 16. CO_2 adsorption capacities of activated samples generated from different parent anthracites

Figure 16 shows the CO_2 adsorption capacities of activated samples generated from different parent anthracites. It can be seen that the activated carbon made from PSOC-1468 has the highest CO_2 adsorption capacity (65.8mg-CO_2/g-adsobent. The CO_2 adsorption capacity of the activated carbons made from AFM 2600 and AFM 800 have similar value (55.4 and 58.3mg-CO_2/g-adsobent at 30^{o}C adsorption, respectively).

3.3.3. Effect of surface treatment on the CO_2 adsorption capacities

The CO_2 adsorption capacities of the activated anthracites and their NH_3 and HNO_3 treated counterparts were determined at 30, 50 and 75^{o}C, as shown in Figures 17 and 18.

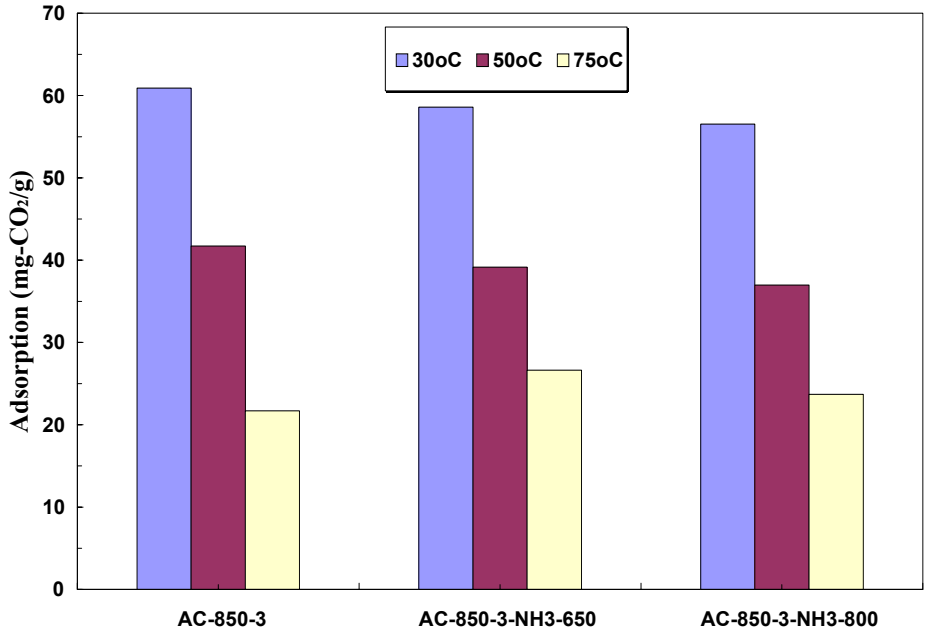

Figure 17. CO_2 adsorption capacities of AC-850-3 and its NH_3 treated samples, AC-850-3-NH_3-650 and AC-850-3-NH_3-800 at different adsorption temperature

It can be seen that there are significant changes in the CO_2 adsorption capacity of the parent and treated anthracites with temperature. At 30°C, the adsorption of the untreated activated anthracites was slightly higher than the treated samples. At higher adsorption temperatures (50°C and 75°C), the adsorption capacities of the treated samples was slightly higher than that of the parent activated anthracite. For instance, at 75°C, the CO_2 adsorption capacity was 21.7, 26.6 and 23.7 mg-CO_2/g-sorbent for AC-850-3, AC-850-3-NH_3-650 and AC-850-3-NH_3-800, respectively.

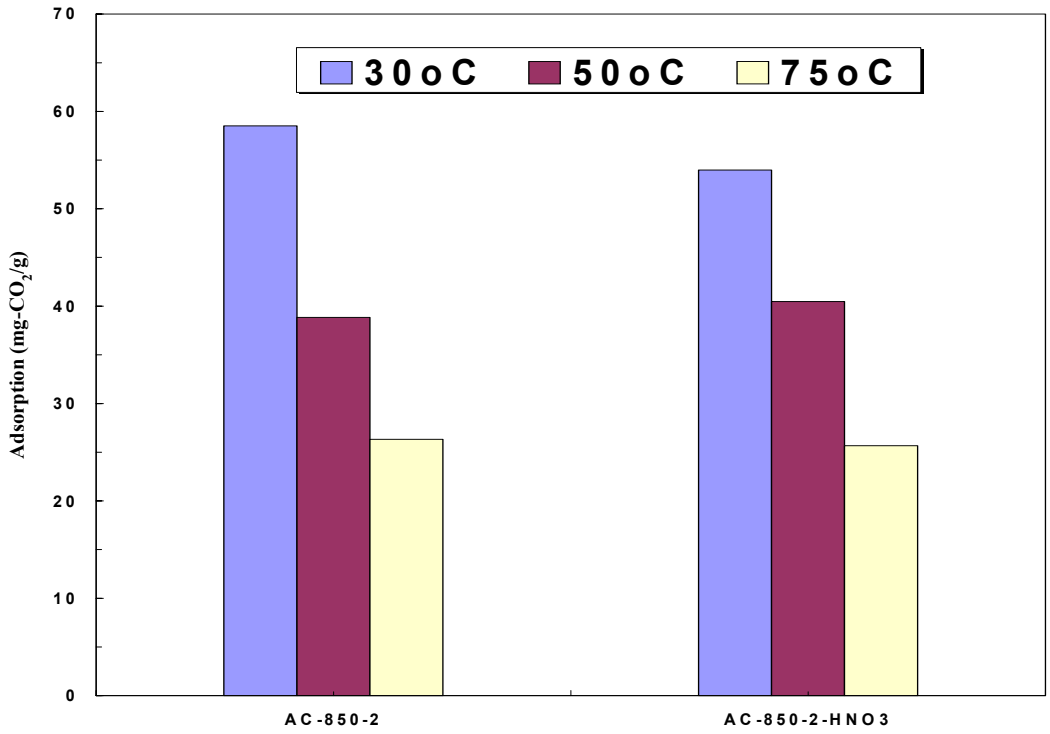

Figure 18. CO_2 adsorption capacities of AC-850-2 and its HNO_3 treated sample: AC-850-2-HNO_3 at different adsorption temperature

For the HNO_3 treatment, the CO_2 adsorption was 38.8 and 40.5 mg-CO_2/g-sorbent for AC850-2 and AC-850-2-HNO_3 at 50^oC, respectively. This indicates that the treatment process can improve the CO_2 adsorption of the anthracite, particularly at higher temperatures. This is probably due to the introduction of nitrogen groups. Further studies were conducted to assess the nitrogen functional groups that affect CO_2 adsorption (Section 3.3.3).

Figure 19 shows the CO_2 adsorption capacities of the AC-850-3 and AC-890-3 samples, and their PEI impregnated samples, AC-850-3-PEI and AC-890-3-PEI. It can be seen that impregnation with PEI increases significantly the CO_2 adsorption capacities, particularly for AC-890-3. For instance, the adsorption capacity increased from 21.6 to 26.3 mg-CO_2/g for AC-850-3 after impregnation. For the AC-890-3 sample, the PEI impregnation increased more significantly the CO_2 adsorption capacity from 16.9 to 37.5 mg-CO_2/g. This increase in the CO_2 adsorbed after amine impregnation is consistent with that reported for molecular sieve materials MCM-41 and fly ash carbons [7, 20]. The higher CO_2 adsorbed amount for AC-850-3 compared to AC-890-3 is probably due to the presence of more micropores (92% vs. 78%). Previous studies conducted on MCM-41 and fly ash carbons have shown that the CO_2 chemical adsorption for PEI impregnated materials is favored by the presence of mesopores that can promote mass transfer within the pores.

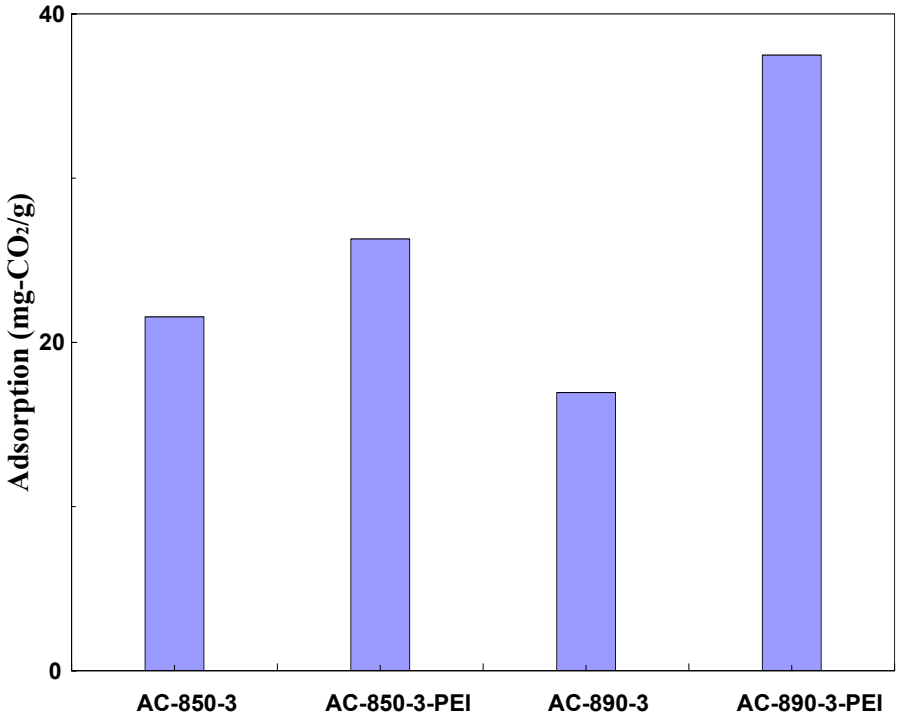

Figure 19. CO_2 adsorption capacities of AC-850-3 and AC-890-3 and their PEI impregnated samples, AC-850-3-PEI and AC-890-3-PEI at 75°C adsorption

3.3.4. Factors that influence the CO_2 adsorption of activated anthracites

From the CO_2 adsorption studies described above, the sample with the highest CO_2 adsorption capacity was the anthracite activated at 800°C for 2 hours, whose surface area was 540 m^2/g, and the adsorbed amount of CO_2 was 65.72mg-CO_2/g-adsorbent. However, the anthracite with the highest surface area and pore volume (1049m^2/g and 0.558ml/g, respectively) was that activated at 850°C for 3 hours and its CO_2 capacity was only 40.0mg-CO_2/g-adsorbent. It should be noted that the experimental adsorbed amount of CO_2 is much

lower than the theoretical amount that can be derived from the total pore volume and taking the liquid density of CO_2 is 0.93g/L (assuming that the adsorbed CO_2 changes to the liquid phase in the nanopores [26]). For example, the calculated theoretical CO_2 adsorption capacity of the anthracite activated at 800^oC for 2 hours and 850^oC for 3hrs are 232.7mg/g, and it is 412.4mg/g for AC, respectively. This indicates that not all the surface area or the pore volume of the activated anthracites contributes to the adsorption of the CO_2.

The relationship between CO_2 adsorption and the microporosity of the activated anthracites is presented in Figure 20. It seems like the samples with the highest microporosity have the highest CO_2 adsorption capacity. Previous studies have shown that only pore sizes less than 5 times that of the molecular size of the adsorbate are effective for gas adsorption at atmospheric pressure. This observation was confirmed empirically [27] as well as by mathematical simulation using grand canonical Monte Carlo (GCMC) and the nonlocal density functional theory (NLDFT) [28]. Since the molecular size of CO_2 is 0.209 nm, only pores less than 1.0nm are effective towards CO_2 capture at atmospheric pressure. Therefore, it is desirable to tailor the pore size distribution of the activated carbons, especially in order to maximize the pore less than 1.0nm, to optimize the physical adsorption of CO_2 onto the carbon surface.

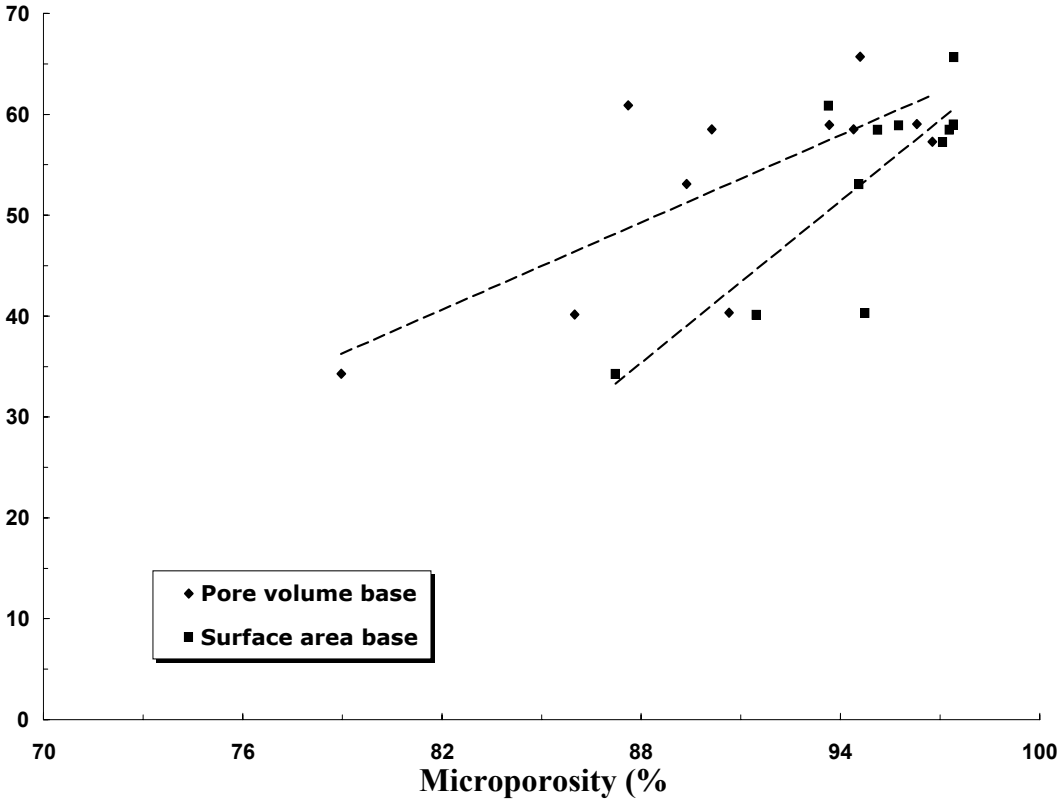

Figure 20. Variation of CO_2 adsorption capacities and microporosity of the activated anthracites

As shown in Figure 15, the raw anthracite can adsorb as much as 38.2mg-CO_2/g-sorbent at 30^{o}C, while its surface area and pore volume are very small (1.39m^2/g and less than 0.001mL/g respectively). There are two hypotheses that can explain this behavior, as described below. Firstly, the raw anthracite has very fine micropores that cannot be reached by N_2 at 77K, where the smallest pore size is 0.5nm using DFT method from N_2 isotherm [18]. However, as previously described, pores less than 0.5nm may also have the capability to adsorb CO_2. The second hypothesis is that there are some surface functional groups on the surface of raw anthracite that can contribute to the chemical adsorption of CO_2. This second

hypothesis is partially supported by the XPS data shown in Tables 7 and 8, as described below.

In order to understand the effect of the surface functional groups on the adsorption of CO_2, XPS analysis was conducted to characterize the functional groups of raw anthracite, activated anthracite (AC-850-3), NH_3 treated activated anthracites (AC-850-3-NH_3-800), HNO_3 oxidized activated anthracite (AC-850-3-HNO_3) and PEI impregnated activated anthracite (AC-850-3-PEI). Figure 21 shows the binding energy spectra of XPS analysis for AC-850-3, AC-850-3-NH_3-800 and AC-850-3-HNO_3, while Figure 22 shows the binding energy spectra of XPS analysis for AC-850-3 and AC-850-3-PEI. The major difference between the activated anthracite and the surface treated samples, is the presence of the peak at 400eV, which corresponds to the element N. This indicates that the surface treatment introduced N into the surface of the activated anthracites, and the amount introduced varied for the different methods.

Figures 23 and 24 show the C 1s and O 1s spectra of AC-850-3, AC-850-3-NH_3-800 and AC-850-3-HNO_3 respectively, and Figures 265 and 26 present the C1s and O 1s of AC-850-3 and AC-850-3-PEI, respectively.

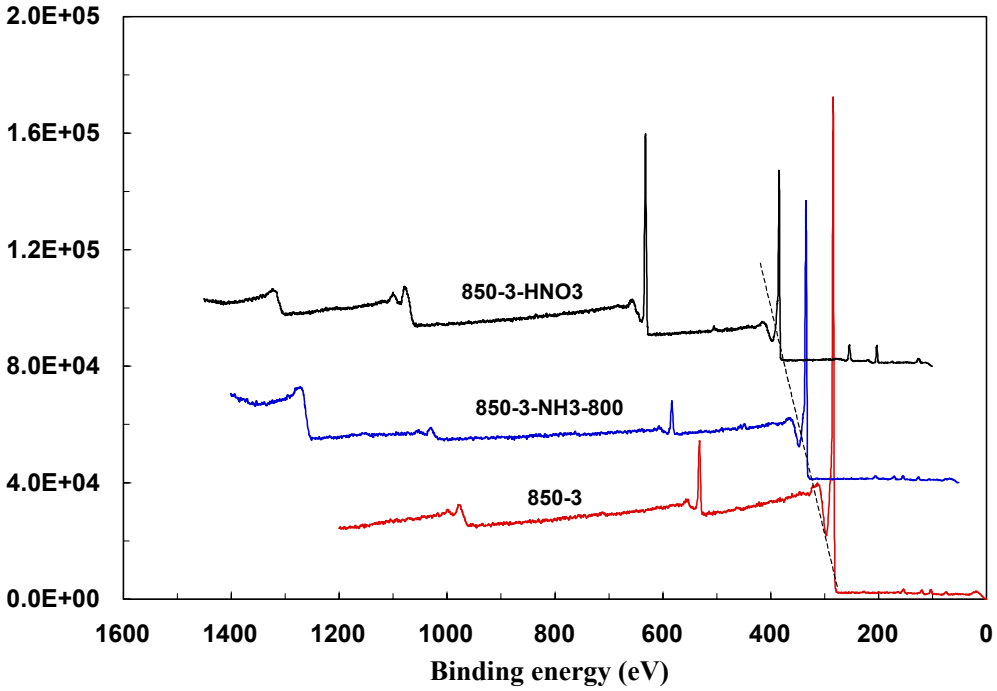

Figure 21. XPS spectra of the activated anthracite AC-850-3 and its HN_3 and HNO_3 treated samples

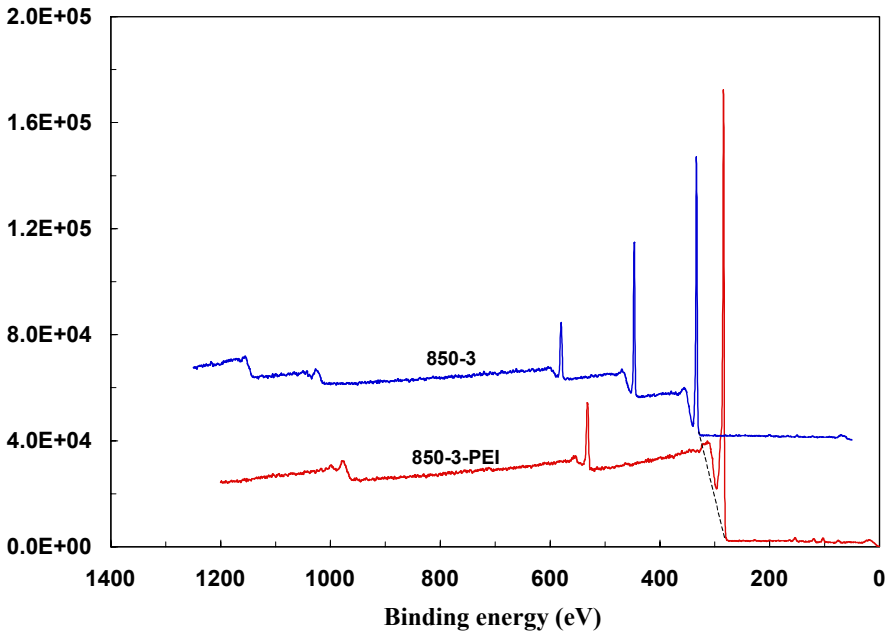

Figure 22. XPS spectra of the activated anthracite AC-850-3 and its PEI impregnated samples

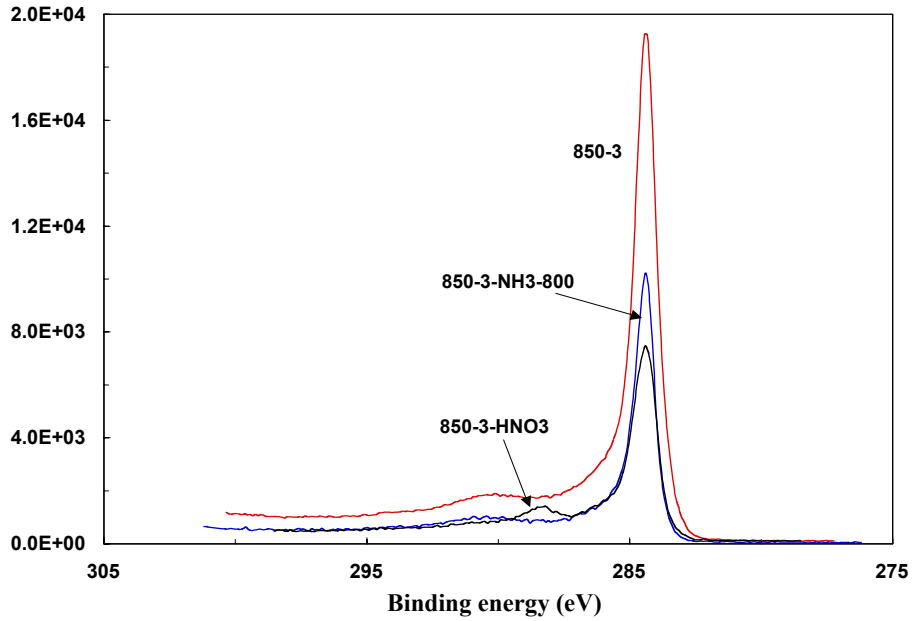

Figure 23. C 1s spectra of activated anthracite (AC-850-3) and its HN_3 and HNO_3 treated samples

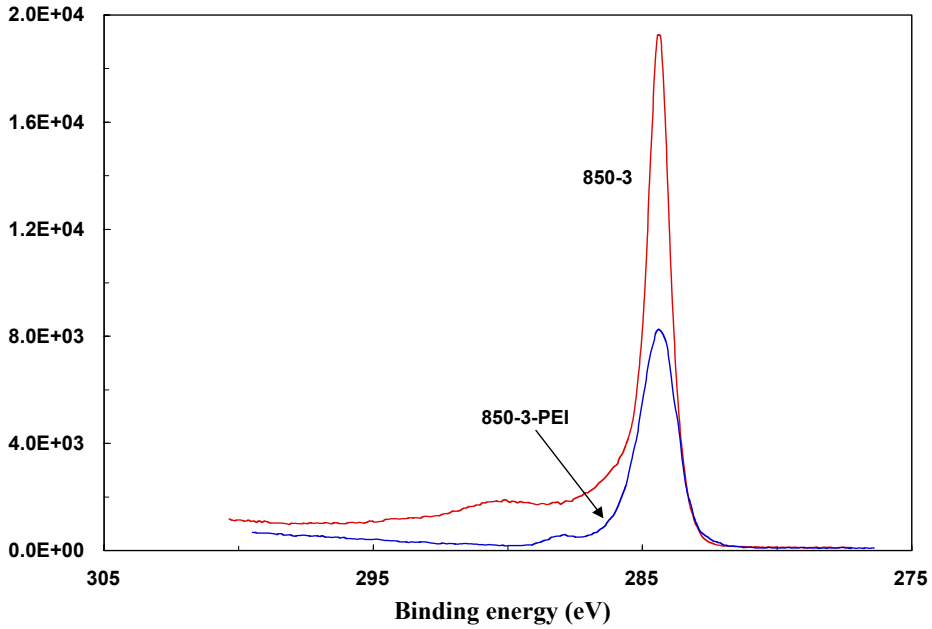

Figure 24. O 1s spectra of activated anthracite (AC-850-3) and its HN_3 and HNO_3 treated samples

For the AC-850-3 sample, there are bands that correspond to C-C, C-N and small quantities of organic oxygen species. Although not acquired in higher resolution mode on every sample, Si and Al (presumably from mineral contamination) were observed in AC-850-2-HNO_3 and AC-850-3-PEI. The Si and Al concentrations were roughly 1 atom%. Assuming the presence of SiO_2 and Al_2O_3, the Si and Al would then account for 3-4atom% of the oxygen observed.

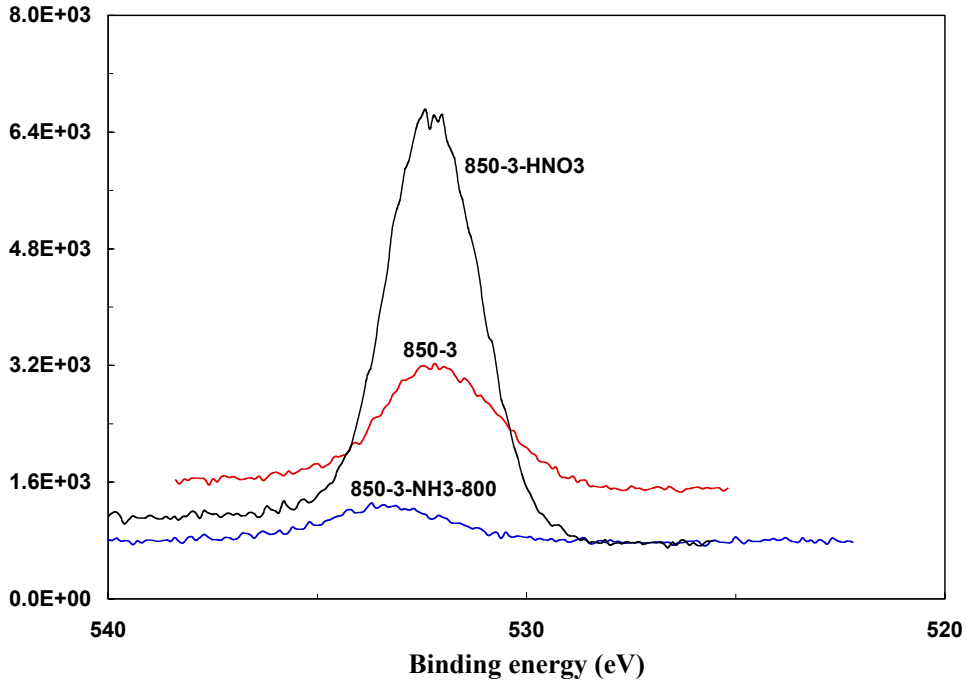

Figure 25. C 1s spectra of activated anthracite (AC-850-3) and its PEI impregnated sample

AC-850-2-HNO_3 contained a large quantity of oxygen (Figure 25). The C 1s spectrum contained a characteristic COO^- peak at 288.4 eV. Finally, two types of nitrogen were observed: C-N and a higher binding energy peak tentatively assigned as NO_2.

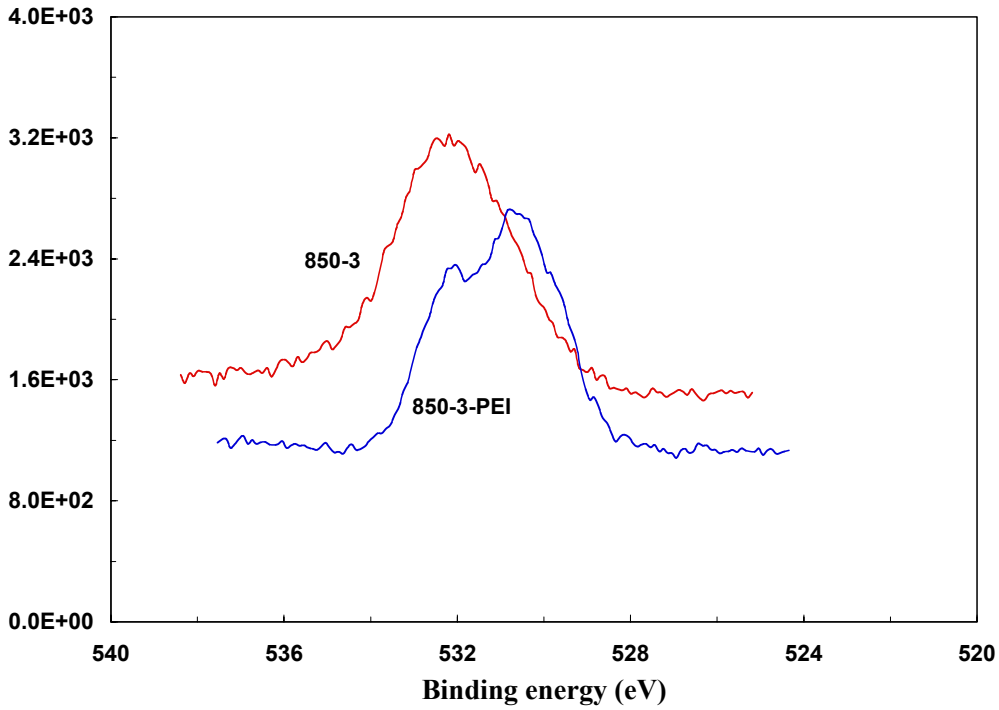

Figure 26. O1s spectra of activated anthracite (AC-850-3) and its PEI impregnated sample

AC-850-3-PEI contained significant quantities of nitrogen, as expected from the PEI impregnation. Assuming that all the nitrogen detected was from PEI, then 60-65% of the signal detected was from PEI. A small amount of COO^- (or possibly O=C-N) was detected on both samples.

The XPS results are summarized in Tables 7 and 8 below. The raw anthracite has 1.1% nitrogen atoms on the surface. After activation, the nitrogen content in the activated anthracite (AC-850-3) was lower than that in the raw anthracite since probably the nitrogen in the anthracite was lost during the activation process. As expected, the NH_3 treatment introduced nitrogen surface groups on the activated carbon, especially at high temperature.

The nitrogen content increased from 0.1% in the untreated activated carbon to 1.1% in the NH_3 treated activated carbon, as shown by the XPS data presented in Table 7.

Table 7. Summary of the elements detected by XPS (Rel. Atom%)

Sample	C	O	N
Raw	90.3	8.6	1.1
AC-850-3	93.6	6.3	0.1
AC-850-3-NH_3-800	94.0	4.9	1.1
AC-850-3-PEI	73.3	8.4	18.3

Since CO_2 is an acid gas, alkaline surface functional groups will favor chemisorption of CO_2. Among the surface functional groups studied on the activated carbon surface, only some nitrogen groups are alkaline. This is also why surface treatment methods are employed to improve the CO_2 adsorption capacity of sorbents by means of increasing the nitrogen content [21, 29]. Therefore, high resolution XPS analysis was conducted on the N 1s and the curve fitting results are presented in Table 8

In addition to the different nitrogen content on the surface of the studied samples (Table 7), the nitrogen functional groups are also different for these samples. The nitrogen groups on the raw anthracite, NH_3 treated activated anthracite and PEI impregnated activated anthracite that have alkaline character are amine groups (around 400.0eV) and imine groups (around 396eV). The presence of these groups also explains why these samples have higher CO_2 capacities, probably due to chemisorption processes. For the same token, the untreated

activated anthracite did not have any imine group and a lower concentration of pyridine groups, resulting in lower CO_2 adsorption capacities.

Table 8. Surface content of nitrogen species obtained by deconvolution of the N 1s XPS peak

	Content of nitrogen (at.%)					CO_2 absorbed at
	N-Imine	Pyridine / C-N	Nitriles	Pyrrolic / amine	Oxides	75°C (mg-CO_2/g)
Raw	-	50.91	-	45.28	3.81	16.05
AC-850-3	-	21.45	29.18	37.86	11.52	21.55
AC-850-3-NH_3-800	43.52	27.86	-	14.09	15.03	23.69
AC-850-3-PEI	33.92	66.08	-	-	-	26.30

4. CONCLUSIONS

Three anthracite samples (PSOC-1468, AFM-800, AFM-2600) were selected for this study to produce activated carbon for CO_2 capture. A lab scale fluidized bed was used for the activation and the activation temperature used was between 700-890°C. Three surface treatment methods (NH_3 heat treatment, HNO_3 oxidization and PEI impregnation) were conducted to modify the surface properties of the activated anthracites and to improve their CO_2 capture capacity. A TGA instrument was used to characterize the CO_2 capture capacity at 30 and 75°C. The N_2-77K isotherms were used to characterize the pore structure of the

activated anthracites. XPS analyses were used to characterize the surface functional groups of the activated anthracites and surface treated activated anthracites.

High surface area (over 1,000m^2/g) activated carbons were prepared from an anthracite sample (PSOC-1468) by steam activation using fluidized bed reactor. N_2-77K adsorption studies show that the activated anthracites are mainly microporous and the microporosity decreased with increasing activation time and temperature. The maximum surface area and pore volume are 1071m^2/g and 0.588mL/g for the anthracite activated at 890^{o}C for 2 hours. The surface areas go through a maximum with increasing solid yields. The initial increase in surface area is probably due to opening of porosity and formation of micropores, while the decrease in surface area for lower solid yields (<40%) is due to the enlargement of micropores and and pore wall removal.

The adsorption of CO_2 on the activated anthracite is mainly a physical adsorption process and the adsorbed amount decreased with increasing adsorption temperature. The CO_2 capture results do not show a linear relationship with the surface area. For example, the sample with the highest CO_2 adsorption capacity (65.7mg-CO_2/g-adsorbent) was the anthracite activated at 800^{o}C for 2 hours, whose surface area was only 540 m^2/g. This is probably due to only certain size pores being effective for CO_2 adsorption.

Two surface treatment methods, including NH_3 heat treatment and polyethylenimine (PEI) impregnation, were used to modify the surface properties of the activated anthracites to increase their CO_2 capture capacity at higher temperatures. The NH_3 treatment increases the

surface area of the activated samples, especially at lower temperatures (650°C). The chemical impregnation with PEI results in a dramatic decrease of the surface area of the activated anthracite, probably due to pore blockage and surface coverage by PEI. Both the NH_3 treatment and PEI impregnation can increase the CO_2 capture capacity of the activated antrhacites at higher adsorption temperature, due to the introduction of alkaline nitrogen groups on the surface.

5. Acknowledgments

This work was funded by the US Department of Energy (DOE) through a grant of the Consortium for Premium Carbon Products from Coal (CPCPC) at Penn State University (DOE Award number: *DE-FC26-98FT40350,* Internal Agreement Number: 2484-TPSU-DOE-0350). The authors would like to thank Dr. Yinzhi Zhang from the Energy Institute, Penn State University for her help to analyze the N_2 isotherms and discuss the analysis data; Dr. Xiaochun Xu from the Energy Institute, Penn State University for his help to provide the PEI sample and helpful suggestion; and Dr. Jeff Shallenberger from MRL (Materials Characterization Laboratory), Penn state University for his help to do the XPS analysis and data treatment. Finally, the authors also thank the Coal Bank at Penn State University and FB Leopold, PA for providing the anthracite samples.

6. Publications resulting of this project

1. Z. Tang, M. M. Maroto-Valer, Y. Zhang, CO_2 capture using anthracite based sorbents. Prepr. Am. Chem. Soc. Div. Fuel Chem., 2004, 49(1), 298-299.

2. Z. Tang, Y. Zhang, and M.M. Maroto-Valer, Study of CO_2 adsorption capacities of modified activated anthracites. Prepr. Am. Chem. Soc. Div. Fuel Chem., 2004, 49(1), 308-309.

3. M. M. Maroto-Valer, Z. Tang, and Y. Zhang, Use of activated anthracites for CO_2 capture, *Proceedings Carbon 2004*, American Carbon Society, Providence, RI, July 11-16, 2004, Paper J022.pdf (CD-ROM publication).

4. Z. Tang, M. M. Maroto-Valer, Y. Zhang, CO_2 capture of activated and impregnated anthracites, Fuel Processing Technology, To be submitted.

7. References

1. C.D., Keeling, T. Whorf. (1998). Trends: A Compendium of Data on Global Change, Oak Ridge.
2. H.J. Herzog, (1998) Proc. Stakeholders' Workshop on Carbon Sequestration, MIT EL 98-002.

3. P.J., Birbara, and T.A. Nalette (1996) US patent No: 4, 810, 266.
4. R.V. Siriwardane, M.S. Shen, E.P. Fisher, J.A. Poston. (2001) *Energy & Fuel*. 15, 279.
5. H.H. Schobert, J.P. Mathews, A.D. Jones, P.J. Pappano, R.H. Hurt (2001). Proc.11th International Conference on Coal Science, CD-ROM publication, Paper No. ICCS~220.PDF.
6. R.C. Bansal, J. Donnet, F. Stoeckl, Activated Carbon, Marcel Dekker, Inc. (1998).
7. T. Wigmans, Carbon 27(1) (1989) 13.
8. A.K. Dalai, A.I. Chowdhury, E.S. Hall, J. Zaman, E.L. Tollefson, Fuel 75 (1996) 384.
9. J.J. Pis, M. Mahamud, J.A. Pajares, J.B. Parra, R. C. Bansal, Fuel Processing Technology 57 (1998) 149.
10. J. A. Conesa, M. Sakurai, M.J. AntalJr, Carbon 38(6) (2000) 839.
11. J. Díaz-Terán, D.M. Nevskaia, J.L.G. Fierro, A.J. López-Peinado, A. Jerez, Microporous and Mesoporous Materials, 60(1-3) (2003) 173.
12. F. Rodríguez-Reinoso, M. Molina-Sabio, Carbon 30(7) (1992) 1111.
13. K. Gergova, S. Eser, H.H. Schobert, Energy & Fuel 7 (1993) 661.
14. J. Pis, J. Parra, G. Puente, F. Rubiera, J. Pajares, Fuel 77(6) (1998) 625.
15. M.M. Maroto-Valer, H.H. Schobert, In: B.Q. Li, Z.Y. Liu (Eds), Prospects for Coal science in the 21st Century, Shanxi Science and Technology Press., Taiyuan, China (1999) 909
16. M. Mittelmeijer-Hazeleger, J. Martin-Martinez, Carbon 30(4) (1992) 695.
17. D. Spencer, J. Wilson, Fuel 55 (1976) 291.

18. Z. Tang, M.M. Maroto-Valer, YZ Zhang, American Chemical Society Fuel Chemistry Division Preprints, 2004, 49(1), 298-299
19. Z. Tang, M.M. Maroto-Valer, YZ Zhang, American Chemical Society Fuel Chemistry Division Preprints, 2004, 49(1), 308-309
20. X. Xu, C.S. Song, J.M. Andresen, B.G. Miller, A.W. Scaroni, Energy & Fuel 16 (2002) 1463.
21. M.L. Gray, Y. Soong, K.J. Champagne, J. Baltrus, R.W. Stevens, Jr. P. Toochinda, S.S.C. Chuang, Separation and Purification Technology 35 (2004) 31.
22. K.S.W. Sing, D.H. Everett, R.A.W. Hual, and et al, Pure & Appl. Chem. 57(4) (1985) 603
23. Y.Z Zhang, Z. Lu, M.M. Maroto-Valer, J.M. Andrésen, H.H. Schobert, Energy & Fuel, 17 (2003) 369.
24. M. Turmuzi, W. R. W. Daud, S. M. Tasirin, M. S. Takriff and S. E. Iyuke, Carbon, 42 (2003) 453.
25. Duong D. Do, Adsorption Analysis: Equilibria and Kinetics (Series on Chemical Engineering, Series Editor: Ralph T. Yang), Imperial College Press, London 1998
26. D. Cazorla-Amorós, J. Alcañiz-Monge, A. Linares-Solano, Langmuir 12 (1996) 2820.
27. J.M. Martín-Martínez, R. Torregrosa-Maciá, M.C. Mittelmeijer-Hazeleger, Fuel 74 (1995) 111.
28. A. Vishnyakov, P.I. Ravikovitch, A.V. Neimark, Langmuir 15 (1999) 8736
29. J. Przepiórski, M. Skrodzewicz, A.W. Morawski, Applied Surface Science 225(1-4) (2004) 235.

CONSORTIUM FOR PREMIUM CARBON PRODUCTS FROM COAL

Nanotube Enhancement of Coal Extract Pitches: Fibers and Foams

SUBCONTRACT NO. 2480-UK-DOE-0350

FINAL REPORT

for Period 1 March through 30 June 2004

by

University of Kentucky

Center for Applied Energy Research

&

West Virginia University

Department of Chemical Engineering

August 2004

Disclaimer

ABSTRACT

The results of Laboratory and supporting technical assessments conducted under Subcontract No. 2480-UK-DOE-0350 are reported for the period March 1, 2002 to June 30, 2004. This contract is with the University of Kentucky Research Foundation, which supports work with the University of Kentucky Center for Applied Energy Research and West Virginia University. This work involves multiwall carbon nanotube enhancement of coal-derived pitches for carbon fiber and carbon foam applications.

TABLE OF CONTENTS

EXECUTIVE SUMMARY

High performance pitch based carbons are typically made from mesophase pitch. The mesophase pitch contains liquid crystal domains that tend to align in the axial direction of the fiber or ligaments of foam so that when carbonized and ultimately graphitized, a highly ordered graphitic lattice is formed, imparting excellent physical, electrical, and thermal properties to the resultant materials. However, the high processing costs and low yields associated with the production of mesophase pitch suitable for these applications makes the pitch expensive to produce, and adds significantly higher costs to the product. Hence, if viable methods of producing high performance carbon fibers and foams from low cost isotropic pitch feedstocks could be developed, a significant cost advantage could be gained. It is the aim of this project to produce high value carbon fibers and foams via the co-processing of a low cost coal extract pitch with well-dispersed carbon nanotubes.

The carbon nanotubes were dispersed in pitch and selected mixtures formed into filaments or foams. During fiber spinning, nanotubes aligned axially with the fiber. The second product was a lightweight high-strength porous carbon, usually referred to as carbon foam.

The presence of nanotubes in these fiber and foams improved strength, modulus, and thermal conductivity. The ability to generate higher value materials with a small addition of nanotubes to a coal extract pitch will result in materials of high commercial and military interest for structures, thermal management and electromagnetic shielding.

1. SECTION ONE

UNIVERSITY OF KENTUCKY

CENTER FOR APPLIED ENERGY RESEARCH

INTRODUCTION

Coal-derived carbon fibers and foams composites containing highly aligned nanotubes were shown to have enhanced physical properties compared to pitch derived foams and fibers. The component materials, coal extract pitches from WVU and UK and high purity multiwall carbon nanotubes from UK, were produced, blended and formed into fibers (UK) and foams (WVU). The materials were heat treated and tested for their physical, and thermal properties.

Multiwalled carbon nanotubes, which have graphene planes wrapped into a cylindrical configuration, have extremely high specific strengths (200x steel), elastic modulus (>1 TPa), and electrical and thermal conductivities. Typically, the nanotubes produced by UK have diameters less than 25 nanometers, and lengths of about 50 μm. Although nanotube-enhanced pitches can be used to form a suite of materials (including carbon pitch matrix composites, artificial graphite, carbon foams, carbon black and carbon fibers), this project focused on two main carbon products. The first is a lightweight high-strength porous carbon, usually referred to as carbon foam. Carbon foams pioneered by West Virginia University have, for a given density, resulted in higher strength and modulus than other known processes for carbon foam. The second product is pitch-derived continuously spun carbon fibers, which has been a major research focus at the University of Kentucky.

The starting point for both materials is the use of coal-derived extract pitches. These materials have a significant content of high molecular weight aromatic hydrocarbons, permitting a high degree of graphitization when heat treated. The tendency to form a graphitic lattice, as opposed to amorphous or turbostratic carbon, is significantly enhanced by the addition of carbon

nanomaterials, which might act to enhance the formation of highly oriented crystalline domains. Yet improved performance and reduced cost can result from the addition of small amounts of carbon nanomaterials, which can significantly enhance the graphitic character of the bulk material. As a result, when this material is converted to carbon, macroscopic domains are created with preferred crystal orientation, and enhanced index of graphitization.

In the case of carbon foam, coal is hydrogenated to about 2 weight percent hydrogen Mild hydrogenation increases the aromatic content of the coal, which is desirable from the point of view of forming carbon materials. The solvent extract is refined by distilling off low molecular weight components, resulting in an aromatic pitch. By carefully controlling the temperature and pressure in a nitrogen-pressurized autoclave, the outgassing volatiles create a porous structure.

In the case of carbon fibers, high modulus as well as high thermal conductivity requires the formation of well-ordered graphite domains, and fibers are usually derived from mesophase pitch or PAN. However, as pointed out previously, added carbon nanotubes not only act as reinforcing composite fibers, but also impose long-range order in the matrix pitch over many microns of interlocking domains, and hence may offer significant advantages compared to conventional mesophase pitch.

It should be also noted that the addition of nanotubes is not necessarily expensive, and can even reduce cost. UK has installed a pilot-scale continuous reactor for the production of 1 to 3 kg/day of high purity multiwalled carbon nanotubes. This unit was be operable in December 2002, and estimated costs of the nanotubes are less than $100/kg. In the future, much lower costs are

projected due to economies of scale and process improvements. In any case, the use of a few grams of nanotubes per kg of pitch will greatly enhance the product properties while having only incremental effect on the material costs. The proposed work offers one promising route to move low cost coal-extract pitches into medium- and high-performance structural, thermal management and electrical shielding applications (with an ensuing increase in value).

Task 1.0 Production of Coal Derived Pitches – UK CAER.

Anthracene oil was used to extract pitch from a Western Kentucky #9 coal (W.Ky), Table 1, using low severity extraction conditions. Extraction conditions produced a high softening point pitch suitable as a feedstock for carbon fibers and nanotube composite carbon fibers. Approximately 1 kg of Western Kentucky coal extract pitch was prepared. The extraction technique can be summarized as follows.

Table 1. Proximate and ultimate coal analysis.

	W.Ky
Moisture (%)	5.2
Ash (%)	19.0
Volatiles (%)	34.6
Fixed Carbon (%)	41.2
Carbon (% daf)	80.0
Hydrogen (% daf)	6.3
Nitrogen (% daf)	1.7
Total Sulfur (% daf)	4.8
Oxygen *by diff.* (% daf)	7.2
Pyritic Sulfur (% db)	2.0
Sulfate (% db)	0.02
Organic Sulfur (% db)	1.9

Digestion of coal with anthracene oil was performed batch-wise in a heated Parr Instruments 2L stirred autoclave reactor. Coal was crushed to < 60 mesh and then slurried with anthracene oil in a coal to solvent ratio of 1:2 w/w and placed into the reactor, typical charge for the digestion was

about 900 g. Digestion of the coal was performed at 425 ^{o}C for 60 min and at a pressure of 200 psi. The reactor was maintained at 200 psi by slowly venting the reactor during digestion as required, the vent line was attached to a cold catch pot (-15 ^{o}C) to trap any light distillates generated during digestion. After the 60 min digestion time, the reactor was allowed to cool to approximately 260 ^{o}C, the reactor de-pressurized and the contents drained into a pre-weighed beaker. After allowing the reactor to cool to room temperature, the reactor, catch pot and vent lines were weighed and this data used to calculate a mass balance for the digestion. QI and THFI were determined on the digests.

Un-dissolved coal was separated from the digest by hot filtration. Filtration was preformed through a GFA filter at 250 ^{o}C with 10 psi of nitrogen over pressure. Filtering rate and cake resistivity was calculated using Darcy's Law [Purchas 1967]. The weight of filter cake and filtrate were also measured. Filtrates were vacuum distilled to recover anthracene oil and extracted pitch (pot residue). Vacuum distillation was used to control the softening point of the pitch, typically pitches with softening points in the range of 220 to 260 ^{o}C are desired for carbon fiber fabrication. A brief summary of extraction data from one of the batch extractions is shown below in Tables 2, 3 and 4.

Table 2 - Coal digestion data summary, digestion performed at 425 ^{o}C for 60 minutes.

	W.Ky	*units*
Coal IN (daf) =	224.5	g
Solvent IN =	584.9	g
Slurry IN (daf coal) =	809.4	g
Extraction Distillates OUT =	53.3	g
Digest OUT (daf coal) =	727.3	g
QI =	21.3	%
THFI =	24.8	%
% Conversion [based on QI] (daf coal) =	68.7	%
% Conversion [based on THFI] (daf coal) =	63.5	%
Mass Balance Extraction (daf coal) =	96.4	%

Table 3 – Summary of filtration parameters for coal/anthrancene oil digests.

	W.Ky	*units*
Filter Charge (daf coal) IN =	727.3	g
Cake (daf coal) OUT =	56.2	g
Filtrate (daf coal) OUT =	624.3	g
Distillates OUT =	4.7	g
Specific Cake Resistance =	2.1	10^{10}m/kg
Filter Rate =	214.5	kg/m^2/h
QI Filtrate =	0.8	%
Mass Balance Filtration (daf coal) =	97.6	%

Table 4 – Distillation Summary.

	W.Ky	***units***
Distillation Charge IN =	624.3	g
Distillate OUT =	391.2	g
Pitch (Pot Residue) (daf coal) OUT =	230.4	g
Pitch Softening Point =	255	^{o}C
Mass Balance Distillation (daf coal) =	99.6	%

Task 2.0 Production of Carbon Nanotubes – UK CAER.

The University of Kentucky Center for Applied Energy Research has developed a synthesis method for producing high purity multiwalled carbon nanotubes. The method is a chemical vapor deposition process and highly selective. A pilot process for producing high purity (>90 %) was installed and commissioned in January 2003, current production capacity is approximately 1 kg per day.

The synthesis process involves decomposition of an appropriate hydrocarbon over a dispersed iron catalyst that is deposited *in situ* on quartz substrates. The process has been described in detail elsewhere [Andrews et al 1999], but can be summarized as follows. The process configuration involves entraining a mixture of xylene and ferrocene into an inert gas stream. Decomposition of the ferrocene at temperatures in the range 625 – 775 °C, and at atmospheric pressure, produces a coating of iron nanoparticles on the quartz surfaces, and these metal sites function as catalysts for the formation and growth of multiwall carbon nanotubes. An example of the carbon nanotube mats produced is shown in Figure1.

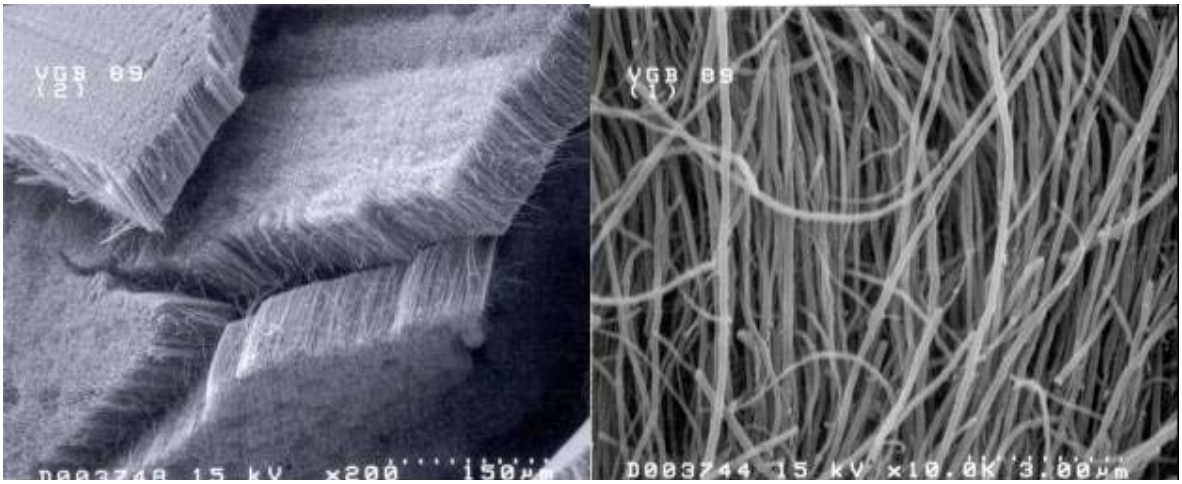

Figure 1 – Multiwall carbon nanotube mats.

In preparation of for fabrication of nanotube/pitch composite fiber and foams, approximately 500 g of multiwall carbon nanotubes was produced.

Task 3.0 Dispersion of nanotubes – UK CAER.

WVU provided UKCAER with a Koppers coal tar pitch, softening point 110 ^{o}C and a pitch/nanotube mix containing 2 wt % of nanotubes prepared. Dispersion of the MWNTs in the pitch matrix was achieved by heating the pitch to a temperature above its softening point in a Haake Polylab Rheomix, where high shear mixing could be applied. Tests were performed to determine the optimum conditions (temperature, mixing time and rotor speed) required to adequately disperse the MWNTs and yield a homogenous product, but without unduly degrading the pitch. At the completion of each test, the composite was allowed to cool, recovered from the mixer, and crushed to yield a granular product. Pitch/nanotube blends were prepared in 50 g batches (the optimum capacity of the mixing bowl), approximately 600 g of pitch/nanotube blend was prepared. The pitch blend was returned to WVU for carbon foam synthesis. Pitch/nanotube blends containing 2 and 4 wt% nanotubes were also prepared with W.Ky coal extract pitch and Ashland A500 pitch (for comparison) using the same techniques described above.

Task 4.0 Fiber forming, processing and testing – UK CAER

Pitches nanotube mixes were formed into continuous filaments using a Wayne bench scale extruder fitted with a 6.2mm diameter screw and 0.3mm dia x 1mm capillary die. Tests were conducted to determine the conditions under which the samples could be successfully extruded to produce a continuous thread. Feed size distribution and the temperature profile along the barrel and nozzle were crucial to this task. The extruded thread was attached to a wind-up drum rotating at speeds up to 1700rpm (12m/s) to draw filament in the range 15 to 30μm.

Tows of fiber cut from the wind-up drum were stabilized by heating slowly in air up to 310^{o}C. The stabilized fibers are then rapidly carbonized by heating to 1000^{o}C in nitrogen. Processing of control fiber samples is shown in Table 5.

Table 5 – Summary of fiber processing data for control fiber samples.

Pitch	**Stabilization**				**Carbonization**			**Carbon Yield (%)**
	Rate (^{o}C/min)	**Linear Shrink (%)**	**Weight Change (%)**	**Status**	**Linear Shrink (%)**	**Weight Change (%)**	**Status**	
WVU#BO44-NDK (QI Free Coal Tar)	0.2	13	-1.9	3	11	-21.3	3	76.8
WVU#BO81-NDK (Coal Extract)	0.2	12.5	-2.2	3	10	-24.3	3	73.5
W.Ky	0.2	11	-2.6	3	13	-31	3	71.2
Status: 0 = melted, 1 = stuck, 2 = slightly stuck, 3 = OK. *n/a = not applicable.*								

Table 6 – Summary of fiber processing data for pitch/nanotube composite fiber samples.

Pitch	Stabilization				Carbonization			Carbon Yield (%)
	Rate (^{o}C/min)	Linear Shrink (%)	Weight Change (%)	Status	Linear Shrink (%)	Weight Change (%)	Status	
W.Ky + 2 wt % MWNT	0.2	0	3.8	3	8	26.9	3	75.9
W.Ky + 4 wt % MWNT	0.2	4	3.4	3	11	22.4	3	80.2
A500 + 2 wt% MWNT	0.2	0	10	3	10	24	3	76
Status: 0 = melted, 1 = stuck, 2 = slightly stuck, 3 = OK. *n/a = not applicable.*								

SEM images of W.Ky pitch/nanotube composite fibers are shown below in Figure 2 and 3. Both images show dispersion of nanotubes as individual nanotubes, aligned axially in the fiber. Exhaustive attempts to measure mechanical properties of these fibers as single filaments produced ambiguous results. Overall mechanical properties measured appeared the same or lower than values determined for blank fibers (ie containing no nanotubes). Inspection of the above SEM images shows that the external surface of the fibers is rough, these “defect” sites in the surface may cause premature failure of the matrix before any stress can be transferred to the nanotubes (reinforcement), during testing of single fiber filaments. To avoid undue influence on the mechanical properties of the fiber by the fiber’s surface characteristics epoxy lay-ups of fiber tows were prepared.

Figure 2 – W.Ky pitch fiber containing 2 wt% nanotubes.

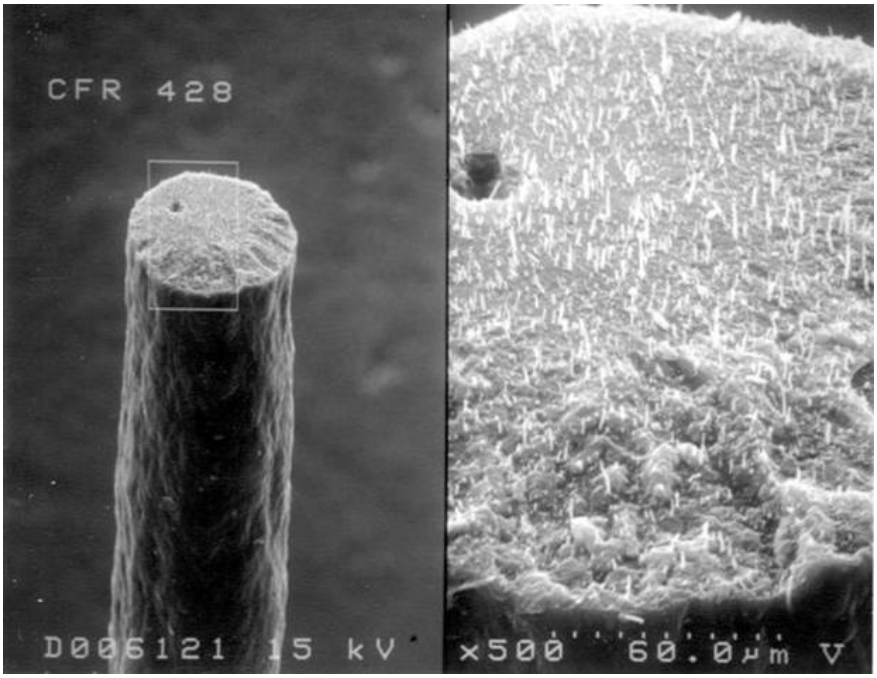

Figure 3 – W.Ky pitch fiber containing 4 wt% nanotubes.

Composite fibers were dip coated in epoxy to reduce the effect that surface defects had on the mechanical properties. Individual fibers were dip coated in epoxy, wiped and then cured at 120 ^{o}C for 1 hour. The resulting epoxy coated fibers were examined under SEM and some examples are shown in Figures 4 and 5. Inspection of these images shows that the epoxy significantly reduced the surface "roughness" of the composite fibers. The reduction in surface roughness also reduces surface defect sites that may have caused the ambiguous mechanical test results previously. Pitch fibers from both W.Ky and A500 feedstocks were also dip coated and used for comparisons with the epoxy coated composite fibers. Epoxy coated fibers were tested on an MTS tensile tester, 100 of each fiber type were tested. A summary of tensile strength and elastic modulus are shown in Table 7.

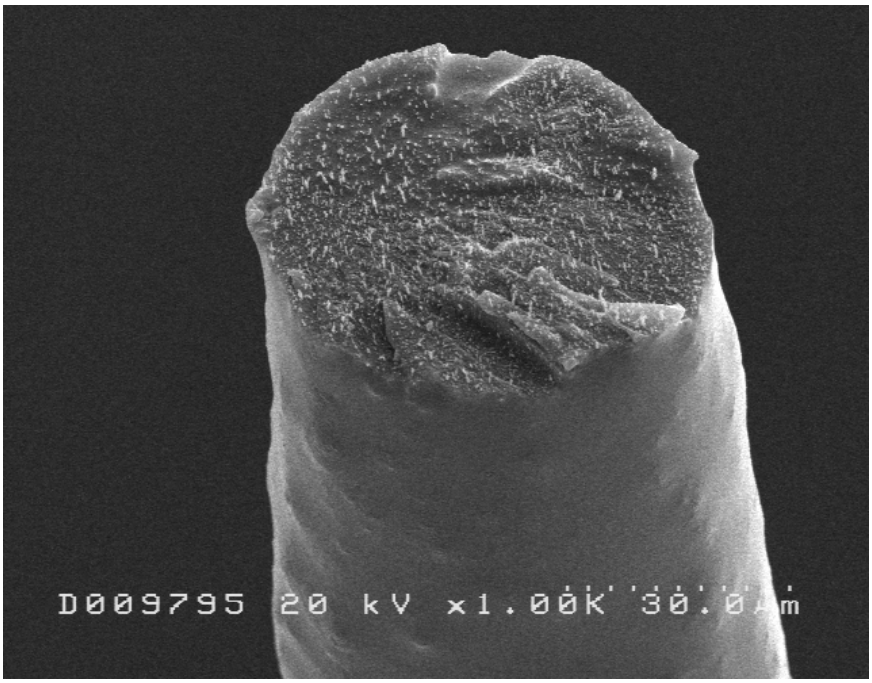

Figure 4 – Epoxy coated W.Ky pitch nanotube fiber.

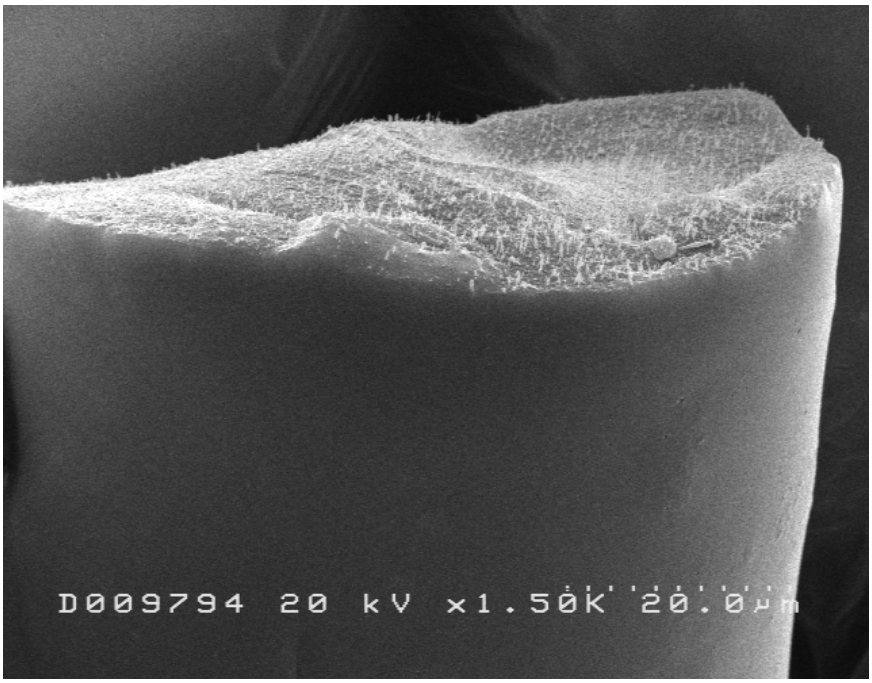

Figure 5 – Epoxy coated W.Ky pitch nanotube fiber.

Table 7 – Mechanical properties of epoxy coated pitch and pitch nanotube composite fibers.

Fiber	Mean Tensile Strength (MPa)	Std. Dev (MPa)	Mean Elastic Modulus (GPa)	Std. Dev (GPa)
A500	282.9	69.2	38.9	6.4
A500 + 2vol% nanotubes	372.2	61.0	36.4	2.8
W.Ky	526.3	60.5	36.0	3.6
W.Ky + 4vol% nanotubes	365.3	64.4	38.8	3.7

The results for the mechanical testing were not definitive. Although the A500 composite fibers did show increases in elastic modulus and tensile strength, the increases were moderate. The W.Ky composite fibers showed a decrease in tensile strength and modulus. These results can be explained by examining some of the fiber fracture surfaces, a sample of 10 fiber fracture surfaces retained after tensile testing were examined under SEM. A typical example of a W.Ky fiber

composite fracture surface is shown in Figure 6. This figure shows the presence of a large void within the fiber, such voids within the fiber were observed in several fiber fracture surfaces. The voids are detrimental to the fibers mechanical properties. The W.Ky composite fibers, which were spun with the highest nanotube loading, 4wt%, also had larger diameters compared to the fibers with lower loadings of nanotubes. Spinning larger diameter fibers also increases the likelihood of introducing larger defects during spinning. Further refinement of spinning techniques to reduce the fiber diameters of composite fibers is required.

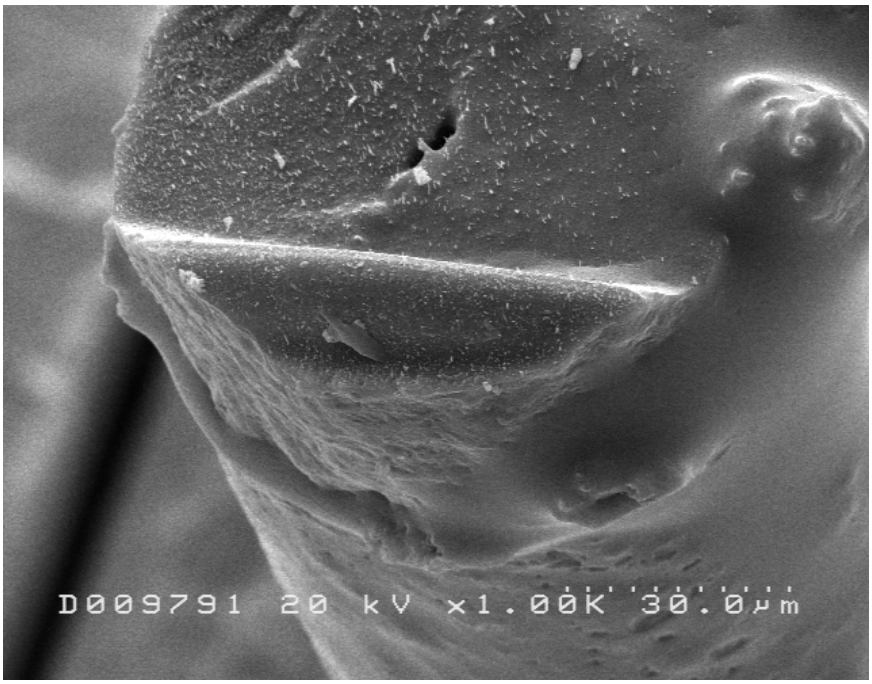

Figure 6 – W.Ky composite fiber fracture surface.

The thermal properties of composite foams were also assessed. The thermal diffusivity of the pitch derived foams and composite foams were measured using a laser flash method. Thermal diffusivities were measured on an Netzsch LFA 427 Laser Flash instrument. The laser flash

technique involves pulsing a laser onto the sample and measuring the heat diffused through the sample. Thermal diffusivity is directly proportional to thermal conductivity. Thermal conductivity can be calculated from the thermal diffusivity if the heat capacity and thermal expansion of the sample is known (or can be measured). Thermal diffusivity measurements require careful sample preparation to ensure that no penetration of the laser through the sample occurs during the measurement and that all of the lasers energy is absorbed by the sample.

Sample preparation of the carbon foams can be summarized as follows. Pitch foams and foam composites were cored to produce samples measuring 10mm diameter and approximately 2mm thick. Samples were coated, top, bottom and side with silicon carbide. The silicon carbide was used to fill the surface pores of the foam to prevent scatter or penetration of the laser pulse during measurement. The silicon carbide coated foam was cured at 400^{o}C for 1 hour, cooled and the polished to produce a smooth surface. The sample was then coated with graphite. Laser flash experiments were performed using a laser voltage of 450V and a pulse width of 0.8ms. Thermal diffusivity was measured in 100^{o}C increments from ambient to 700^{o}C, 3 shots per point were used with a delay time of 10 min between each shot. Results of thermal diffusivity test are summarized in Table 8.

Table 8 – Thermal diffusivity data for carbon foams.

	Thermal Diffusivity (mm^2/s)	
Temperature (^oC)	A240	A240 + 2wt% nanotubes
25	1.335	1.483
100	1.217	1.366
200	1.173	1.295
300	1.155	1.237
400	1.152	1.215
500	1.162	1.210
600	1.153	1.229
700	1.172	1.236

Comparison of thermal diffusivity between the foam and composite foam shows an approximate 30% increase in thermal diffusivity for the composite foam. It should be noted that this increase in thermal diffusivity was the result of only a 2wt% loading of nanotubes. It should also be noted that the thermal diffusivity of these foams did not change over the 700^{o}C temperature range. This is in comparison with graphite, where its thermal diffusivity drops dramatically above 400^{o}C.

2. SECTION TWO

WEST VIRGINIA UNIVERSITY

Task 5.0 Foam processing and testing - WVU

In last quarterly report, we reported on the pretreatment of pitches as a way of tailoring their foaming performance. In this report on we will report the subsequent foaming process and the characterization of the resultant foams.

Experimental:

Raw A240 petroleum-derived pitch and coal-based SynPitch were used as the starting pitches. A portion of each was sent to the CAER in Kentucky where 2% MWNT were incorporated into each pitch. Treated pitch samples, both with and without the addition of nanotubes, were ground to certain mesh size(50~100 mesh) and charged into a high pressure foaming reactor. The foaming was carried out in a N_2 atmosphere with pressure up to 500psi and temperature up to 500°C. The obtained green foam was then calcined at 1000°C in inert atmosphere to increase its strength and carbon content.

The carbon foams were characterized by SEM to investigate the distribution of nanotubes in carbon foam matrix. The general properties of carbon foam, such as bulk density and porosity and % of open cell structure were also measured. The porosity and % open cell were measured by means of a He pycnometer.

$$\text{Porosity}\% = (1 - D_b / D_p) \times 100$$

$$\%\ \text{open cell} = D_f / D_p \times 100$$

where D_b bulk density; D_f true density of the foam; D_p true density of pulverized foam

Results:

2 wt% MWNT was added into the raw pitch by the CAER workers, but after the heat treatment of pitch, foaming and calcinations, the amount of nanotubes in the carbon foam has been changed to 4.3%, 3.7% and 3.4%, respectively, as shown in Table 1. This is due to the loss of volatile matter during the various steps of foam preparation.

Table 1. Correction of the amount of nanotube in the carbon foam

Samples	Original MWNT added, wt%	Weight loss in different steps, wt%			Finial concentration of MWNT in the carbon foam, wt%
		pitch heat treatment	foaming	calcination	
A240	2	49.5	4.3	4.3	4.3
Coal-based SynPitch	2	36.4	10.7	5.7	3.7
Coal Tar Pitch	2	35.7	5.3	4.8	3.4

Table 2. General properties of carbon foam derived from pitches

Sample	Bulk density, g/cc	Porosity, %	% open cell
A240	0.34	82.9	97.2
A240/MWNT	0.41	78.6	95.7
Coal-based SynPitch	0.42	79.7	95.6
Coal-based SynPitch/MWNT	0.34	82.6	96.1
Coal Tar Pitch	0.67	64.8	83.5
Coal Tar Pitch/MWNT	0.68	65.4	82.9

The foam microstructure and the distribution of nanotubes in the foam matrix were investigated by SEM. Figure 1 shows the overall cross section of these pitch-derived carbon foams. A240 generates more uniform cell size, while SynPitch-dervived carbon foam shows a wider cell size distribution.

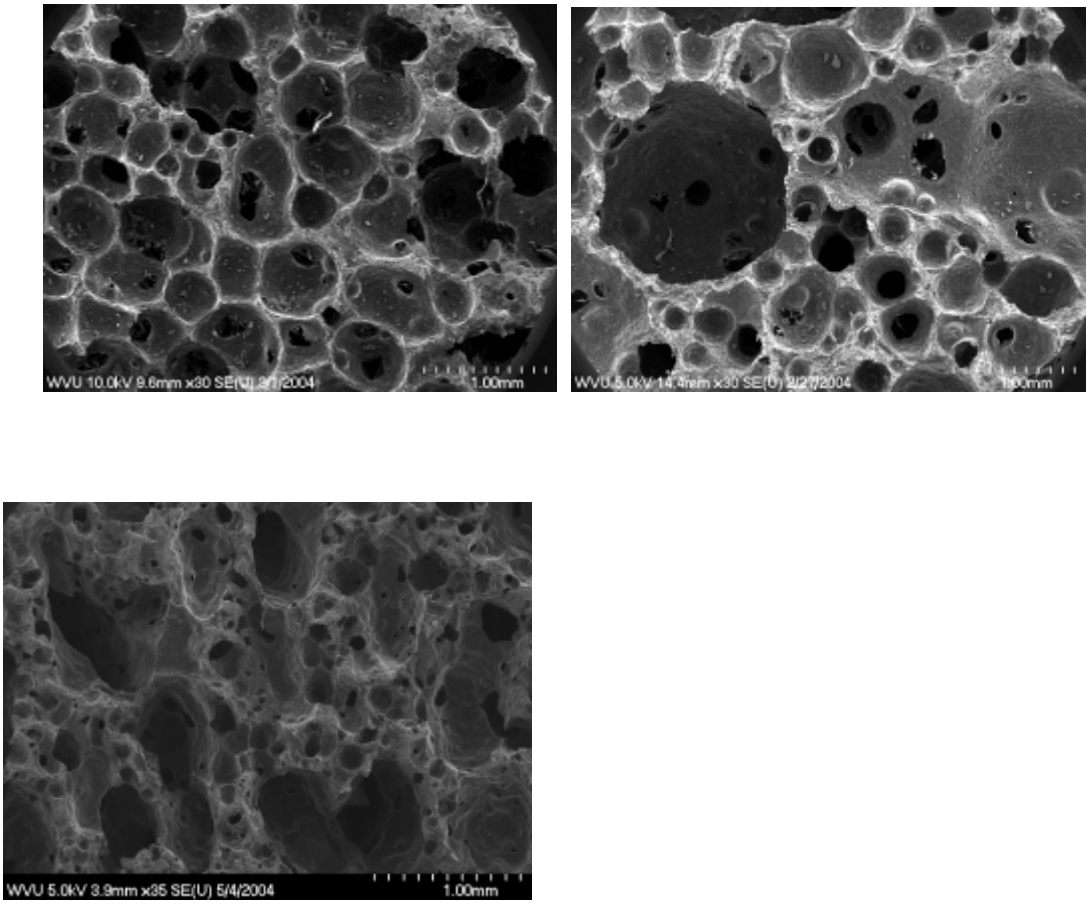

Figure 1. SEM images of MWNT reinforced carbon foam. A240-based, left, SynPitch-based, right and coal tar pitch-based, bottom center

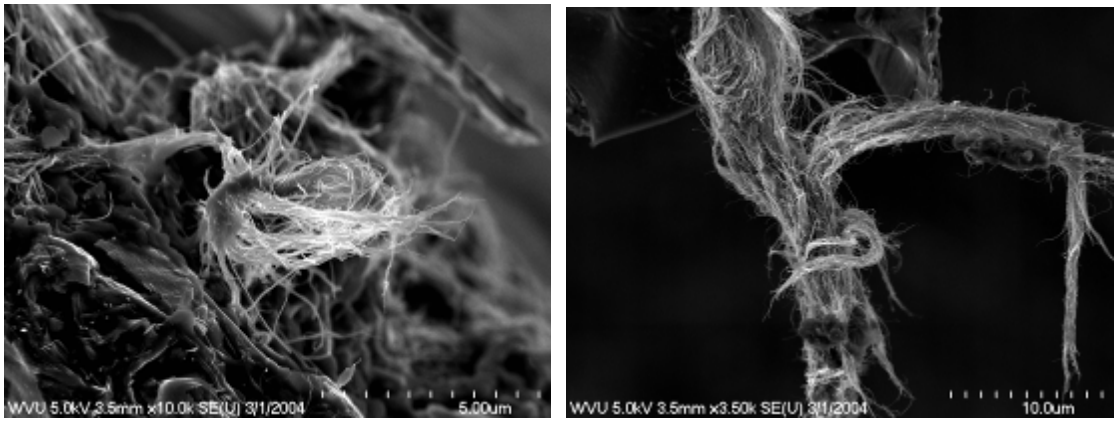

Figure 2. Agglomerated MWNT found in the carbon foam matrix

The interaction between the nanotube and composite matrix is in part responsible for the enhancement of mechanical strength. For the carbon foam/MWNT system, due to the lack of the knowledge of surface chemistry of nanotubes and carbon at this moment, we are unable to specify the precise interactions between nanotubes and carbon matrix, but *van Der Walls* and π-π interactions might be involved. The enhanced mechanical properties are believed to be due to the "bridging" effect of the nanotubes and the ability to transfer the load to the nanotubes. If the nanotubes are strongly bonding or interacting with the foam matrix, the nanotubes will bridge the microscopic cracks and the matrix residues should be observed adhering to the tube surface in the fracture sites. Figure 3 shows the nanotubes found on the fracture surface of foam matrix. Most of these tubes appear to have a clean surface without matrix residues adhering to it. The results indicate that the MWNT may have weak interactions with carbon foam matrix and hence not strongly bound to the matrix.

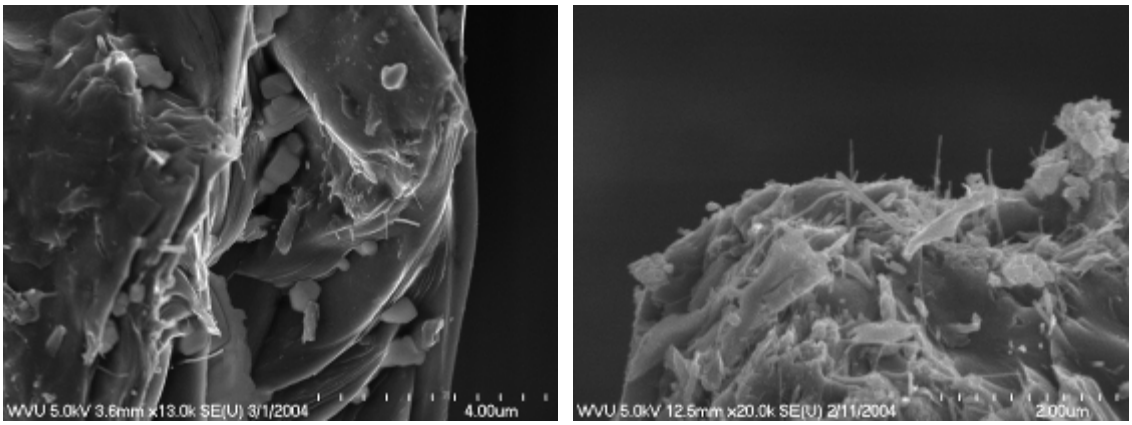

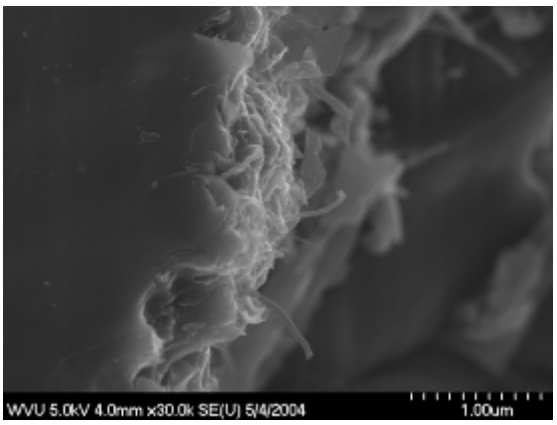

Figure 3. MWNT appeared on the cross section of carbon foam, A240-based, left and SynPitch-based, right, coal tar pitch-based, bottom.

The alignment(orientation) of nanotubes in the matrix also affects the property enhancement of the carbon foam. The nanotubes found on the fracture surface, as shown in Figure 3, were supposed to “bridge” the matrix together. This kind of alignment would be effective in enhancing the overall strength of the foam. However, the nanotubes found on the cell membrane are, for the most part, oriented perpendicular to the foam wall and are not effectively bridging the matrix together, as shown in Figure 4. In addition, the nanotubes bridging between the graphitic layers or microcracks should enhance the strength of the foam, but such structures were difficult

to find at least for the samples investigated here(see Figure 4). The nanotubes may need a high shearing force to align them in a certain direction. Unlike the spinning of the carbon fiber, which subjects the pitch a high shearing forces during extrusion from a nozzle, the shearing force applied to the carbon foam matrix during foaming is from the gas bubble evolution, which might not be strong enough to align the nanotubes parallel to the cell wall.

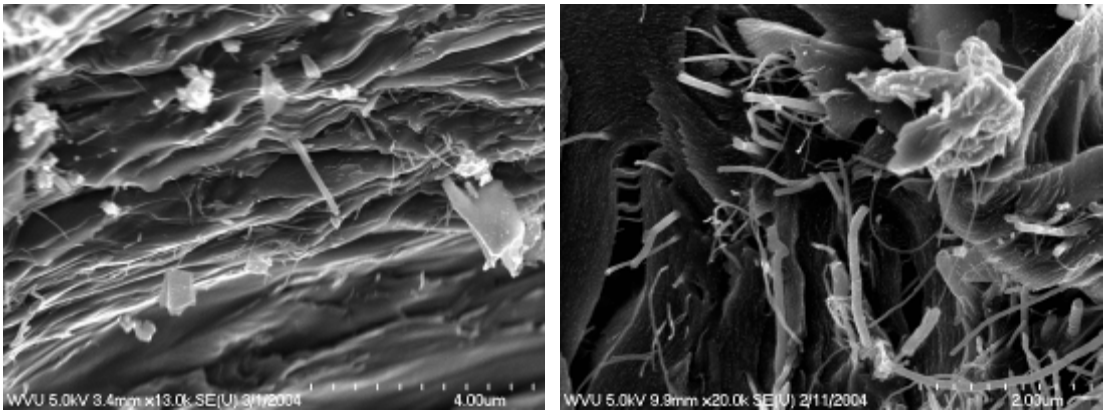

Figure 4. MWNT found on the foam cell membrane, A240-based, left; SynPitch-based, right.

Compressive strength was measured by means of Instron 5869 using a cylindrical shaped sample(25mm diameter by 20~30mm height) with a matched stainless steel sample holder cylinder and piston. The compressive strength is obtained from the yield strength of the stress-stain curve for the foam.

Figure 5 shows the compressive stress-strain curves. The stress increases as the load is applied to the sample and then the sample fractures but still resists the load as the cells are compressed. To compare the effect of nanotubes, the compressive strength along with the relative density of samples was measured and is listed in Table 3. An accurate comparison should be carried out among the samples with same relative density, but due to the technical difficulty, it is hard to get

the samples with and without nanotubes to have exactly the same relative density. However, the relative densities of the actual sample are close for the foams tested here. The results listed in Table 3 indicate that the nanotubes do not significantly affect the strength of carbon foam at least under compression. It is not clear at this moment what causes this result. Further testing of the tensile strength may be necessary to clarify the effect of nanotubes on the carbon foam strength and such tests are currently under way.

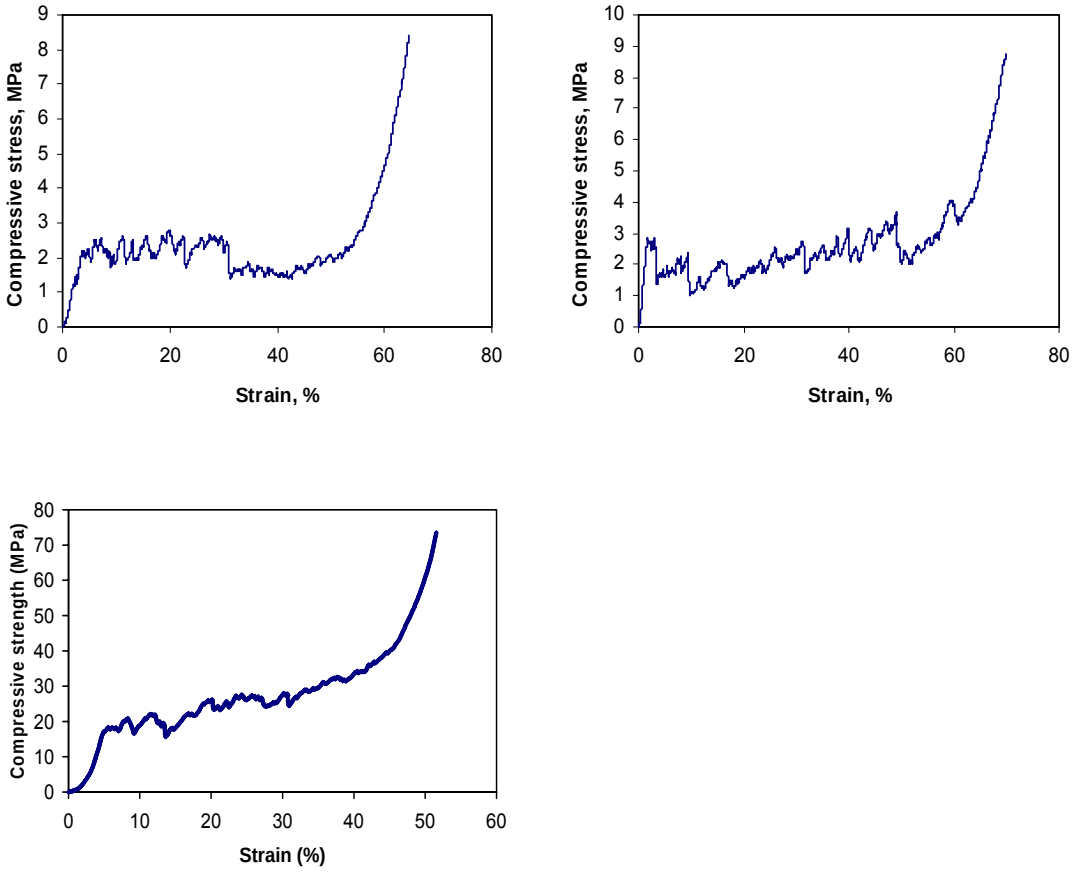

Figure 5. Compressive stress-strain curve. A240/MWNT, left; SynPitch/MWNT, right; and coal tar pitch/MWNT, bottom.

Table 3. Comparison of the compressive strength of carbon foam with and without MWNT addition

Sample	Compressive yield strength, MPa	Relative density
A240	3.9	0.17
A240/MWNT	2.3	0.21
SynPitch	2.5	0.20
SynPitch/MWNT	2.7	0.17
Coal Tar Pitch	18.2	0.35
Coal Tar Pitch/MWNT	18.2	0.35

References

Andrews, R., D. Jacques, A.M. Rao, F. Derbyshire, D. Qian, X. Fan, E.C. Dickey, and J. Chen, *Continuous production of aligned carbon nanotubes: A step closer to commercial realization.* Chemical Physics Letters, 1999. **303**(16): p. 467-474.

Purchas, D.B, 1967, “Industrial Filtration of Liquids”, Leonard Hill, London, England.